Republic of Iraq
Ministry of Higher Education
and Scientific Research
University of Baghdad
College of Education for pure
Sciences / Ibn Al-Haitham

Characterization of ($Mg_xCr_yZn_{1-x-y}O$) Nanoparticles Prepared by Sol-Gel Auto Combustion Technique

A thesis
Submitted to the Council of the College of Education for Pure
Sciences / Ibn Al-Haitham / Baghdad University in Partial
Fulfillment of Requirements for the Degree Master of
Sciences in Physics

By

Radhwan Shopan Muhssen

(B.Sc. in Physics 2013)

Supervised by:
Assist. Prof. Tagreed Muslim Marush

2017 A.D. **1439 A.H.**

بِسْمِ اللَّهِ الرَّحْمَٰنِ الرَّحِيمِ

وَاصْبِرْ لِحُكْمِ رَبِّكَ فَإِنَّكَ بِأَعْيُنِنَا ۖ وَسَبِّحْ بِحَمْدِ رَبِّكَ
حِينَ تَقُومُ (48)

صدق الله العلي العظيم

سورة الطور الآية (48)

Supervisors Certification

We certify that Radhwan Shopan Muhssen Al-Afraijy has presented this thesis under our supervision at physics department, College of Education for Pure Sciences Ibn- AL-Haitham, the University of Baghdad as a partial requirement for the degree of Master of Science in physics.

Signature:
Name: ***Dr. Tagreed Muslim Marush***
Title: Assistant Professor
Address: College of Education for Pure Science / Ibn –Al-Haitham
University of Baghdad
Date: 18 / 9 / *2017*

In view of the available recommendation, I forward this thesis for debate by the examination committee.

Signature:
Name: ***Dr. Kareem Ali Jasim***
Title: Professor
Address: College of Education for Pure Science / Ibn –Al-Haitham
University of Baghdad
Date: 18 / 9 / *2017*

Certification of Examiners

We certify, that we have read the thesis titled **"Characterization of ($Mg_xCr_yZn_{1-x-y}O$) Nanoparticles Prepared by Sol-Gel Auto Combustion Technique"**, presented by **Radhwan Shopan Muhssen** and as an examining committee, we examined the student on its contents, and in what is related to it, and that in our opinion it meets the standard of a thesis for the degree of Master of Science in Physics.

(Chairman)

Signature: N. A. Bakr
Name: Dr. Nabeel Ali Bakr
Title: *Professor*
Address: *University of Diyala*
Date : 13 / 2 / 2018

(Member)

Signature:
Name: Dr. Farouq Ibrahim Hussain
Title: *Assistant Professor*
Address: *University of Baghdad*
Date : 14 / 2 / 2018

(Member)

Signature:
Name: Dr. Suad Hammed ALeabi
Title: *Assistant Professor*
Address: *University of Baghdad*
Date : 14 / 2 / 2018

(Supervisor)

Signature:
Name: : Dr. Tagreed Muslim Marush
Title: *Assistant Professor*
Address: *University of Baghdad*
Date: 14 / 2 / 2018

K. F. Ali

Prof. Dr. Khalid Fahad Ali

The Dean of College of Education

For Pure Science / Ibn –Al- Haitham

Linguistic Amendment

I certify that this thesis titled ***"Characterization of ($Mg_xCr_yZn_{1-x-y}O$) Nanoparticles Prepared by Sol-Gel Auto Combustion Technique"*** *presented by (**Radhwan Shopan Muhssen**) has been corrected linguistically; therefore, it is suitable for debate by the examining committee.*

Signature:

Name: ***Dr. Muntaha Motashar AbdulSahib***

Title: Assistant Professor

Address: College of Education for Pure Science / Ibn –Al-Haitham

Date: 16 / 10 / 2017

Dedication

To My Beloved Country ……… Iraq

…

To Whom God Crowned him With Prestige and Dignity, To Whom I am So Proudly Carrying his Name ……… My Dear Father

To My Angel In Life, To The Character of Love, Compassion and Dedication, To The Secret of My Existence, To The One Who's Prayers Is The Key Of My Success ……… My Beloved Mother

To The Pure and Kind Hearts and The Innocent Souls, To The Basils Of My Life ……… Brothers & Sisters

…

To My Loyal Friends ……… Haider Faisel, Hussain Jani, Thaer AbdulSada, Mohammad Odah, Muayad Shihab & Mohammad AbdulHassan.

Radhwan

Acknowledgements

All praise to Allah who enabled me to overcome all the difficulties I faced, until putting the thesis in its final form.

I would like to thank **the Deanship of College of Education for Pure Science / Ibn al-Haitham and Presidency of the Department of Physics to allow for the completion of the master study.**

I would like to thank my supervisor **Dr. Tagreed Muslim Al-Saadi** for her inspiration, guidance and valuable suggestions throughout this research, and to my beloved spiritual father **Dr. Tariq A. Al-Dhahir** for his helpful discussions and encouragement. I would also like to express my gratitude to the professors and all the staff members of the Department of Physics/ College of Education for Pure Science/ Ibn Al-Haitham, especially **Assistant Pro. Dr. Farouq Ibrahim Hussain, Assistant Professor Dr. Ahmed Rafeeq Abdul - Majeed, Prof. Dr. Khalid Hilal Harbi and Dr. Shatha Hashim** for their great help, helpful discussions and encouragement.

I would like to express my thanks to my best friend **Bassam Thuaban, Ali Saad, Rashid Latif, Mohammad Abdallah, Haydar Abdul Zahra, Ibrahim Khalil, Maitham Al-Rikaby, Karrar Amin, Rusul Alaa** for their continuing support and help.

Abstract

In the present work, nanosized pure and ($Mg_xCr_yZn_{1-x-y}O$) doped ZnO nanoparticles were synthesized, with different doping concentrations for nine doped samples. A simple and cost-effective sol-gel auto combustion technique was used, utilizing Zinc Nitrate ($Zn\ (NO_3)_2.6H_2O$) and Ammonia solution (NH_3) as precursors, in addition to the Citric Acid ($C_6H_8O_4$) as the combustion agent and Distilled water (DW) as a solvent. Where the concentrations of Mg and Cr were divided into two groups, the first in which Mg concentration is constant ($x = 0.05$) and y = (0, 0.05, 0.1, 0.15, 0.2); while the second in which Cr concentration is a constant equal to ($y = 0.05$) and x = (0, 0.05, 0.1, 0.15, 0.2). The optimized preparation conditions for forming the gel were pH of 7.0 at 85 °C.

X-ray diffraction analysis (XRD), scanning electron microscopy (SEM), energy dispersive spectroscopy (EDX), Ultraviolet-visible spectroscopy (UV-Vis) and LCR meter techniques were used to study structural, optical and electrical properties of prepared samples. The results obtained from these examinations of the doped samples were compared and matched with their counterparts of the un-doped ZnO.

The XRD patterns have revealed that the diffraction peaks of pure and (Mg, Cr) doped ZnO nanoparticles, can be indexed to a hexagonal wurtzite structure. From the diffraction patterns of all prepared samples, strongest four clear peaks of zinc oxide were observed, within the angular range of the X-ray diffraction (20^o - 80^o), attributed to the crystalline planes (101), (100), (002) and (110). The average crystallite size of ($Mg_xCr_yZn_{1-x-y}O$) was calculated using the Scherrer and (Williamson – Hall) formulas. The resulting powder was found to have a crystallite size on the nanoscale, lying between (22-33) nm, and was noted to decrease as doping rate increased. Several structural parameters were calculated, including

lattice parameters, inter-planner spacing, xrd density, specific surface area, texture coefficient and the morphology index. The morphological and elemental analysis was carried out for the sample (M1) with concentrations of ($Mg_{0.05}Cr_{0.05}Zn_{0.9}O$). SEM micrographs have shown the particles have a spherical or semispherical formation aggregated in the form of clusters. EDX spectra have revealed the presence of Zn, Mg, Cr and O, which confirmed the formation of the analyzed sample.

The optical studies were carried out using ($Mg_xCr_yZn_{1-x-y}O$) Nanopowder as a solution, within the wavelength range of (300-900) nm. The obtained results have revealed that the absorbance spectra decreases with increasing the doping rate for all samples. As concerning to values of allowed band gap obtained by Tauc's plot, it was found to decrease from 3.36 eV to 2.61 eV as the doping rate with both Mg and Cr increased.

The a.c. electrical measurements were studied as a function of the frequency within the range (50Hz - 3MHz). Frequency dependent dielectric constant and dielectric loss were studied, and they were observed to decrease with increasing frequency. This decrease can be explained by the increase in the frequency of the electric field, which caused a decrease in the contribution of the space charge polarization, and this phenomenon is common in most of the dielectrics. The variations of a.c. conductivity dependent frequency and temperature had also been studied at room temperature, 50, 100 and 150 ^{0}C. A Linear increase in conductivity with increasing frequency and temperature was observed, which confirms the semiconducting behaviour of the synthesized material. At room temperature, un-doped ZnO sample has shown a minimum electrical conductivity than rest-doped samples. Thus, we found that the doping with (Mg, Cr) has enhanced or modified the electrical conductivity of zinc oxide at room temperature.

List of Contents

Chapter Two : Theoretical Background

Chapter Three : Experimental Work

Chapter Four : Results and Discussions

Chapter Five : Conclusion and Future Works

List of Tables

List of Figures

Symbols

Symbol	Description	Units
n_i	Intrinsic carrier density	cm^{-3}
$\boldsymbol{n}$	The diffraction order	-
$\boldsymbol{\lambda}$	The wavelength of the X–ray source	nm
$\boldsymbol{d_{hkl}}$	Inter atomic spacing	Å
$\boldsymbol{\theta}$	Bragg's angle	degree
hkl	Miller indices	-
a, c	Lattice constant	Å
$\boldsymbol{\rho}_{x\text{-}ray}$	X-ray density	g/cm^3
$\boldsymbol{Z}$	Number of molecules per unit cell	-
$\boldsymbol{M_{wt}}$	Molecular weight	g/mol
$\boldsymbol{V}$	The unit cell volume	$(Å)^3$
$\boldsymbol{N_A}$	Avogadro number	1/mol
$\boldsymbol{D}$	The average crystalline diameter	nm
β	The full width at half maximum	rad
$\boldsymbol{\varepsilon}$	The internal Micro-strain	-
SS.A	The specific surface area	cm^2/g

$\mathbf{T_c}$	The texture coefficient	-
M.I	The XRD morphology index	-
$\mathbf{FWHM}_h$	The highest FWHM value that obtained from peaks	Degree
$\mathbf{FWHM_p}$	A particular peak's FWHM for which M.I. is to be calculated	Degree
$\boldsymbol{\alpha}$	The absorption coefficient	cm^{-1}
A	The absorbance	-
ξ	The molar absorbance	$(M.cm)^{-1}$
C	The molar concentration	M
L	Length of light path	cm
$\boldsymbol{hv}$	The incident photon energy	eV
E_g	The optical energy gap	eV
$\boldsymbol{E_p}$	Phonon energy	eV
T	Transmittance	-
$\mathbf{I_t}$	The intensity of transmitted light	mW/cm^2
$\mathbf{I_o}$	The intensity of the incident light	mW/cm^2
r	The exponent of Tauc's relation	-
$\boldsymbol{E_g^T}$	Tauc energy gap	eV
$\boldsymbol{\varepsilon'}$	Real part of Dielectric constant	-

$\boldsymbol{\varepsilon}''$	Imaginary part of Dielectric constant	-
$\varepsilon_{\circ}$	The permittivity of vacuum	F/cm
ε	The permittivity of the semiconductor	F/cm
t	Thickness of the pellet	cm
$\boldsymbol{C_p}$	Parallel capacitance	F
d	Diameter of guard electrodes	cm
tan δ	The loss factor	-
$\boldsymbol{\sigma_{a.c}}$	Alternative Electrical conductivity	$(\Omega.cm)^{-1}$
f	Frequency of the applied ac electric field	s^{-1}
ω	The angular frequency	s^{-1}
ρ	The electrical resistivity or specific resistance	Ω.cm
R	The Ohmic resistance	Ω
A´	Represents cross-sectional area of the sample	cm^2
l	The length of the sample	cm

Abbreviations

Symbol	***Meaning***
ZnO	Zinc oxide
n-type	Semiconductor of electrons Majority
eV	Electron- volt
GPa	(Giga-Pascal) Extremely high-pressure
NPs	Nanoparticles
hcp	Hexagonal closed packed structure
XRD	X-ray diffraction
SEM	Scanning electron microscopy
UV	Ultra violet
Vis	Visible light
EDX	Energy dispersive spectroscopy
LED	Light-emitting diode
a.c .	Alternating current
e.g.	stands for *exempli gratia*, which means “for example.”
(0-D)	Zero-Dimensional
(1-D)	One- Dimensional

(2-D)	Two- Dimensional
(3-D)	Three- Dimensional
CVD	Chemical vapour deposition method
pH	Potential of hydrogen
E_C	The lower edge of the conduction band
E_f	The Fermi energy level
E_V	The upper edge of the valence band
P-type	Semiconductor of holes Majority
xerogel	A solid formed from a gel by drying with unhindered shrinkage
(JCPDS)	Stands for Journal Committee on Powder Diffraction Standards
IR	Infrared radiation
Temp.	Temperature

Chapter One

Introduction and Historical Review

1.1. Introduction

Nanotechnology exactly denotes any technology performed on a nano scale, which has implementations in the real world. Nanotechnology involves the production and application of chemical, physical and biological systems at scales extending from individual molecules or atoms to submicron dimensions, as well as the combination of the resulting nanostructures into larger systems [1]. In this volume, the material varies in its chemical, physical and biological properties than in the macroscopic sizes [2].

Nanotechnology is likely to have a profound impact on our economy and society in the early twenty-first century, incomparable to that of semiconductor technology, information technology, or cellular and molecular biology. On the other hand, it contains some risks that must not be neglected [3].

Nanotechnology attains it's being to the amazing development within the field of microelectronics. Since the invention of the integrated circuit in 1958 nearly half a century ago, there has been an exponential growth in the number of transistors per the microchip and an associated decrease in the smallest width of the wires in the electronic circuits. As a result, extremely powerful computers and efficient communication systems have appeared with a subsequently ingrained change in our daily lives [4].

The choice of the preparation methods is a basis to improve the final properties of nanoparticles that are designed for a specific application, and this choice should be guided by a series of factors, such as physical and chemical parameters of the compound, the nanoscale diameter, structure and morphology, or environmental considerations, which certainly constitute a criterion indisputable [5].

One of the nanomaterials preparation methods is the solution-gel or colloidal solution (sol-gel) method of auto-combustion, which is considered one of the distinctive methods, due to the ease in preparation, shortness of time and require no high temperatures [6].

1.2. Zinc Oxide Overview

Zinc oxide (ZnO) is an n-type semiconductor, and classified within the compounds semiconductors group (II - VI) of the periodic table. It is widely used in technological and industrial applications due to its direct and wide band- gap about (3.37) eV, as well as, has a unique properties comparing with features of other competitors, such as (SiC, In_2O_3, SnO_2, $CdSnO_4$ and GaN) [7, 8], so it was found that:

1. Can be produced at low cost, due to the abundance of its raw materials

2. Nontoxic.

3. Possesses high chemical stability.

4. Possesses high irritation energy.

5. Characterized by a good thermal, optical and piezoelectric behavior.

6. Possesses high and stabilized irradiation energy, where some experiments proved that the (ZnO) is very resistant to high radiation energy, making it suitable for space applications [9].

1.2.1. ZnO-Based applications

Zinc oxide can be utilized in many optoelectronic applications such as optical sensors, surface audio waves devices, gas sensors devices, capacitors, transparent conductors, optical sites sensors, laser diodes, variable resistors, solar cells and blue / violet light emitting devices, where it's considered the most important material in light emitting diodes chemical and biological sensors fields. In addition, it is widely used in cosmetics, as ointments, powders for the skin and as a primary compound in sunscreen cosmetics. ZnO has been widely used as an additive material to common materials, such as rubber, ceramics, glass and coatings such as glass coating, aircraft and buildings [10, 11].

1.2.2. Physical Characteristics of ZnO

1.2.2.1. Crystal Structure

Zinc oxide crystallizes in three structures; hexagonal-wurtzite, cubic (zinc blende) and the rarely observed cubic-rock salt. The wurtzite crystal structure is most common, because it is more stable at ambient conditions than its other forms, and it has lattice parameters (a= 3.25 Å & C=5.12 Å) at the ideal condition. Zinc blende form can be more stable via growing ZnO on a substrate with a cubic structure. The rock-salt (NaCl-type) structure is relatively observed only at high pressures about (10 GPa), as shown in Fig. (1-1) [12, 13].

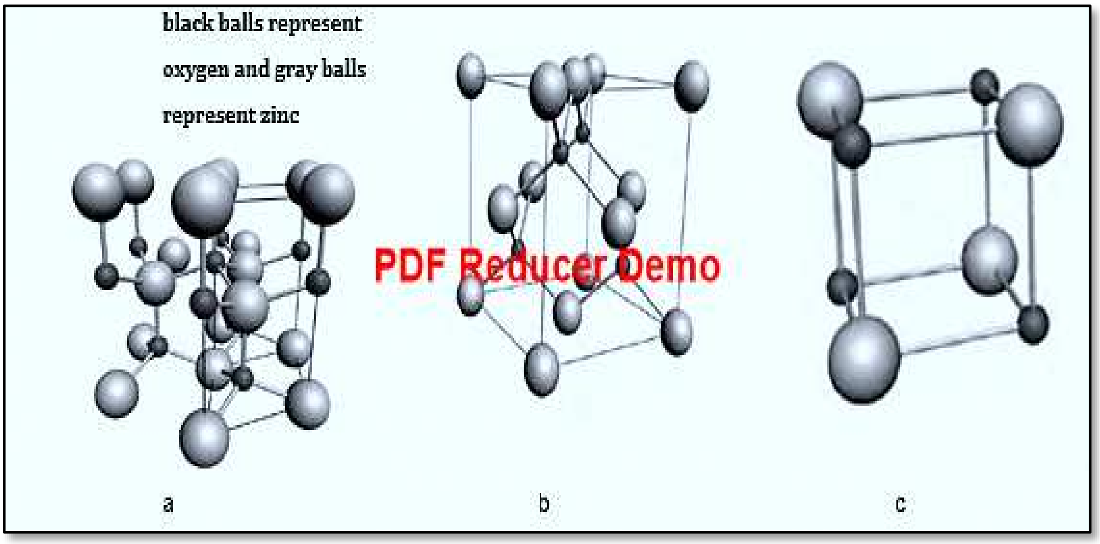

Fig. (1-1): *Lattice structures of three ZnO structures: (a) Hexagonal (wurtzite); (b) Cubic zinc-blend and (c) Cubic rock salt* [14].

1.2.3. Chemical characteristics of ZnO

Zinc oxide is a white solid compound. Crystalline zinc oxide when heated in air, its colour change from white to yellow and return to white at cool. This colour change is due to a small loss of oxygen at high temperatures [15]. Zinc Oxide is an amphoteric oxide, because it does not dissolve in water and alcohol, but dissolves in ammonia, metallic acids, ammonium carbonate and alkaline hydroxides [16].

In addition, these are some physical and chemical properties of ZnO, as shown in the table (1-1):

Table (1-1): *Some physical and chemical characteristics of ZnO* [10, 17]

Molecular Weight (g/mol)	*Crystal Structure*	*Density (g/m^3)*	*Melting Point (°C)*	*Ionic Radius (Å)*	*Solubility*		*Colour*
81.389	*Cubic & Hexagonal*	*5.60*	*1975*	*0.74*	*soluble in most acids*	*Insoluble In water and alcohol*	*White*

1.3. Characteristics of materials used for doping ZnO-NPs

1.3.1. Magnesium oxide MgO

Magnesium oxide can be obtained from magnesium silicate and magnesium carbonate. Magnesium oxide is a white powder with a high melting point, and it is a semiconductor that has a wide energy gap (7.8 eV), molecular weight (40.3044 g/mol), density (3.85g/cm^3) and a melting point about (2852°C). In addition, it has a cubic crystal structure with lattice parameter (a = 0.4212 nm), as shown in figure (1-2) [18, 19]. Magnesium oxide is used in the refractories and insulators as it has a high melting point, as well as it is used as an inner lining of the metal and glasses furnaces because of its low expansion and resistance to cracking, it is also used for manufacturing the reflective layers in optical devices [20].

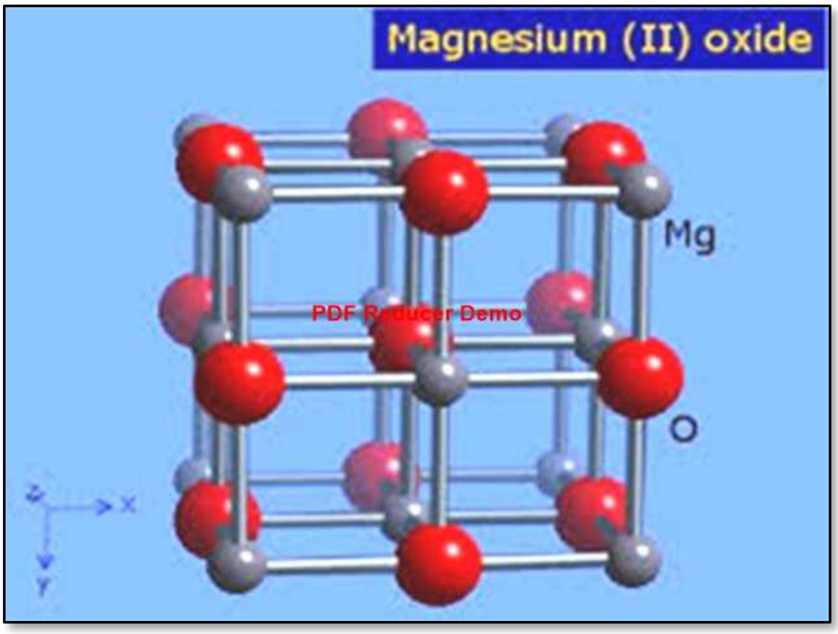

Fig. (1-2): *The lattice structure of MgO* [21].

1.3.2. Chromium (III) Trioxide Cr_2O_3

Chromium oxide has many oxidations conditions. In this study, it has been studied in the stable status Cr_2O_3, as it is a transitional element, and these elements are characterized by their wide applications [22]. The properties of chromium oxide vary between alkaline, amphoteric and acidic, depending on the oxidation of chromium in the oxide, where the acidic properties increase with increasing oxidation number, and for (Cr_2O_3) chromium oxide is considered as an amphoteric oxide. Chromium oxide is characterized with green colour and varies between bright green, brown green and olive green depending on the crystallization state, table (2-1), and it has hexagonal closed packed (hcp) crystal structure [23], as shown in figure (1-3).

Table (1-2): *Some physical and chemical characteristics of* Cr_2O_3 [23, 24].

molecular weight g/mol	***Colour***	***Density (g/cm ^{3})***	***Solubility***		***Melting point ^oC***	***Boiling point ^oC***
151.99	*green*	*5.21*	*insoluble in* H_2O *and alcohol*	*soluble in common acids*	*2266 ± 25*	*4000*

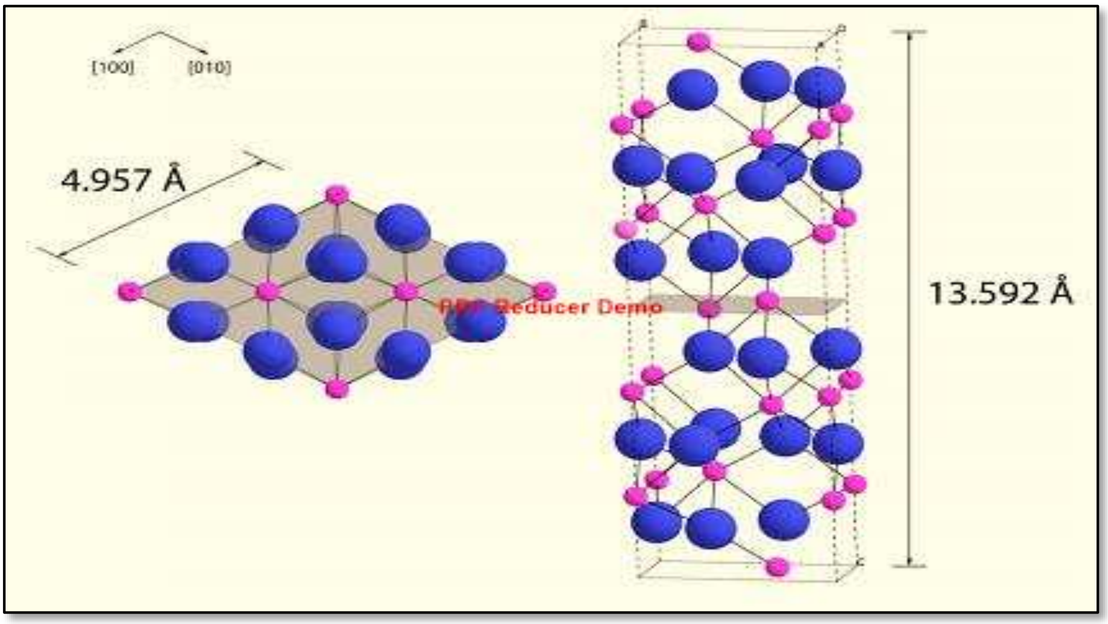

Fig. (1-3): *The Top view (left) unit cell of* Cr_2O_3*, at the right, the intersection of the (0001) plane with the bulk unit cell of* Cr_2O_3*. The large blue spheres are oxygen atoms and small purple are chromium atoms* [25].

1.4. Historical Review

In (2010), S. B. Rana, et al., have synthesized undoped and doped ZnO nanoparticles by direct precipitation method using wet chemical reaction. The crystallite size and phase purity of as-grown particles were investigated by X-ray diffraction (XRD) and scanning electron microscopy (SEM). The XRD results showed that the synthesized ZnO powders have a pure single-phase wurtzite structure and the average particle size was about 40 nm. The dopant elements Cu and Co influenced the particle size of the powders. The EDS analysis used to study the elemental analysis revealed the presence of Zn and O pure ZnO, and confirmed that Cu, Co and O are present in doped samples [26].

In (2010), A. K. Zak et al., have prepared ZnO nanoparticles by the sol-gel method of auto-combustion from zinc acetate as a precursor and acetic acid. Prepared samples were sintered at temperatures of 650°C and 750°C for 1hour. ZnO-NPs were studied by (XRD) technique. XRD results showed that the produced sample was crystalline with a hexagonal-wurtzite phase. The unit cell volume was noted to decrease as calcination temperature increased. They depended on Williamson-Hall (W-H) analysis and size-strain plot method to study the individual contributions of lattice strain and crystallite sizes on the peak broadening of the ZnO-NPs. From the results, the strain value was observed to decreases but the particle size increases as calcination temperature increased [27].

In (2011), J. Zhang, et al., have prepared $Zn_{1-x}Zr_xO$ nanoparticles via the sol-gel technique. The results of XRD showed that all samples have hexagonal wurtzite lattice structure with no any other new phase. In addition, the Zr atoms have been successfully entered into the ZnO lattice instead of forming other lattices. The lattice parameters monotonously were found to increase with increasing the (×), they thought it was due to the difference of the ionic radius of Zr^{4+} (0.84 Å) and Zn^{2+} (0.74 Å). The SEM images exhibit that the NPs of scanned samples with different sizes are partly accumulated together, with about 60 nm diameter [28].

In (2011), T. V. Kolekar et al., have prepared ZnO nanoparticles using the simple chemical method. Prepared samples were characterized using XRD and UV- Visible spectroscopy. XRD patterns revealed the hexagonal structure of prepared samples. No impurity peaks were observed, this indicate the high purity of the obtained ZnO. They calculated the optical band gap from UV-Visible absorption measurements, found to be 3.2 eV, and estimated the particles size from XRD pattern. The average crystallite size was calculated from Scherrer formula and found to be (10 nm) of ZnO-NPs that were calcined at 673 K [29].

R. Garcia, et al., in (2011), have prepared Indium-doped ZnO nanopowder by the solution combustion technique, using the metal nitrates as oxidizer agents and the carbohydrazide as fuel. The powders prepared by this method were spongy clusters, involving platelet-shaped nanocrystals with narrow particle size distribution and wurtzite structure. SEM studies confirmed that the doping with indium had no significant effect on the morphology of prepared powder. The Scherrer's formula was employed to determine the grain diameter (d) and found to be equal to 30 nm [30].

In (2012), S. P. Ghosh et al., have synthesized ZnO nanoparticles using the sol-gel method, and they have used zinc acetate dehydrate and triethnolamine (TEA) as basic materials. The obtained ZnO powder were calcined at 700^{o}C and 900^{o}C temperatures. They studied the prepared samples by (XRD), (SEM), and UV- visible spectroscopy. The results showed that the crystalline nature, particle size, and optical properties of the processed ZnO nanoparticles were significantly affected by calcination temperature. The XRD patterns showed that the ZnO crystal has a hexagonal wurtzite structure. SEM studies clearly demonstrate the spherical formation of ZnO nanoparticles, with a particle size of 20 nm. The optical properties were studied at room temperature by measuring the UV-VIS absorption. With increasing calcination temperature, the size of the particles increased and the band gap of the samples remained almost same i.e. (3.17 eV) [31].

In (2012), by the precipitation method, ***R. Viswanatha, et al.,*** have prepared Mg-doped ZnO nanoparticles with different doping concentrations. They studied the effect of Mg doping on the morphology, crystal structure and optical properties of the synthesized nanoparticles. The surface morphology of prepared material had studied by (SEM). They analyzed the structure and phases of Mg-ZnO powder by X-ray diffraction (XRD). XRD confirmed that the resultant ZnO nanoparticles were pure with a hexagonal structure. Scherrer equation was used to calculate the crystallite size and found to be lying between (60-90) nm. They used UV–Vis spectrophotometer to measure the optical band gap and it was found to be decrease as Mg content increased, in comparing to undoped ZnO, which is equal to (3.41 eV) [32].

In (2012), V. D. Mote et al., have synthesized Cr doped ZnO at room temperature by co-precipitation technique. They studied the structural and optical properties of prepared samples by using XRD and UV-Vis. The XRD results confirmed that the samples have hexagonal (wurtzite) structure without additional peak, which suggests that Cr ions go to the regular Zn sites in the ZnO crystal structure. The lattice constants were calculated using X-ray diffraction data and it was noticed that the lattice parameters increased as Cr content decrease. The unit cell volume decreased with increasing Cr concentration. Scherrer's formula was used to calculate the average grain size for pure and Cr doping samples and found to be in the range of (11 – 17) nm. The band gap of the samples has been evaluated by the UV-Visible spectrometer. They found that the band gap decreases as Cr increased; which is may be attributed to the s-d and p interactions and the smaller average grain size [33].

In (2012), M. A. Hassan has prepared high purity ZnO nanoparticles at low temperature using the chemical method. The effect of annealing at high temperatures were studied. He found that the reaction between zinc acetate solution and sodium hydroxide solution at 0°C suddenly occurred, and the annealing temperature of product surfactant powder played a significant role in the morphological changes. The nanoparticles were characterized by (XRD), (SEM) and UV-visible. XRD result confirmed the hexagonal wurtzite ZnO structure. The crystallite size was determined using Scherrer's formula and found to be 35nm and 37nm, he found that the particles size increased and more defects such as oxygen vacancies at preparation process. SEM measurements showed homogeneities regarding of particle size distribution. For the UV- Visible studies, the band gap was found to be (Eg =3.3 eV). The absorbance spectra were observed to decrease as wavelength increased [34].

In (2012), T. M. Hammad, et al., have prepared Co-doped ZnO nanopowder at low temperatures by the simple chemical method, with an atomic ratio of Co: Zn (0 to 7) %. XRD analysis showed that the Co-doped ZnO samples have a wurtzite crystal structure and crystal size of 12–5 nm calculated from the Scherrer's formula. XRD, SEM and EDX have proved the spherical super-structure formation of doping of Co in ZnO and revealed that the Co^{2+} was successfully substituted into the ZnO host lattice of the Zn^{2+} site. The optical band gap of ZnO nanoparticles noticeably increased from 3.32 to 4.12 eV as Co content levels increased from (0 to 7) %. Thus, they have concluded that the current doping method is considered to be another efficient technique to modify the optical properties of ZnO nanomaterial [35].

In (2013), S. Kumar et al., have synthesized $Mg_xZn_{1-x}O$ ($0 \le x \le 5\%$) using the sol-gel method. XRD, SEM and Uv-Vis, these techniques were employed to study the properties of prepared samples. XRD study revealed the existence of polycrystalline hexagonal wurtzite phase of ZnO for 0-5% of mg doping ZnO. The lattice parameters were observed to decrease as Mg content increased. Average crystallite Size was noted to increase from 34 nm for pure ZnO to 41 nm as Mg content increased. The energy gap of the nanoparticles samples has been determined by Tauc plots. Results showed that the optical band gap increases from 3.1 eV to 3.35 eV, this increase might be attributed to the defects presences. Change in the band gap of the material, there are essential tails recognized towards lower energy side of the absorbance spectra. These tails maybe occured due to the scattering of a range of particulate sizes or some type of Urbach tail effect due to inter-grain depletion regions. They deduced that the prepared nanoparticles would be quite valuable for UV LED's implementations [36].

T. M. Hammad et al., in (2013), have prepared Fe doped ZnO NPs using the sol-gel process. They have studied the structural, magnetic and optical properties of the prepared samples. The following techniques XRD, EDX and UV-VIS spectroscopy were employed to study these properties. The structural results showed the single phase with hexagonal wurtzite structure of Fe doped ZnO, also showed that the increase in the (Fe) dopant content led to a reduction in particle size, where the average particle size was (6, 8 and 3) nm for undoped ZnO and Fe doped ZnO of (2% and 5%) respectively. It was found that the Fe^{2+} ions were successfully substituted Zn^{2+} ions in the ZnO host lattice without changing its wurtzite structure. The optical band gap of synthesized nanoparticles was found to increase from (3.5 eV to 3.71) eV as (Fe) concentration increased up to (5%). They have concluded that their preparation method has improved the optical properties of Fe doped ZnO [37].

In (2013), S. F. Shayesteh and A. A. Dizgah have prepared undoped and Mg-doped ZnO NPs using basic chemical solution method. They studied the effect of doping with Mg and the heat treatment on the structural and optical response of synthesized nanomaterial. They characterized the prepared samples by using (XRD), (EDX), (SEM) and UV–Vis optical absorption. XRD Results revealed that the prepared NPs had a hexagonal structure. EDX technique had indicated the Mg substitution in the ZnO host material.

SEM micrographs have confirmed the spherical form of the as-prepared ZnO, also it indicated that the average size increased as the annealing temperatures increased. Due to the incorporation of Mg, the crystallite sizes were found to decrease, while the optical band gap increased. From the UV–Vis spectrum, a blue shift was observed, which was regard as a typical signature of size confinement of ZnO nanoparticles [38].

In (2014), A. Ghosh et al., have studied the prepared undoped and Cu-doped zinc oxide nanoparticles using a chemical route. Structural results confirmed that all prepared samples having polycrystalline nature. Crystallite size was noted to change as increasing the doping concentration of Cu. SEM studies were carried out to identify grain size and texture. UV-Vis measurements exhibit absorbance peaks in the region (200 – 800) nm; they found that absorbance did not change much. [39].

C. Jayachandraiah and G. Krishnaiah, in (2015), have studied the synthesized pure and erbium (1.30, 1.79, 2.83 and 3.53 at. %)-doped ZnO nanostructures using the wet chemical co-precipitation method. XRD, EADX, UV-Vis and LCR meter, these devices were used to study characterization of prepared nanoparticles. The XRD results confirmed the hexagonal wurtzite structure of all samples. The particle size was found to decrease from 23 nm to 17 nm with Er content. The chemical composition was identified using EDAX; it showed that the product was composed of only Zn, O and Er with no any other impurities. The energy gap was noted to decrease with increasing Er content. Dielectric constant, dielectric loss and A.C. conductivity were observed to decrease as Er content increased [40].

In (2015), N. K. Divya et al., have synthesized erbium doped ZnO nanoparticles using solid-state reaction route. The XRD data showed a change in the hexagonal wurtzite structure of ZnO, due to the incorporation of Er^{3+} based on crystallite size. (EDS) Spectra confirmed that were no impurities in the parent ZnO sample. The calculated crystallite size from Scherrer's formula was found to decrease from 57.71 nm to 45.26 nm, as erbium content increased. The A.C. electrical conductivity of doped samples was found to decrease with frequency. Dielectric constant and loss was found to decrease with increasing Er dopant and frequency [41].

S. R. Brinth and M. Ajitha, in (2015), have synthesized ZnO nanoparticles by an aqueous solution method, sol-gel and hydrothermal method. Prepared particles have been studied using following techniques XRD, EDX, SEM and UV-Vis. The XRD studies showed that the synthesized nanoparticles have wurtzite structure and the particle size was determined using Scherrer's equation and found to vary between 13 nm and 18 nm. SEM investigations revealed that the surface morphology of ZnO-NPs have spherical in the hydrothermal process and varies to flower like the arrangement in the sol-gel and aqueous solution process. EDX studies confirmed the existence of Zn and O. Absorbance spectrum was observed to decrease as the wavelength increased. The UV-visible spectrum of the nanoparticles showed a blue shift compared with that of the bulk sample [42].

In (2015), A. Sh. AL-Gurabi, et al., have prepared zinc oxide nanoparticles via chemical method, using ($Zn(NO_3)_2.6H_2O$) and (NaOH) with various concentrations (0.25, 0.5, 0.75, and, 1M) at 70^0C.

They studied the effect of temperature on particle size and shape. The following techniques were employed to study the prepared samples such as XRD and SEM. X-ray diffraction results showed that the ZnO-NPs have wurtzite structure, with no impurities in XRD pattern. In addition, the results showed that the diffraction peaks are intensive and very sharp. The SEM morphology studies have revealed that the particle size increase as the NaOH concentration increased. They observed that the change in concentration of NaOH led to change in pH value, which led to change in the size and shape of ZnO NPs [43].

In (2015), S. Jurablu et al., have synthesized Zinc oxide (ZnO) nanoparticles by a sol-gel technique, using the ethanol solution of zinc sulphate heptahydrate with diethylene glycol surfactant. Structural and optical investigations were studied using XRD; SEM and UV-Vis. XRD results revealed that the ZnO nanoparticles possessed a hexagonal-wurtzite structure. The average crystallite size of ZnO has achieved about 25 nm computed from Sherrer's formula. The morphological studies of the surface of SEM depicted spherical particles with the formation of clusters. Absorbance peak of UV-Vis spectra revealed the wide band gap energy of 3.49 eV [44].

In (2016), M. S. Hamza et al., have prepared ZnO nanoparticles using the Hydrothermal technique. They used zinc nitrate hexahydrate [$Zn(NO_3)_2 \cdot 6H_2O$] as a precursor. XRD and SEM have been employed to study the morphology and structure of ZnO nanostructure. The obtained results showed that the prepared ZnO nanostructures had a hexagonal wurtzite structure. SEM images of nanorods and nanospheres with pH found to increase as the ammonia concentration decreased [45].

In (2016), Y. Cherifi et al., have synthesized Fe doped ZnO NPs using a sol-gel technique. SEM and XRD results confirmed that all samples had fine-scale and single-phase hexagonal wurtzite structure. The Scherrer's formula was used to calculate average crystallite size and found to decrease from 20.12 nm to 17.8 nm as the Fe content increased. The band gap energy was found to decrease from 3.11 eV to 2.53 eV as Fe doping content increased. Dielectric constant and dielectric loss were found to decrease as increasing the frequency of applied A.C. electric field; they imputed this behaviour to the existence of the space charge in the nanostructure, such as vacancies, dangling bonds, and the microspores due to the grain boundaries of their large surface grain. The A.C. conductivity was noted to increase with increasing the frequency. This increase has been explained by the increased number of the charge carriers that were derived from either the replacement of Zn by Fe ions or the incorporation of Fe ions in the interstitial sites of ZnO lattice [46].

T. IQBAL, et al., in (2016), using the sol-gel auto-combustion method have synthesized undoped and Mn-doped ZnO nanoparticles with various doping concentrations. The structural, morphological and dielectric were studied using XRD, SEM, and precession impedance analyzer. The XRD results confirmed the hexagonal wurtzite structure of prepared samples. The average crystallite size was found to be in the range of (100 nm), also noted to decrease as Mn increasing due to a decrease in the agglomeration process. Dielectric constant and dielectric loss were observed to decrease as Mn content increased. The variation of A.C. conductivity at room temperature found to increase exponentially as the applied A.C. frequency increased [47].

1.5. Aim of the Work

This work aims to:

- Preparation of zinc oxide nanoparticles doped with chromium and magnesium ($Mg_xCr_yZn_{1-x-y}O$) with various percentages by the sol-gel auto-combustion method.

- Study of the structural, optical and electrical properties of the prepared samples.

1.6. Methodology

- Prepare pure and doped ZnO Nanopowder utilizing sol-gel combustion method and studying the doping effect on the final properties being studied.
- Splitting of the prepared Nanopowders into three amounts, the first, in the form of a tiny powder for structural properties (X-ray test). The second, in the form of a suspension solution consisting of distilled water and nanopowders of prepared materials, which is specially intended for the optical properties (UV-Vis spectrometer). The third is in the form of compacted pellets by using a hydraulic press, and this is specific for the morphological (SEM), elemental (EDX) and electrical characteristics (LCR meter).
- Calcining synthesized Nanopowder at 600 ^{0}C and sintering the compacted pellets at 1100 ^{0}C using a high-temperature furnace.
- Measure and compare the resulting average crystallite size by two methods, Debye-Scherrer and the Williamson-Hall.

- Analyze the obtained findings to summarize the final conclusions.

1.7. Outline of the Thesis

The thesis is organized according to the following scheme. The current chapter (Chapter One) provides a brief introduction to the research topic and a statement of the motivations and objectives of the research and provides a survey of the literature on powder preparation and studying of ZnO. Chapter Two provides a theoretical framework for the research area. The details of the experimental procedure performed in this work are presented in Chapter Three; this chapter includes powder preparation, compaction process and sintering of Zinc oxide nanopowder. The results and discussion are presented in Chapter Four. Chapter Five contains the conclusions of preparation and study of un-doped and (Mg, Cr) doped ZnO Nanopowder; as well as recommendations for future works.

Chapter Two

Theoretical Background

2.1. Introduction

This chapter includes the theoretical concepts of the research subject, in terms of scientific explanations, laws and mathematical relations that have been adopted for interpreting the obtained findings of the present study.

2.2. Nanoscience Concept

Nanoscience primarily is defined by the unit of length, the nanometer scale ($1nm = 10^{-9}m$) at which lies the ultimate control over the form and function of matter. This smallest scale is a combination of different types and numbers of atoms that are used to manufacture a new form of the matter, this smallest scale at which we have the freedom to practice our inventions. While the nanoscience concentrates on the fundamental sides of nanoscale which are formation, characterization, and assembly. The conclusive goal of nanotechnology is to develop devices and materials that will outweigh present technologies, also make new ones with completely new functions [48, 49].

2.3. Nanomaterials: Definitions and Advantages

Nanomaterials can be described as the materials that have structural component clusters in form of molecules or crystallites, which have dimensions in the range (*1 to 100*) nm, and figure (2-1) shows visual objects of the nanoscale. Typically, these clusters of the atoms consist of hundreds to thousands in the nanometer scale (nm), which generally called Nano clusters. These small aggregations of atoms are generally known by several names, such as nanocrystals, nanoparticles and quantum dots**.** The nanostructured materials have led to new scientific fundamental phenomena and many applications in short, medium and long range. In addition, examples of these applications include (nanoelectronic devices, electron field emitters of ultra-thin TV screens, quantum wires, nanoprobes, high-resolution tips for atomic force and scanning microscopes, sensors, gas storage, nano-devices and the parts of the nano-machines) [50,51].

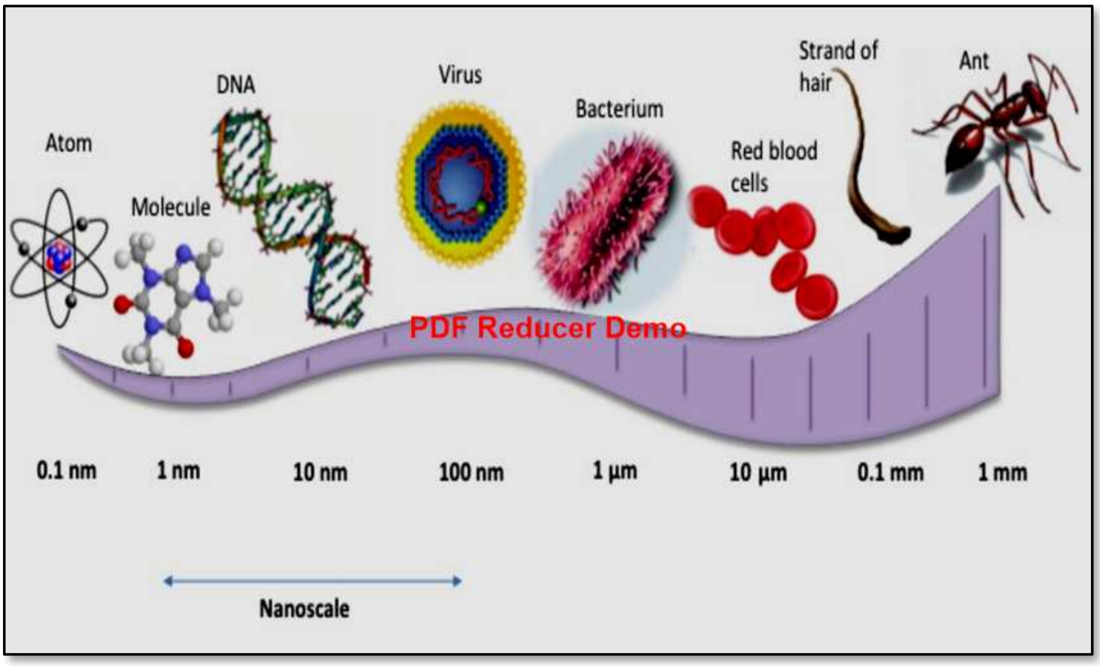

Fig. (2-1): *Examples of size and scale of the nanotechnology* [52].

2.3.1. Classification of Nanomaterials

Minimizing the spatial dimension or restriction of the particles within a given structure and a particular crystalline direction, generally, results changes in physical properties of the system in that direction. One classification of nanomaterials is that based on the number of dimensions, where the nanomaterials that are in one dimension system, e.g. thin films or laminate structures, while in two dimensions, e.g. nanorods and nanotubes or what are called (filamentary structures), and for three dimensions nanomaterials, e.g. structures composed typically of consolidated crystallites. Either material of zero dimension system, e.g. nanoparticles and nanopores.

Figure (2-2) shows classification of nanomaterials depending on the number of dimensions [53, 54].

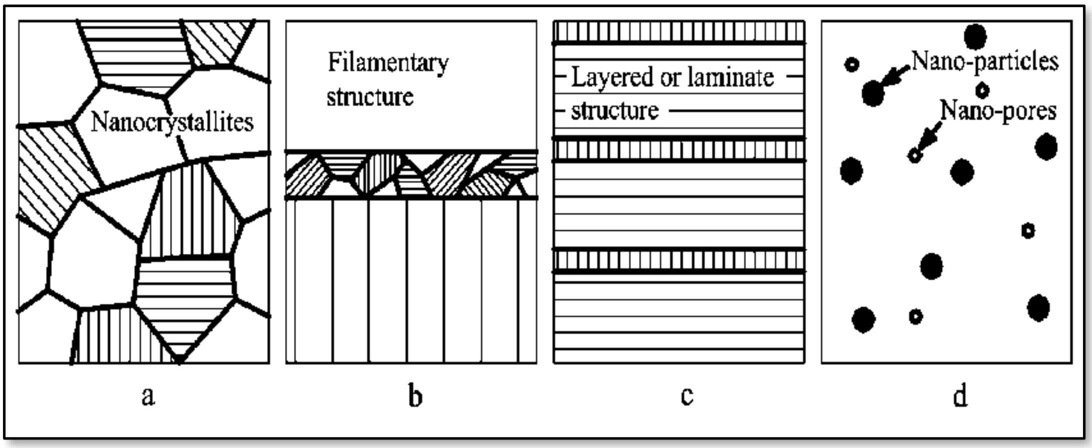

Fig. (2-2)*: The Schematic classification of nanomaterials: (a) 3-D system, (b) 2-D, (c) 1-D and (d) zero –D system* [53].

2.3.2. Synthesis Techniques of the Nanomaterials (Top-down Vs. Bottom-up)

In general, there are two methods for manufacturing nanomaterials. one of them is *Top-down* method, which is represented by reduction the bulk materials into nanoparticles, by using mechanical, chemical or physical processes, this method usually includes thermal, mechanical-energy and high energy lasers. Examples of these denominations are annealing, atomization, and laser ablation [55]. The other one is *Bottom-up* method, which imposes for beginning from atoms or molecules joined together by using special processes to generate materials with nano-dimensions [56].*The bottom-up* method generally includes chemical reactions such as the sol-gel method, precipitation method, flame or plasma spraying synthesis, chemical vapour deposition *CVD* and molecular or atomic condensation [57].

Moreover, figure (2-3) demonstrates methods of manufacturing nanomaterials of both types Top-down and Bottom-up approaches.

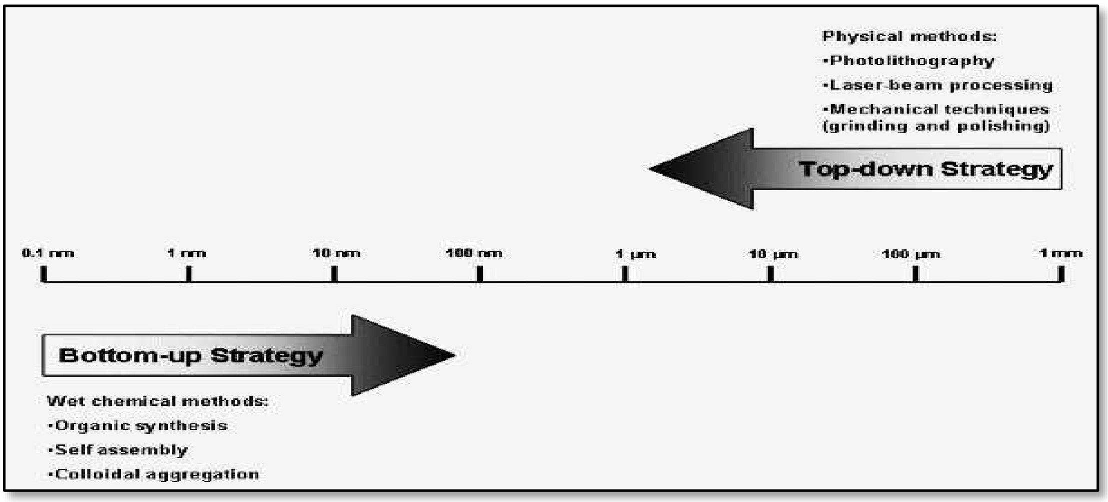

***Fig. (2-3)**: Top-down and Bottom-up methods* [58].

2.5. Sol-Gel Auto Combustion Technique

The *sol-gel* approach is along well defined an industrial method, for producing the colloidal nanoparticles from the liquid phase. The name of "*sol-gel*" can be explained by the transition from the liquid phase (solution or colloidal solution) into the solid phase (di- or multiphase gel) [59]. The part '*sol'* is defined as a stable dispersion of the colloidal particles in a solvent, where *the colloidal* is defined as a suspension of the dispersed solid particles (*~1–1000 nm*) that does not comprise as sedimentation or agglomeration. Whereas the part '*gel'* it is a continuous solid three-dimensional porous network surrounding the continuous liquid phase, in other words, it is a gelatinous compound [60].

In the recent years, it has been amended for fabricating coatings and advanced nanomaterials. The sol-gel method is a chemical method, which is based on the condensation or hydrolysis reactions [61]. Basic stages of this method are displayed in figure (2-4).

The raw materials used in the preparation of (sol) are usually inorganic mineral salts or mineral organic compounds. The sol-gel process undergoes a series of decompositions and polymerization reactions to form a colloidal suspension, and with further processing, we can make the materials with different forms. In addition, thin films with variety properties also can be obtained by this method. The sol-gel process represents a wet chemical mode, also it was known as the process of deposition of the chemical solution to produce solids of small particles. It is an inexpensive and low-temperature technique, allows controlling the chemical composition of the product [62, 63].

Sol-gel auto combustion technique is based on the *redox* reaction between the oxidant and the fuel in the precursor solution. The precursor solution involves the nitrates of the metal cation, a fuel and or a chelating agent in an aqueous medium, where the nitrates act as the oxidant and provide an environment for combustion of the fuel. With dehydrating the precursor solution, a complex net is formed, or the chelating agent leads to the formation a viscous gel at the final stage of dehydration. With further heating, this viscous gel swells with the decomposition of the present nitrates and finally burns out [64].

Some factors must be taken into consideration during the sol-gel auto combustion process, which is addition of ammonia solution in form of droplets until pH is modified to reach degree 7.0, and the system should be acidic to maintain a clear solution, as well as to prevent undesirable aggregates before the gel forming and before the actual combustion starts [65].

The combustion process is an oxidation-reduction reaction [66], where the redox mixture of the oxidant (nitrates) and the reductant (carboxyl groups) collapse with exothermically reaction, with evaporating a large amount of gases, such as CO_2, H_2O and N_2 [67].

ZnO nanoparticles can be prepared by several methods, such as hydrothermal, co-precipitation and a sol-gel method, among these techniques, the sol-gel method is appropriate for synthesizing ZnO nanoparticles due to its versatility, simplicity, and low cost. Comparing with other methods, sol-gel technique exhibits advantages in the production of nanoparticles such as relatively low temperatures and short reaction time [68].

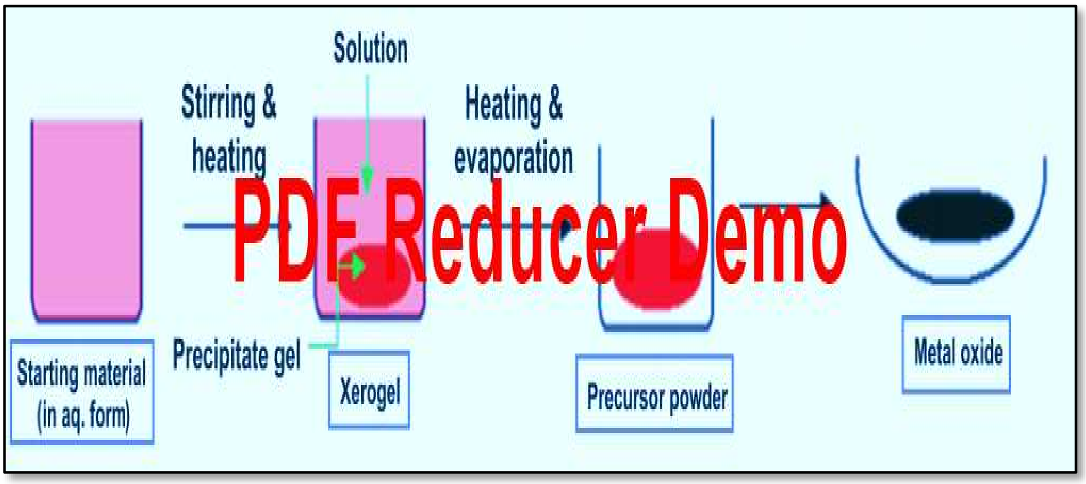

Fig. (2-4)*: A scheme demonstrates basic steps of the sol-gel process* [69].

In fact, sol-gel auto combustion technique used for synthesizing of nanocrystalline oxide materials is an integrated approach for both bottom-up and top-down processes, as the desired oxide products nucleate and grow from the combustion residue [70].

2.5.1. Advantages and Drawbacks of Sol-Gel Process

The sol-gel method is a perfect technique for synthesizing the nanoparticles with high purity. This technique has advantages of the product material, such as good stoichiometric control, pure and homogeneous product, due to mixing in the molecular scale. In addition, the production has tiny particles with a narrow size distribution; also, this method permits to reduce the firing temperatures due to its high surface areas with small particle sizes [71, 72]. On the other hand, there are some disadvantages of this method, such as, the high price of raw compounds and solvents [73], moreover; it can be considered as a multistage process, therefore, takes time [74], and when this method used to prepare ceramics products, the resulting material would contain many pores with relatively low density [75].

2.6. General Principles of Semiconductor Materials

Materials in nature are classified in terms of their electrical conductivity at room temperature into [76]:

- Conductors with high electrical conductivity lying between (10^{3}-10^{8}) (Ω.cm)$^{-1}$.
- Insulators with very low conductivity ranging between (10^{-18}-10^{-8}) (Ω.cm)$^{-1}$.
- Semiconductors with conductivity to the limits of (10^{-8}-10^{3}) (Ω.cm)$^{-1}$, that's mean this conductivity lies in between conductor and the insulator material.

In recent years, semiconductor nanoparticles have much noticeable attention due to their perceptive mechanical, optical and electrical properties, compared with their equivalents in the bulk scale [77]. Among them, zinc oxide (ZnO) nanostructure, basically an n-type semiconductor, is a gorgeous multifunctional material, as it has wide applications in the area of sensors, varistors, solar cells, gas sensors, displays and UV light-emitting devices [78].

2.6.1. Characteristics of Semiconductors

Most important semiconductors characteristics can be summarized as follows [79, 80]:

- Semiconductors have a resistance of a negative thermal coefficient that is the dependence of their electrical conductivity on the temperature is contrary to metals, as a resistance of semi-conductor decreases with increasing temperature.
- For a pure semiconductor, the electrical conductivity increases exponentially with temperature.
- The conductivity for an impure semiconductor depends strongly on the impurity concentration.
- Semiconductors have two types of charge carriers, electrons and holes, unlike conductive materials.
- The impurities play a major part in reducing the electrical resistance of the semiconductor.
- It's conductivity is affected by the magnetic field.
- Semiconductor materials are a light-sensitive, whereas the semiconductor resistance changes when exposed to an effective wavelength light.

2.6.2. Conventional (in-organic) Semiconductors

Semiconductor materials can be classified into two major categories as follow:

A. Intrinsic Semiconductors

If a semiconductor is pure and free of impurities then it is called *intrinsic*. A conventional inorganic semiconductor material, like silicon (Si) consists of covalently bound atoms forming a crystalline lattice structure. At absolute zero, the valence band is completely filled with electrons, as shown in fig. (2-5), whilst the conduction band is empty, and when the semiconductor temperature increases, electrons will be thermally excited and a certain number of electrons in the valence band relocate to the conduction band left behind a number of holes. The electrons that reach the conduction band, will partially fill this band, and be ready for electrical conduction when an electric field is applied, either holes which are formed in the valence band, are directly filled by moving neighbourhoods electrons in an opposite direction to the direction of the field. At room temperature, and for an intrinsic semiconductor, the Fermi energy lies in the middle of the band gap (E_g). For an intrinsic semiconductor [81, 82]:

$$n' = p = n_i \qquad \text{... (2-1)}$$

Where:

n´: electron density,

p: the hole density,

n_i: is called intrinsic carrier density.

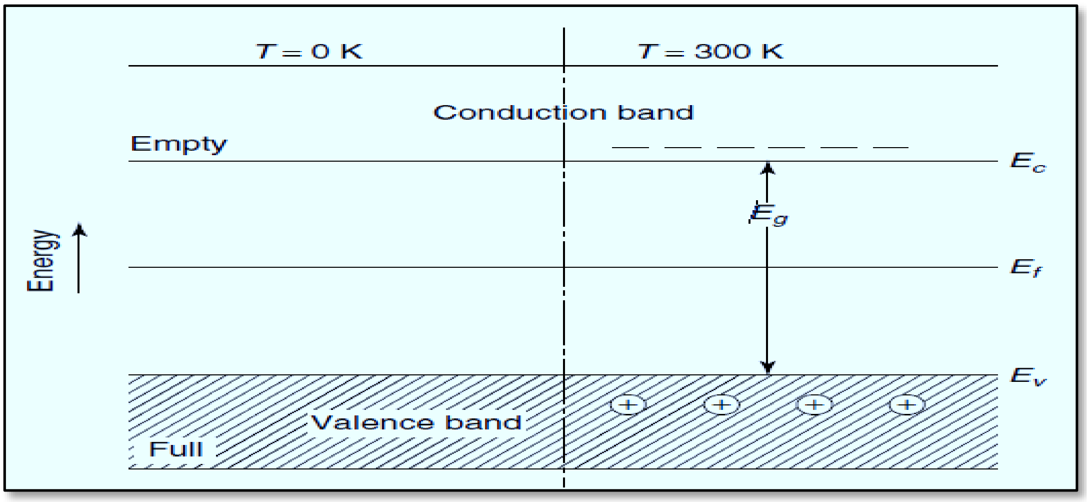

***Fig. (2-5)**: Energy bands of an intrinsic semiconductor: Ec is the lower edge of the conduction band; E_f is the Fermi energy level; Ev is the upper edge of the valence band, and Eg is the band gap* [83].

B. Extrinsic Semiconductors

Practically, all traditional semiconductors are extrinsic; that is, the impurities determined the electrical behaviour, that which, present in even slight concentrations, introduce excess of electrons or holes. For example, when the concentration of impurities of one atom is about $(10^{12})\frac{\text{atom}}{cm^3}$, which is sufficient to make silicon an extrinsic at room temperature [84].

Extrinsic semiconductors are classified into two types, depending on the type of impurities that are doped with. For instance, by adding pentavalent impurities, by a process known as doping, into silicon crystal, which has a valence of more than four, can obtain a semiconductor with electrons concentration is much larger than the concentration of holes. This kind of semiconductors is called as an *n-type* semiconductor. Nevertheless, if we add trivalent impurities into Silicon, such as boron (B), which have a valence less than four, then the concentration of holes is much greater than that of electrons. This type is called as *p-type* semiconductor [85, 86].

Semiconductors resulting from the doping process, are distinguished from their pure counterparts, by the fact that their conduction results from the participation of only one type of charge carriers (abundance or majority) for transmitting the generated current. Moreover, the charge carriers in the *n-type* semiconductor are the electrons. Whereas, in a *p-type* semiconductor, the charge carriers are the holes [87].

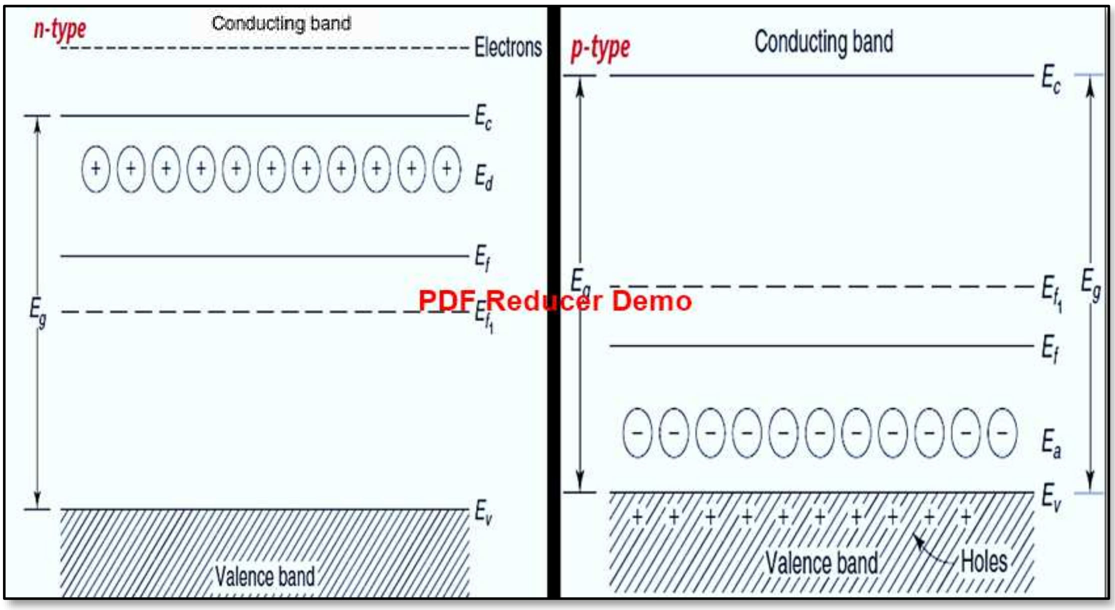

***Fig. (2-6)**: Schematic illustration the energy bands in an extrinsic semiconductor for both p-type and n-type* [83].

The energy difference between the conduction band and the valence band is called as the band gap. The properties of the material can change, depending on the amount of the band gap; in the case of metal, insulator and semiconductor. Figure (2-7) shows in the band gap in materials [88].

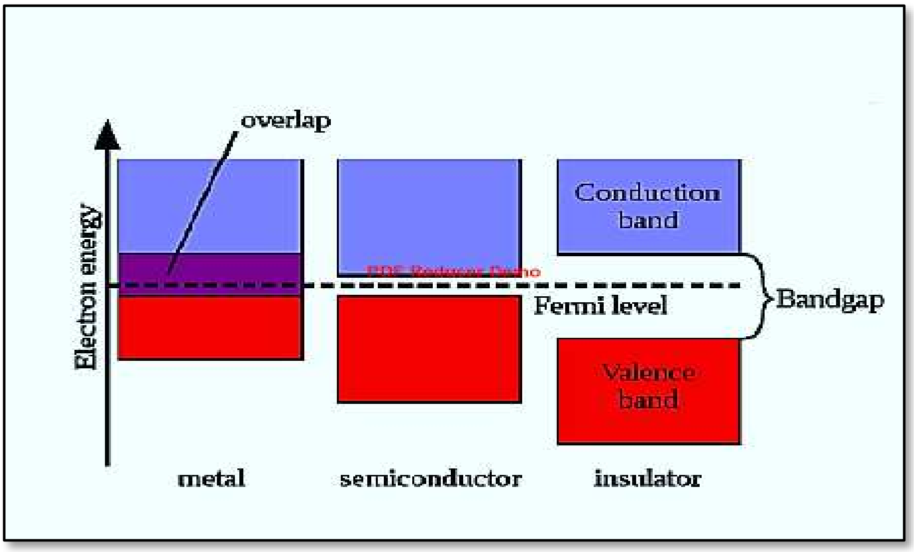

Fig. (2-7): *The band gap in materials* [88].

2.6.3. Doping of Semiconductors

Doping of semiconductors is central to present day for electronic and optoelectronic gadgets. Doping empowers control of both the optical and the electrical properties of semiconductors keys to device usefulness. The properties of the doped semiconductors emphatically rely on upon the electronic levels presented by the dopants. Upon increasing the dopant concentration, the discrete impurity levels in the band gap of the host semiconductor evolve into an impurity band that can overlap with the conduction/valence band in n-/p-type semiconductors, respectively, resulting in band gap narrowing (BGN) [89].

Doping of intrinsic inorganic semiconductors induces localized energy levels close to the conduction (n-type) or valence (p-type) band edge of semiconductor, fig. (2-8) extrinsic semiconductors. By this technique, the energy for the introduction of an electron or hole is tremendously lowered and the compound becomes more suitable for the common devices [90].

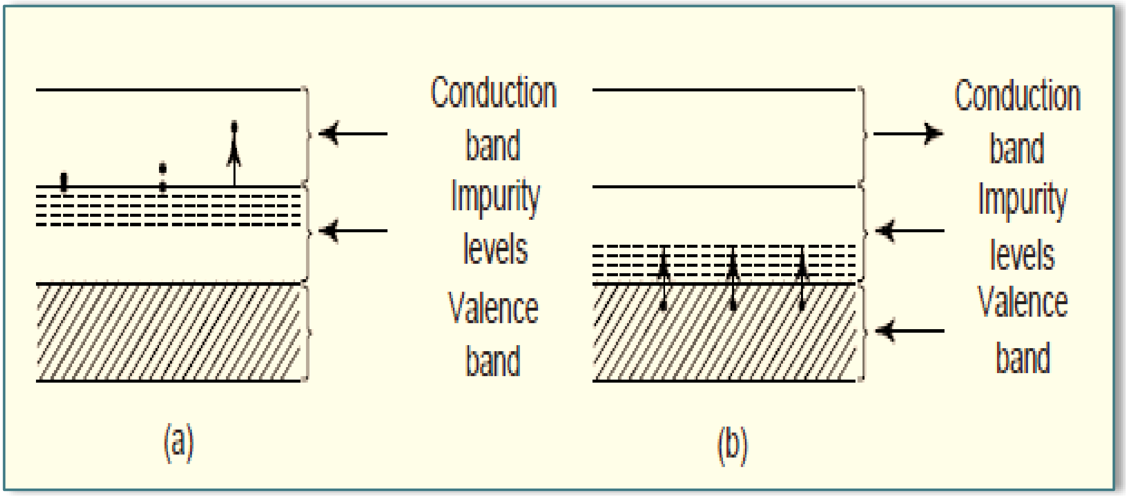

***Fig. (2-8)**: Impurity levels in extrinsic semiconductors (a) donors, or n-type and (b) acceptors, or p-type* [51].

There are several methods for doping semiconductors, depending on the mechanism in which it is carried out, which are as follow [91]:

- *Mixture Doping*
- *Co-evaporation Doping*
- *Thermal Diffusion Doping*
- *Ion Implantation Doping*
- *Laser Doping*

In our study, the mixture doping method had been used, which is performed by mixing the material to be doped with the dopant material, with specific weight ratios in the case of the convergence of their melting temperatures, in order to melt and incorporate them together to complete the doping process [92].

2.7. Structural Properties

X-ray diffraction is the most widely used technique to study the crystalline structure of solids and the least vague method for the accurate determination of the positions of atoms in all kinds of matter, as it is non-destructive technique, that provides a detailed information about the materials being examined.

2.7.1. X-ray Diffraction (XRD)

X-rays are electromagnetic radiation having exactly the same nature of light, but with very much shorter wavelength, approximately lying in the range (0.5 – 2.5) Å. This wavelength of x-rays is analogous to the inter-atomic spacing in solids. X-ray diffraction provided information of characterization of crystalline materials such as phases, crystal structure, preferable crystal orientation and other structural parameters such as crystallite size, lattice parameters, strain, and crystal defects. To determine the crystal structure of a specific material, it requires calculating the crystallite size, lattice constants and x-ray density [93].

The English scientist Bragg has assumed an easy model of the crystalline structure, that can detect the direction of X-ray diffraction from the crystal after it falls on. This model states that the different levels of crystalline atoms can reflect x-rays [94].

In addition, Bragg's law [95]:

$$n\lambda = 2d_{hkl} \sin \theta \qquad \text{... (2-2)}$$

Where, λ: The wavelength of the X–ray source, d_{hkl}: refers to the atomic space, θ : Bragg's angle (angle of the incidence or reflection), and n : is the diffraction order, which is an integer equal to 1, 2, 3 ....etc.

The basic condition for the occurrence of Bragg's reflection is when ($\boldsymbol{\lambda \le 2d_{hkl}}$). Through equation (2-2), we notice the existence of two variables ($\boldsymbol{\lambda, \theta}$), where their values can be controlled to determine the value of ($\boldsymbol{d_{hkl}}$), thus identifying the crystal structure of the material being studied, as well as its crystalline defects. The only way to diagnose the material in terms of its structure is shown in Fig. (2-9), since the sample is fixed and the angle of the source and the detector is changed, as long as the used x-ray is with single wavelength [96].

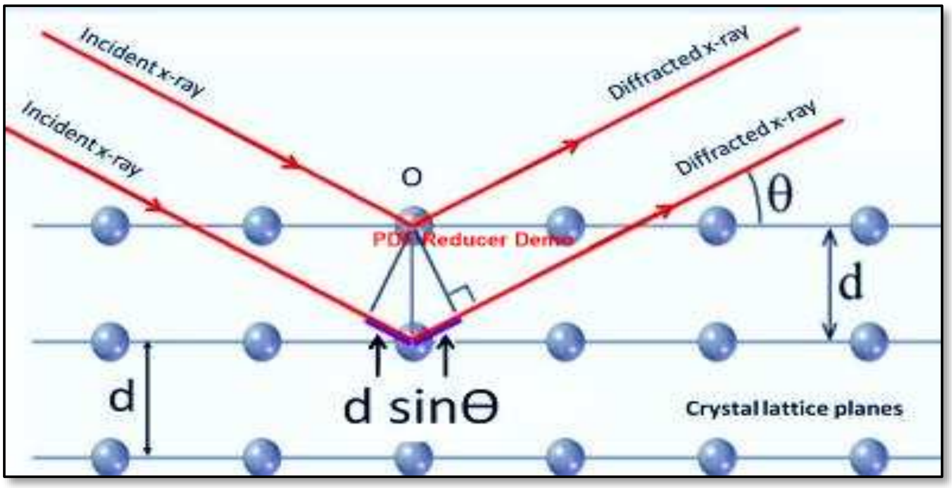

***Fig. (2-9)**: The Principle of X-ray diffraction* [97].

2.7.2. Indexing of XRD Patterns

The indexing is the process of determining of unit cell dimensions, (hkl) indices of each reflection and crystal symmetry. It is an essential step in the structure determination. Compared with single crystal data, whereas the problem can be easily solved, from the three-dimensional location of the nodes in the reciprocal lattice [98].

The mathematical method: in which we calculate the values of (2Θ), from the values of (Θ) resulting from X-ray diffraction pattern. Then ($sin^2\theta$) is calculated, and then all ($sin^2\theta$) values are divided by the lowest value of ($sin^2\theta$), then the division resultant for all values is multiplied by the number (2) and then by (3), and more until we get integer numbers. These integers represent the summation of squares of Miller indices (h^2+K^2+l^2) [99].

In general, programs especially intended for this purpose carry out the indexing of the diffraction patterns process; this is known as the auto-indexing. In order to get the lattice dimensions with more precisely, a refinement process should be carried out, using one of the available methods, including refinement based on the (Rietveld software analyzes) [100, 101].

2.7.3. Structural Parameters Calculation

The structural parameters of a material powder are considered an important issue for interpreting many physical properties of the material. The most important structural parameters that can be obtained from the XRD patterns are:

A. Lattice Constants

In the case of Hexagonal system, which is typical of ZnO, fig. (1-1a), where a, b, c, since, (a=b), Therefore, the lattice constants (a) and (c) can be calculated using the XRD pattern by the following formula of the hexagonal system [102]:

$$\frac{1}{d^2_{hkl}} = \frac{4}{3}\left(\frac{h^2 + hk + k^2}{a^2}\right) + \frac{l^2}{c^2} \qquad \text{... (2-3)}$$

Where, d_{hkl} : The d-spacing, (a, c): The lattice constants, and (hkl): are Miller indices [9].

B. X-ray Density (ρ)

The density of the material can be calculated from X-ray diffraction data using the following relationship [6]:

$$\rho_{x\text{-}ray} = \frac{Z\,M_{wt}}{V\,N_a} \qquad \text{... (2-4)}$$

Where:

$\rho_{x\text{-}ray}$: the density (g/cm^3), Z: number of molecules per unit cell which is (2) for hexagonal structure, M_{wt} : molecular mass (g/mol), V: the unit cell volume (cm^3) which is ($\boldsymbol{V = \frac{\sqrt{3}}{2}\,a^2.\,c}$) for hexagonal and N_A is Avogadro number (1/mol).

C. Crystallite Size (D)

The crystallite size can be calculated by two methods as follows:

First: - by using the Scherrer's formula, which given as [103]:

$$D = \frac{k\lambda}{\beta\cos\theta} \qquad \text{... (2-5)}$$

Where: (D) Is the crystallite size, λ : is the wavelength of used x-ray (1.504 Å), β: represents *(FWHM)* the full width at half maximum in radians, θ : is Bragg's angle and k : a constant with value approximately equal to (0.89) [104].

Second: - by using an equation of (Williamson – Hall), as taking into consideration the micro-strain of the grains, as follows [105]:

$$\beta * \cos\theta = \left[\frac{k\lambda}{D}\right] + 4\varepsilon * \sin\theta \qquad \text{... (2-6)}$$

Where, $\boldsymbol{\sin\theta}$: is the effect of the strain. Nevertheless, through the above equation (2-6) of (W-H), and to calculate the average crystallite size (D), a graph is drawn with ($4\varepsilon\, \sin\theta$) along the x-axis and ($\beta_{hkl}\, \cos\theta$) along the y-axis, for the prepared ZnO nanoparticles [106].

D. Specific Surface Area (SS.A)

The Specific surface area is a property of materials. It has a particular importance in case of reactions on surfaces, adsorption, and heterogeneous catalysis. The Specific area (SS.A) can be obtained from Sauter's formula [107]:

$$SS.A = \frac{6*10^3}{D_p * \rho} \qquad \text{... (2-7)}$$

Where: SS.A is the specific surface area, D_p is the particle size and ρ is the density of the synthesized material.

E. Texture Coefficient ($\mathbf{T_c}$)

The texture coefficient (T_C) represents the texture of a specific plane; deviation of a plane from unity reveals that this is the preferred direction of growth. The T_C (hkl) values should be greater than one, for the preferential orientation [108].

The quantitative information about the discriminatory crystal orientation can be obtained from the texture coefficient (T_c) relation, as follows [109]:

$$T_c(hkl) = \frac{I(hkl)/I_0\,(hkl)}{\frac{1}{n}\sum_n I(hkl)/I_0\,(hkl)} \qquad \text{... (2-8)}$$

Where, $T_c(hkl)$: represents the texture coefficient, $I(hkl)$: is the measured intensity of XRD, (n): is the number of peaks considered for diffraction, and $I_0\ (hkl)$: represents the standard intensity of the plane which is taken from (JCPDS) data. The numerator of the equation, which includes the multiplying of the number of considered peaks by the relative intensities, this magnitude is divided by the sum of the relative intensities of the same peaks [110].

F. Morphology Index (M.I)

Sharper XRD peaks are typically indicative of high nano crystalline nature and larger crystallite materials. The morphology index (M.I) is calculated from FWHM of XRD data. The (M.I) has direct relationship with crystallite size and specific surface area [111].

(M.I) is obtained by using the equation [112]:

$$M.I = \frac{FWHM_h}{FWHM_h + FWHM_p} \qquad \dots (2\text{-}9)$$

Where, (M.I): is the morphology index, ($FWHM_h$): is the highest FWHM value that obtained from peaks and ($FWHM_p$): is a particular peak's FWHM for which M.I. is to be calculated.

2.8. Optical Properties

For many reasons, studying the optical properties of the materials is an interesting. Firstly, using the materials for optical applications such as optical fibres, reflective coating and interference filters, requires an accurate diagnoses of their optical properties. Secondly, the optical properties of all materials may be regarded to their electronic band structure, electrical properties and the atomic structure [113, 114].

2.8.1. The Fundamental Absorption Edge

The absorption edge can be described as the rapid increase in the absorption, when the absorbed radiation energy is approximately equal to the energy gap; thus, the fundamental absorption edge represents the smallest difference in energy between the upper point of the valence band to the lower point of the conduction band [115].

2.8.2. Absorption Coefficient (α)

The absorption coefficient of the materials considered as a very strong function of the band gap energy and the photon energy. It can be described as the attenuation in the flux of radiation energy or the intensity per unit of area in the direction of the wave in the medium and depends on the incident photon energy, semiconductor properties and the type of the electronic transitions that occur between the energy bands. The absorption processes considered as the main cause for the attenuation in incident photon energy [116, 117]. Whereas, absorption coefficient is related to the absorbance by the following equation [118]:

$$\alpha = 2.303\left(\frac{A}{d}\right) \qquad \text{... (2-10)}$$

Where: α is absorption coefficient, A: the absorbance and d : the thickness of the sample.

For the analysis of solutions, there is what has called length of the path (L), according to (Beer's–Lambert) law, which states that the molar absorbance is fixed and that absorption is proportional to the concentration of a material dissolved in a specific solvent being measured at a given wavelength. Accordingly, for the solution, the absorption coefficient is called molar absorptivity, which is also known as the extinction coefficient, which is related to the absorbance by the following relationship [119]:

$$A = \xi \, C \, L \qquad \text{... (2-11)}$$

Where:

ξ: is the molar absorbance (extinction coefficient) $(\mathrm{M.cm})^{-1}$, C : the molar concentration, L : Length of the light path in centimetres 1(cm) the thickness of the quartz tube.

The following relation relates the absorption coefficient (α) and the extinction coefficient, as follow [120]:

$$\xi = \frac{\alpha \, \lambda}{4\pi} \qquad \text{... (2-12)}$$

Where λ : represents the wavelength of the incident radiation.

2.8.3. Electronic Transitions

The study of optical properties is one of the most important studies for determining the electronic transitions, which occur within the solid material; through this study, we can identify the energy gap (E_g) of the solid material that helps to use the material in many electronic applications [121].

Electronic transitions occur between the valence and conduction bands, as a result of the absorption of radiation, which split these transitions into direct and indirect [117].

Nevertheless, the following empirical equation described these transitions [122]:

$$\alpha h\nu = B(h\nu - E_g)^r \quad \text{... (2-13)}$$

Where, (α) : represents the absorption coefficient, $(h\nu)$: is the incident photon energy, *(B) :* a constant amount does not change with the photon energy, and directly related to the properties of the material and the transition probability. *(E_g)*: is the value of the optical energy gap and the exponent *(r)*: is a constant depending on the material and the type of the optical transition whether it is direct or indirect [123].

A. Direct Transitions

Occurs when both of the bottom of the conduction band and the top of valence band are at the same point in k-space and have the same wave vector value $(\Delta k = 0)$, and this is called (*Allowed direct Transition*), (r=1/2), as in Figure (2-10). In the case of transitions from adjacent sites to the highest point in the valence band to adjacent locations near the lowest point in the conduction band, with constant value of the wave vector $(\Delta k = 0)$, before and after the transition, this transition is called (*Forbidden direct Transition*), (r=2/3) [124].

B. Indirect Transitions

For indirect electronic transitions, the bottom of the conduction band and the top of valence band are at different regions of (k-space). This type of transition requires absorption or emission of phonons to conserve the momentum resulting from the change of the wave vector of the electron (Δk≠0). The exponent (r) in equation (2-14), may take as (r=2) for allowed indirect transition, and (r=3) for the forbidden indirect transition. Fig. (2-10) shows direct and in-direct transition [125].

For indirect transitions, the absorption coefficient can be obtained by the following equation [126]:

$$\alpha h\nu = B(h\nu - E_g \pm E_p)^r \qquad \text{... (2-14)}$$

Where, $\boldsymbol{E_p}$ **:** Phonon energy associated with emission or absorption (eV), (+) : phonon emission, (-) : Phonon absorption.

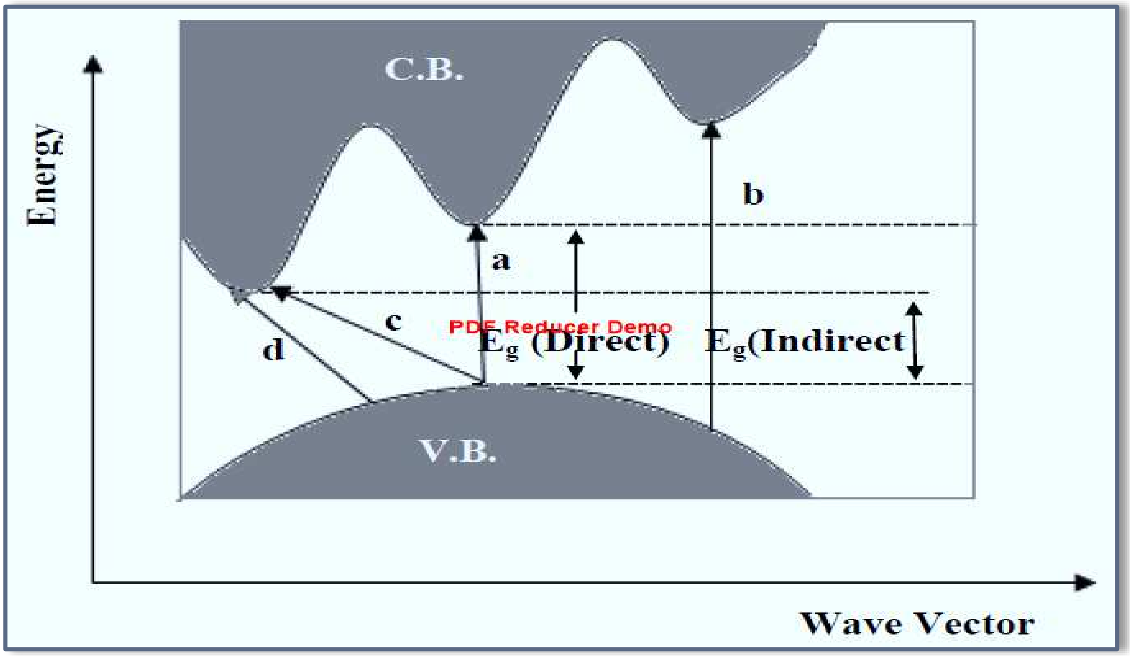

Fig. (2-10): *Electronic transitions: (a) allowed direct, (b) Forbidden direct, (c) allowed indirect and forbidden indirect* [127].

2.8.4. Optical Parameters

A. Transmittance (T)

Is the ratio between the intensity of the transmitted light (I_t) and the intensity of the incident light (I_o), and symbolized by the symbol (T), it is given by the following relation [128]:

$$T = \frac{I_t}{I_o} \qquad \text{... (2-15)}$$

Moreover, the transmittance depends on several factors including thickness of the material, temperature and doping process.

B. Absorbance (A)

The absorbance (A) or the optical density can be defined as the inverse logarithm of the transmittance (T), and it can be expressed as follows [129]:

$$A = log\ T = log\ \frac{1}{T} = log\ \frac{I_o}{I} \qquad \text{... (2-16)}$$

C. Reflectance (R)

Depending on the spectrums of transmittance (T) and the absorbance, (A), from relation (2-17) the reflectance (R) was calculated in accordance to the energy conservation law [130]:

$$R = 1 - T - A \qquad \text{... (2-17)}$$

D. Optical Band Gap (Eg)

The energy gap is defined as the lowest energy required for raising the electrons from the top of the valence band to the bottom of the conduction band, or the energy space between the valence and conduction bands. It has been called prohibited or forbidden, because it’s a place almost devoid of levels, where the electrons do not settle in, for pure semiconductor, but for doped semiconductor, the electrons are present for a very short time. This gap determines the type of solid material [131, 132]. It is one of the most important optical constants that are based on the physics of semiconductors, to manufacture many electronic devices such as solar cells, reagents, optical diodes and others. The selection of the semiconductor materials for manufacturing, based on the forbidden energy gap, which must be approximate to the energy of the photons within the visible UV and IR of the electromagnetic spectrum, in order to identify the amount of transmitted, absorbed or reflected photons affecting on the material under analysis [133].

The value of allowed band gap can be obtained from Tauc's plot, by extrapolation the straight part of resulting curve at the point $(\alpha h\nu)^2 = 0$, which is between values of $(h\nu)$ (eV) along the x-axis and $(\alpha h\nu)^2$ $(cm^{-1}\ eV)^2$ along the y-axis, where the intersection represents the optical energy gap of the material [134, 135].

From Tauc's relation [136]:

$$\alpha = \frac{B(h\nu - E_g^T)^r}{h\nu} \qquad \text{... (2-18)}$$

Where, E_g^T : Tauc's energy gap.

2.9. Electrical Properties

- **Electrical Properties of ZnO**

As a direct wide band gap semiconductor with a large exciton binding energy of (60 meV), ZnO is representing a great attraction for electronic and optoelectronic devices. For instance, a device that is made by a material with a larger band gap, may have a lower noise generation, high breakdown voltage, and can run at higher temperatures with high power operation. In semiconductors, the performance of electron transport is different at high and low electric field. When the electrical field is increased, the energy of the electrons of the applied electrical field is equivalent to the thermal energy of the electron [137, 138].

2.9.1. Dielectric Properties

- **Dielectric in Terms of Polarization and Electric Field**

The dielectric material consists of positive and negative charges. Ordinarily, the centre of negative charges is often applicable to the centre of the positive charges of these molecules. In the presence of an external electric field, positive and negative charges in dielectrics are displaced from their equilibrium positions to form local electric dipoles and the dielectric is said to be polarized. These molecules of the dielectric material are characterized with this, called as non-polar molecules. However, there are molecules of other dielectric materials, where the centre of the negative charge is permanently separated from the centre of the positive charge; these molecules have a permanent dipole moment and are called polar molecules, which have permanent momentums, but the directions of these momentums are random. Nevertheless, if placed under effecting of an alternating external electric field, it rotates these dipoles toward the applied electric field [139, 140].

When dielectric material is exposed to an electric field, the positive charges will be removed in the direction of the field and the negative charges will be moved in the opposite direction leading to form a distance (d) between these two different charges (q), as a result, an electric dipole moment (μ) is created. Accordingly, the electric polarization can be defined as the resultant of the electric dipole moment per unit volume, and is expressed by the following [6]:

$$p = I\ \mu \qquad \text{... (2-19)}$$

Where, I: number of dipoles per unit volume and (μ) is the electric dipole moment which is given as [6]:

$$\mu = qd \qquad \text{... (2-20)}$$

2.9.1.1. Dielectric Constant (ε') and Dielectric Loss (ε'')

The dielectric parameter as a function of the frequency is described by the complex permittivity [141]:

$$\mathcal{E}\ (\omega) = \varepsilon'(\omega) - \varepsilon''\ (\omega) \qquad \text{... (2-21)}$$

Here are the real part (Ɛ') and imaginary part (Ɛ"), which represent the components of the energy storage and loss, respectively, in each cycle of the electric field, and (ω) is the angular frequency (**$\omega = 2\pi f$**), f is applied frequency.

The dielectric constant (permittivity) is defined as the ratio of the permittivity of an electrical capacitor with two-pole insulation (ε) to the permittivity in the case of air presences (ε_{o}) rather than insulator between the poles. Moreover, the dielectric constant is used to classify the types of dielectrics [140].

Where:

$$\varepsilon' = \frac{\varepsilon}{\varepsilon_o} \qquad \text{... (2-22)}$$

Where, ε_o : the permittivity of vacuum equal to = 8.854×10^{-14}, measured by (F/cm), In addition, the ratio between the capacities (C) with existence of the dielectric material to its capacity in the vacuum (C_o) gives us the dielectric constant, which can be expressed utilizing the following relationship [137]:

$$\varepsilon' = \frac{C}{C_o} \qquad \text{... (2-23)}$$

The dielectric constant $\mathcal{E}(\boldsymbol{\omega})$, consists of real permittivity or relative dielectric constant which is generally called dielectric constant of the test material. Dielectric constant of the test material ($\boldsymbol{\varepsilon}'$) is calculated from the measurement of capacitance value, which can be obtained using the following equation [142]:

$$\varepsilon' = \frac{t * C_p}{A * \varepsilon_o} = \frac{t * C_p}{\pi\left(\frac{d}{2}\right)^2 * \varepsilon_o} \qquad \text{... (2-24)}$$

Where,

(t): is thickness of the pellet, C_p : equivalent parallel capacitance which obtained from the data of measurement, $\boldsymbol{\varepsilon_o}$: the permittivity of vacuum equal to = 8.854 x 10^{-14} (F/cm), A: area of the electrode and d: Diameter of guard electrodes.

Whereas, the imaginary permittivity or dielectric loss($\boldsymbol{\varepsilon}''$), is obtained from the value of dissipation factor (D). Where [143]:

$$tan\delta = D \qquad \text{... (2-25)}$$

In addition, dissipation factor (D) is relative and equals to:

$$D = \frac{\varepsilon''}{\varepsilon'} \qquad \text{... (2-26)}$$

The above equation can be written as:

$$\varepsilon'' = D * \varepsilon' \qquad \text{... (2-27)}$$

The energy losses are determined by (ε''). In the engineering applications of dielectrics in capacitors, smaller ε'' is always preferred for a given (ε'). The relative magnitude of ε'' with respect to ε' is defined as (tan δ), which called as the loss factor or dissipation factor (D).

The losses in dielectric materials are usually occurred due to the consumption current. The orientation of the molecules along the direction of an applied electric field in the polar dielectrics requires a part of the electric energy to overcome the forces of internal friction. Another part of the electric energy is specified for rotating of the dipolar molecules and other kinds of molecular transfer from one position to another, which also involve energy losses [144].

2.9.2. A.C conductivity ($\sigma_{a.c}$) and Resistivity ($\rho_{a.c}$)

Electrical conductivity gives a significant information of conduction mechanism of the dielectric materials. The electric conductivity of doped dielectric materials depends on various parameters, like doping mechanism, preparation methods, temperature and sintering conditions and time [145].

The alternating conductivity of dielectric is a scale of the heat generated by the rotation of the dipoles in their positions and depends on the frequency value and given as follow [139, 146]:

$$\sigma_{a.c} = 2\pi f\ \varepsilon_o\ \varepsilon'\ \ \tan\delta \qquad \textbf{...}\ (2\text{-}28)$$

At low frequencies, two components consist [139]:

$$\sigma = \sigma_{a.c} + \sigma_{d.c} \qquad \textbf{...}\ (2\text{-}29)$$

Where, $\sigma_{a.c}$: Electrical conductivity of alternative current is measured by $(\Omega.\text{cm})^{-1}$, ($\sigma_{d.c}$) conductivity of direct current and does not change with frequency, (f) is the measuring frequency of the applied ac electric field (Hz) and (tan δ) is the dissipation factor which describes the difference in phase between current and voltage with respect to the applied ac electric field [146].

One of the most important features of semiconductor that it has a negative thermal coefficient, this leads to increase electrical conductivity of the semiconductor with increasing temperature due to the collapse of the bonds and the transfer of electrons from the valence band to the conduction band, these features have made semiconductor very useful in many electronic applications [147].

Moreover, Specific resistance can also be written as an inverse of the a.c conductivity [147]:

$$\rho_{a.c} = \frac{1}{\sigma_{a.c}} \qquad \textbf{...}\ (2\text{-}30)$$

The length of the sample associated with resistivity according to the following relation [148]:

$$\rho_{d.c} = \frac{RA'}{l} \qquad \text{... (2-31)}$$

Where, (ρ): the electrical resistivity or specific resistance (Ω.cm), (R) : the Ohmic resistance (Ω), (A′) : represents a cross-sectional area of the sample (cm^2) and (l) : the length of the sample (cm).

Chapter Three

Experimental work

3.1. Introduction

This chapter includes raw materials and devices that were used in the preparation process, and it includes the method of preparation and the forms of prepared samples, and there are tables of chemical quantities that have been utilized to prepare the nanomaterial samples, as well as, a general description of devices that were used.

3.2. Starting materials

According to the research project required for the synthesis of un-doped and (Mg, Cr) doped ZnO using sol-gel auto combustion technique, the following chemicals have been selected, as shown in the table (3-1).

Table. (3-1): *Raw materials*

Materials	***Chemical Formula***	***Molar Mass g/mol***	***Purity %***	***Country Product & Company***
Citric acid	$C_6H_8O_7.H_2O$	*210*	*99 %*	*Spain* *Panreca*
Zinc nitrate	$Zn\ (NO_3)_2.6H_2O$	*297.39*	*99 %*	*India* *HIMEDIA*
Magnesium nitrate	$Mg\ (NO_3)_2.6H_2O$	*226.305*	*99 %*	*Germany* *Riedel*
Chromium nitrate	$Cr\ (NO_3)_3.9H_2O$	*399.996*	*99 %*	*Germany* *Merck*
Ammonia solution	NH_3	*17*	*99 %*	*India* *Loba Chemie*

3.3. Tools and Equipment

Some devices were used in the preparation of zinc oxide, which are

i. Sensitive electronic balance

It is one of the essential devices used in the laboratory to measure masses of the raw materials used in the preparation process, and it has a digital counter gives the result directly and has a high ability to determine the masses accurately with four digits, which have been used to reduce measurements errors. The used device brand is (KERN), as is shown in Figure (3-1).

***Fig. (3-1)**: The electronic balance*

ii. Magnetic Stirrer

It is a device used for mixing the chemical solutions. It essentially consists of a rotor magnet by magnet or another magnetic field unconnected with it, and it is often provided with thermal plates or other means for heating the mixture. Usually, one of the two permanent magnets is connected to an electric motor, while the other magnetic bar is immersed in the liquid mixture. When the lower magnet rotates, the immersed magnetic bar is affected by that rotation and trying to spin in the same direction of the magnet orbit without any mechanical contact. This type of mixers is very important in the chemical laboratories and places that require a complete isolation between the mechanical parts in order to avoid friction, corrosion and leak of liquid through the rotation axes. The used device brand is (FALC), as shown in figure (3-2).

Fig. (3-2): *The Magnetic Stirrer*

iii. High-Temperature Furnace

It is an electrical device with a thermal insulator controlled by a temperature thermostat, and it is used for drying, heating, sintering and calcining processes, the used device brand is (Schneider) Korean Origin, as shown in fig. (3-3).

Fig. (3-3): *The Laboratory Furnace*

iv. pH Indicator Paper

It used to measure the degree of acidity or basicity for a particular liquid. This is done by immersing a piece of paper in the solution, the resulting colour is compared to the paper catalogue, this process is repeated until reaching degree (7), which is considered to be neutral, as shown in fig. (3-4).

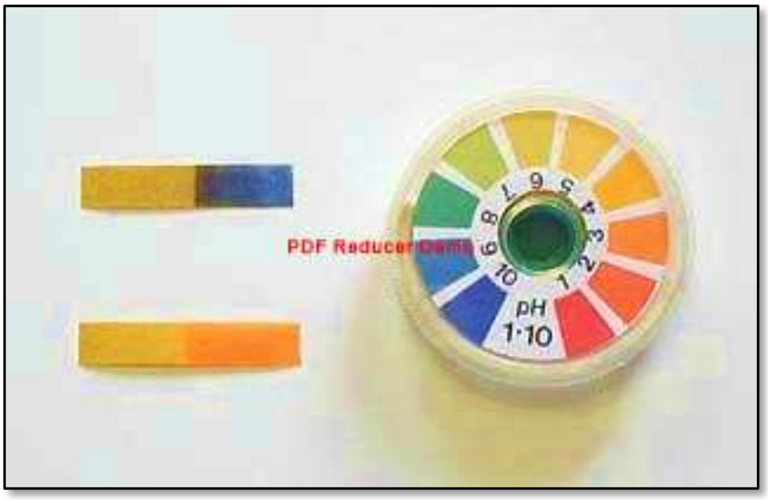

Fig. (3-4)*: pH Indicator Paper*

3.4. Preparation of Un-Doped Zinc Oxide Nanoparticles

Pure zinc oxide has been prepared by the sol-gel method, the procedures and steps of preparation ZnO, can be clarified as follows:

First :- Mass calculation

Masses have been calculated using the molecular formula of the constituent elements of the compound, As follows:

1. Hexahydrate zinc nitrate **$Zn\ (NO_3)_2.6H_2O$**

65.39+ 2(14+3*16) + 6(2*1+16) = 297.39 g

2. Citric acid **$C_6H_8O_7.H_2O$**

(6*12) + (8*1) + (7*16) + (2*1+16) = 210 g

Second:- Molarity calculation

Molarity is the number of the dissolved moles in a litre of solution, and measure with units of mol/Liter, according to the following relationship:

$$M=\frac{n}{V} \qquad \text{... (3-1)}$$

Where: **V:** volume, measured by units of liter, **n:** the number of moles and it is the ratio between the solute mass to the molecular weight of the solvent, measured by units of mol, and:

$$n=\frac{W_t}{M_{wt}} \qquad \text{... (3-2)}$$

By substituting equation no. (2-3) in the equation of no. (1-3), we get:

$$M=\frac{W_t}{M_{wt}*V} \qquad \text{... (3-3)}$$

Third :- Preparation Method

To prepare ZnO nanoparticles by colloidal solution (sol-gel) method of auto-combustion, the following steps have been implemented:

1- (40g) of zinc nitrate ($Zn\ (NO_3)_2.6H_2O$) were dissolved in (30 ml) of distilled water with a molar concentration of (1M), which is calculated from equation (3-3).

2- (14.12g) of citric acid ($C_6H_8O_7.H_2O$) were dissolved in (30 ml) of distilled water with a molar concentration of (0.5 M), which is calculated from equation (3-3).

3- The two solutions were mixed in a heat-resistant beaker by a magnetic stirrer for (40 min) at room temperature, to ensure the full homogeneity of the solution.

4- Acidic function pH has been modified by (pH) indicator paper until reaching approximately to the degree (7) by adding ammonia solution drop by drop.

5- Then, the temperature was gradually raised and stabilized at 85^0C. After a duration of time, gases began to evaporate, after this the interaction left for a period with continuation stirring until the viscous gel form consists.

6- 50 minutes later, the gel began ignition to form a dry gel, then the heat source has been turned off and the material left to be cooled, and then collected. After that milled well by a mortar of ceramic to ensure powder homogeneous and to get rid of the conglomerates that have taken place during the preparation process.

7- The resulting powder is put in a vessel of porcelain characterized with high temperature resistant, and entered into the oven for calcining at (600 ^{o}C) for two hours, thus the preparation process of zinc oxide nanoparticles ZnO ends, which is a white powder as shown in figure (3-5).

Fig. (3-5): *The prepared ZnO nanoparticles*

The interaction equation for the sample (P1) can be written as follows [67]:

$$Zn\,(NO_3)_2.6H_2O + C_6H_8O_7.H_2O + NH_3 \longrightarrow ZnO + 1.5\,N_2 + 6CO_2 + 5.5H_2 + 7H_2O$$

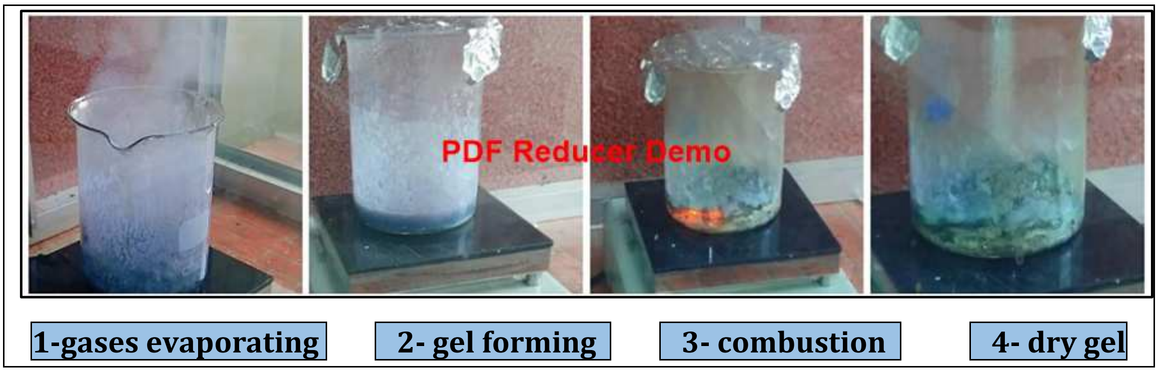

Fig. (3-6): *Steps of preparation samples of the group (P)*

The following fig. (3-7) shows steps of the preparation method:

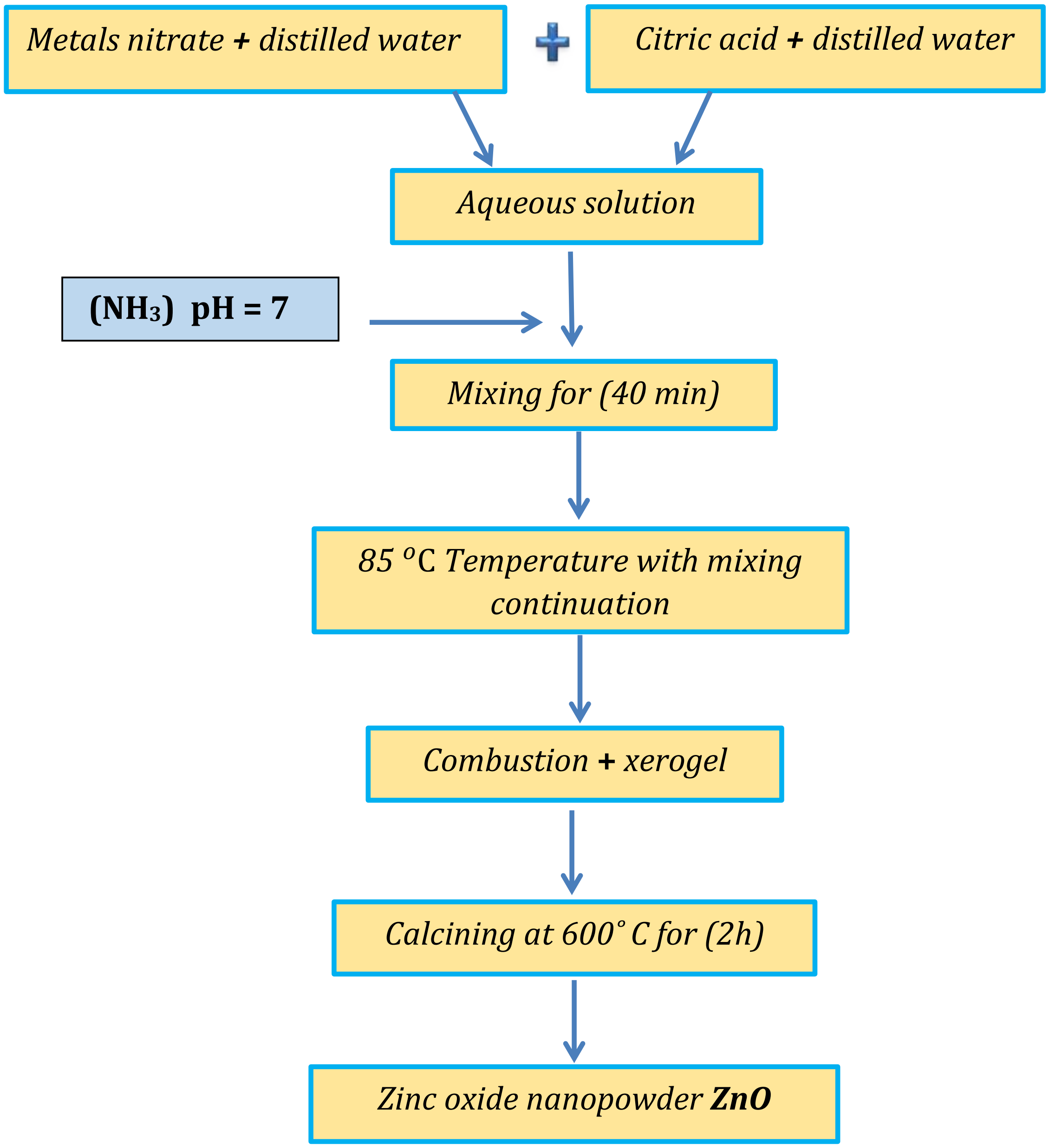

Fig. (3-7)*: Steps of the colloidal solution of auto Combustion method*

The entire experimental procedure of sol-gel combustion technique can be achieved in most of the literature studies, which are included in this study.

3.5. Preparation the Compound ($Mg_xZn_{1-x}O$) By Sol-Gel Method with X Value Equal to (x = 0.05)

The compound ($Mg_{0.05}Zn_{0.95}O$) have been prepared by sol-gel method, in addition, the effect of magnesium ion Mg^{2+} on the zinc oxide was studied. The preparation steps are as follows:

First :- Mass calculation

The molecular weight of the reactants materials in the interaction had been calculated as previously mentioned, in addition to the magnesium nitrate:

Hexahydrate magnesium nitrate **$Mg(NO_3)_2.6H_2O$**

$24.305 + 2(14+3*16) + 6(2*1+16) = 226.305$ g

Second:- Calculation the reactants compounds ratios

The quantities of reactants materials in the interaction can be calculated from the structural formula and molecular weight of the constituent elements of the compound ($Mg_xZn_{1-x}O$). Molecular ratios formula has been used, that depends on the total mass, the weights summation of the salts involved in the reaction and the value of (x= 0.05), according to the following equation:

$$(0.95)\,Zn(NO_3)_2.6H_2O + (0.05)\,Mg(NO_3)_2.6H_2O + C_6H_8O_7.H_2O + NH_3$$

$$\longrightarrow Mg_{0.05}Zn_{0.95}O + 1.5N_2 + 6CO_2 + 5.5H_2 + 7H_2O$$

When the number of moles n =1, the weight will be equal to the molecular weight, by using the method of molecular weight ratio to calculate the mass of reactants materials to prepare doped zinc oxide by magnesium and chromium.

To prepare (40 g) of the compound ($Mg_xZn_{1-x}O$) at the value of (x = 0.05), according to the following relationships:

$$\textit{Quantity to be prepare} = \left[\frac{\textit{Molecular Weight of metal Nitrate} * \textit{total mass}}{\textit{The total molecular weights of all compound salts}}\right]$$

(1-x) * Molecular weight of zinc nitrate = (1-0.05)* 297.39 = 282.5205 g

x * Molecular weight of magnesium nitrate =0.05* 226.305 = 11.3152 g

---

Total molecular weight = 293.835 g

1- Quantity of zinc nitrate Zn $(NO_3)_2.6H_2O$

$$\frac{(1-0.05)*(297.39)*40}{293.835} = 38.4597 \text{ g}$$

2- Quantity of magnesium nitrate Mg $(NO_3)_2.6H_2O$

$$\frac{(0.05)*226.305*40}{293.835} = 1.5403 \text{ g}$$

Third :- Preparation Method

By using the same previous method of preparation and by adding magnesium nitrate Mg $(NO_3)_2.6H_2O$, the compound $(Mg_{0.05}Zn_{0.95}O)$ was obtained, and the table (3-2) shows the quantities of used materials.

Table. (3-2): *The amounts of materials used to prepare the compound* $(Mg_{0.05}Zn_{0.95}O)$

Sample	*X*	*Mass of Zn nitrate (g)*	*Mass of Mg nitrate (g)*	*Total mass nitrate (g)*	*Volume of distilled water (mL)*	*Mass of Citric Acid (g)*	*Volume of distilled water (mL)*
P2	*0.05*	*38.4597*	*1.5403*	*40*	*30*	*14.1222*	*30*

At the end of preparation steps, the nanoparticles powder of the compound $(Mg_{0.05}Zn_{0.95}O)$ was obtained, as shown in figure (3-8).

Fig. (3-8): *The powder of the compound* $(Mg_{0.05}Zn_{0.95}O)$

3.6. Preparation the Compound ($Cr_xZn_{1-x}O$) by Sol-Gel Method with X Value Equal to (X = 0.05)

The compound ($Cr_{0.05}Zn_{0.95}O$) has been prepared by the same previous method that was used to prepare the compound ($Mg_{0.05}Zn_{0.95}O$), fig. (3-9), and the table (3-3) shows the quantities of the materials that are used in the preparation process, according to the following equation:

$$(0.95)\ Zn\ (NO_3)_2.6H_2O + (0.05)\ Cr(NO_3)_3.9H_2O + C_6H_8O_7.H_2O + NH_3 \longrightarrow$$
$$Cr_{0.05}\ Zn_{0.95}\ O + 1.525N_2 + 6CO_2 + 5.2H_2 + 7.3H_2O$$

Table. (3-3): *Amounts of materials used to prepare the compound ($Cr_{0.05}Zn_{0.95}O$)*

Sample	X	Mass of Zn nitrate (g)	Mass of Cr nitrate (g)	Total mass nitrate (g)	Volume of distilled water mL	Mass of Citric Acid (g)	Volume of distilled water mL
P3	0.05	37.335	2.6444	40	30	14.1222	30

Fig. (3-9): *The powder aspect of the compound ($Cr_{0.05}Zn_{0.95}O$)*

3.7. Preparation the Compound ($Mg_xCr_yZn_{1-x-y}O$) By Sol-Gel Method for Values of (x+y) According To ($0\leq x+y \leq 0.25$)

Seven samples of doped zinc oxide with Mg and Cr have been prepared by the sol-gel method with various values of (x+y), these values have been classified into two groups, as shown in table (4-3).

Table. (3-4): *Concentrations of (x) and (y) of the Compound ($MgxCryZn1-x-yO$)*

Samples Codes	*(x)*	*(y)*	*Compound ($Mg_xCr_yZn_{1-x-y}O$)*
M1	*0.05*	*0.05*	($Mg_{0.05}Cr_{0.05}Zn_{0.9}O$)
M2	*0.05*	*0.10*	($Mg_{0.05}Cr_{0.1}Zn_{0.85}O$)
M3	*0.05*	*0.15*	($Mg_{0.05}Cr_{0.15}Zn_{0.8}O$)
M4	*0.05*	*0.20*	($Mg_{0.05}Cr_{0.2}Zn_{0.75}O$)
C1	*0.10*	*0.05*	($Mg_{0.1}Cr_{0.05}Zn_{0.85}O$)
C2	*0.15*	*0.05*	($Mg_{0.15}Cr_{0.05}Zn_{0.8}O$)
C3	*0.20*	*0.05*	($Mg_{0.2}Cr_{0.05}Zn_{0.75}O$)

Molar concentrations of these compounds have been calculated by using the special formula, and the following steps was implemented:

First :- Mass calculation

In addition to zinc nitrate and magnesium nitrate and for the same molecular weights, chromium nitrate was added to prepare of the samples of the compound ($Mg_xCr_yZn_{1-x-y}O$) doped with both Mg and Cr, and as follows:

1. Aqueous chromium nitrate **$Cr(NO_3)_39H_2O$**

51.996+3(14+3*16)+9(2*1+16) = 399.996 g

2. Citric acid **$C_6H_8O_7.H_2O$**

(6*12) + (8*1) + (7*16) + (2*1+16) = 210 g

To prepare (40g) of the compound ($Mg_xCr_yZn_{1-x-y}O$), the special formula was used to calculate the masses, while the percentage of citric acid; was constant in every interaction, according to the following equation of sample (M1) with x = 0.05 and y = 0.05:

$$0.9\ Zn\ (NO_3)_2.6H_2O + 0.05\ Mg\ (NO_3)_2.6H_2O + 0.05\ Cr(NO_3)_39H_2O + C_6H_8O_7.H_2O + NH_3 \longrightarrow Mg_{0.05}Cr_{0.05}Zn_{0.9}O + 1.525N_2 + 6CO_2 + 5.35H_2 + 7.3H_2O$$

In addition, the following table (3-5) shows the amounts of the materials used to prepare the compound ($Mg_xCr_yZn_{1-x-y}O$) with various values of x and y, as follows:

Table (3-5): *The amounts of materials used to prepare samples of the compound ($Mg_xCr_yZn_{1-x-y}O$)*

Samples	*Mass of Zn nitrate (g)*	*Mass of Mg nitrate (g)*	*Mass of Cr nitrate (g)*	*Total mass nitrate (g)*	*Volume of distilled water (mL)*	*Mass of Citric Acid (g)*	*Volume of distilled water (mL)*
M1	*35.8102*	*1.5139*	*2.6755*	*40*	*30*	*14.1222*	*30*
M2	*33.2501*	*1.4883*	*5.2614*	*40*	*30*	*14.1222*	*30*
M3	*30.7751*	*1.4636*	*7.7612*	*40*	*30*	*14.1222*	*30*
M4	*28.3807*	*1.4397*	*10.1794*	*40*	*30*	*14.1222*	*30*
C1	*34.2276*	*3.0642*	*2.7080*	*40*	*30*	*14.1222*	*30*
C2	*32.6625*	*4.6532*	*2.7410*	*40*	*30*	*14.1222*	*30*
C3	*30.9455*	*6.2796*	*2.7748*	*40*	*30*	*14.1222*	*30*

These samples have been prepared by the same previous method in preparation the samples (P1, P2, and P3). In addition, the figures (3-10a), (3-10b) and figures (3-11a), (3-11b) represent the preparation steps and aspects of the samples of the compound ($Mg_xCr_yZn_{1-x-y}O$) respectively.

***Fig. (3-10a)**: The preparation steps of samples of the group (M)*

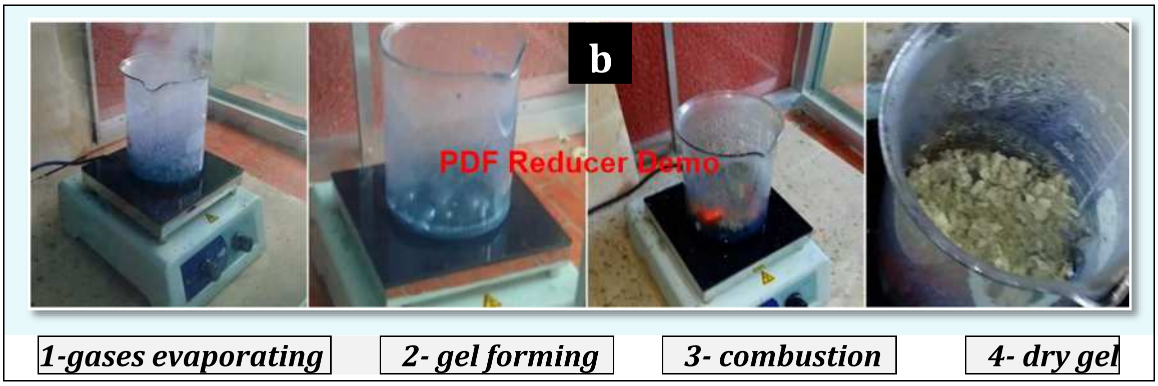

***Fig. (3-10b)**: The preparation steps of samples of the group (C)*

***Fig. (3-11a)**: The Samples (M1, M2, M3 and M4) and **(3-11b)** samples (C1, C2 and C3)*

3.8. Powder Compaction

The obtained powders were pressed in form of pellets, and these pellets are especially intended for electrical properties. The process of moulding is carried out by a hydraulic press with force pressing up to (15 ton), by using the dry pressing method. For each sample, (2.5 g) amount has been prepared, and pressed with (5 ton) of pressure by a hydraulic press in form of pellets with a diameter (1.5 cm), while remaining under pressure for (2 min) by using homemade molds of stainless steel material corrosion resistant. Figure (3-12) shows the components of used mould.

***Fig. (3-12)**: The mold used for forming samples in form of pellets*

3.9. Sintering Process

It is described as the thermal treatment that carried out as soon as the pressing process finished, by placing the pellets in the electric furnace at a temperature (1100 °C) for (3 h), then, samples were left in the furnace to be cooled gradually until reaching room temperature. The purpose of the sintering process is to convert the model from brittle to strong and coherent. The selection of this temperature degree, for being an appropriate degree, in order to be zinc oxide ZnO as a binder phase for other materials, as it has the lowest melting point comparable with magnesium oxide MgO and chromium oxide (III) Cr_2O_3 which are considered as high melting points materials.

3.10. Structural and Morphological Measurements

3.10.1. X-ray Diffraction Measurements

The type of device used in X-ray diffraction is (Shimadzu XRD – 6000), which exists in the central service laboratory in the College of Education for Pure Sciences (Ibn Al-Haitham), with the following specifications of wavelength = 0.15405 nm for copper target Cu - $K\alpha_1$, scanning step (5^0 / min), the current = 30 mA and voltage (40 kV). Figure (3-13) shows the used device.

The device has diagnosed the X-ray diffraction pattern within the angular range ($2\theta = 20^\circ - 80^\circ$) and indicated the nature of the crystalline structures of prepared powders. This test gives information within a specific table showing the diffraction angle, the inter-planner spacing, full width at half maximum (FWHM) of the peak and the relative intensities of each peak. (PCPDFWIN) program has been used for comparing the resulting diffraction patterens and crystalline structures in addition to (Full prof) program that was used for refining the crystalline diffraction data and identifying the lattice constants. Through this measurement, it became possible to do many structural calculations in our study.

Fig. (3-13): *The (Shimadzu XRD – 6000) device*

3.10.2. Scanning Electron Microscope (SEM) Measurements

SEM technique is one of the most widely used techniques in the characterization of Nanomaterials. SEM is an important instrument to get information about morphology, topography, composition and microstructural information of materials. It is suitable for studies that interact with external air and affected by temperature. The electronic microscope has a magnification ability higher than the optical microscope, where the resulting image has a high resolution, which is white & black colours.

The surface of the sample to be examined is scanned with an electron beam, the reflected or back-scattered beam of the electrons is collected, then displayed at the same scanning rate on the cathode ray tube (comparable to the T.V screen). The resulting image on the screen, which may be photographed, represents the surface feature of the sample. The surface of the specimen that may or may not is polished and drilled, but it must be electrically conductive; a very thin metallic surface coating, that must be applied for nonconductive materials [149].

For imaging samples in the nano scale, and because of the magnification capacity of (SEM) device is limited, so that SEM images have been processed by (Image – j) software program, which works on the automatic selection to identify the diameter of the particle from atoms area [150]. In our current study, a microscope of the type (Inspect S 50) was used, as shown in figure (3-14).

Fig. (3-14): *SEM device*

3.10.3. Energy Dispersive X-ray Spectroscopy (EDX)

It is an analytical technique used to recognize the chemical elements that exist in the sample. The principle of this technique that is the produced x-ray by the mutual influence of charged particles such as a band of electrons within the sample material, and then the structure can be identified by the emitted photons. In other words, since each element has a distinctive atomic structure, so that they possess a set of characteristic peaks in the X-ray spectrum [151].

Moreover, to obtain x-ray, when accelerated electrons fall on atoms of the target material, these electrons capture one of the atoms electrons from the internal orbits of the target and causing ionization state, or an electron may rise to a higher energy orbit and that will cause excitation state, in both cases the atom tries to reach stability. When an electron moves from a higher energy orbit to a lower energy orbit, the relocated electron emitting photon with energy equal to the energy difference between the atomic orbits, and this difference in the energy is a distinctive characteristic of each chemical element. There are a number of allowed transitions between the atomic orbits symbolized as (K_α, K_β, and L_α) [152]. The components of a modern digital EDX system are shown in fig. (3-15).

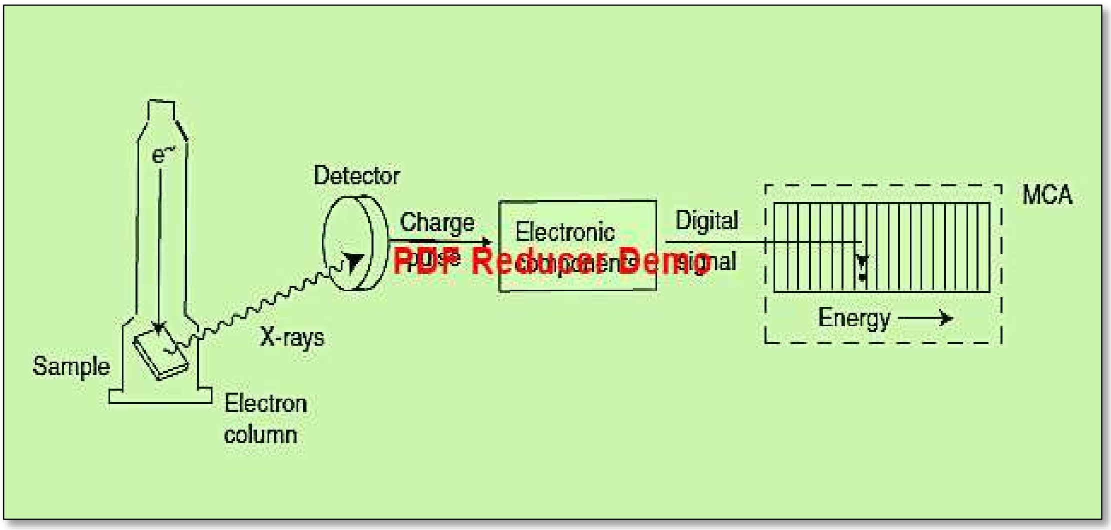

***Fig. (3-15)**: The components of a modern digital EDX system. Where, (MCA) is multichannel analyzer* [153].

3.11. Optical Measurements

3.11.1. UV- visible spectroscopy

Includes measurement of the absorbance for wavelength ranging between (300 - 900) nm, through a double beam by using (UV-Visible 1800) Spectrophotometer (Shimadzu), as shown in figure (3-16). Due to the lack of a device that can measure the absorption of the powder, so that, a solution containing the powder with molar concentration (0.01M) was prepared, where the solution is placed in tubes of quartz with a diameter of (10 mm), shown figure (3-17). Then the tubes are placed in the ultrasonic device to homogenize and spread well. At the end, the tubes were put in the UV- visible device to measure the Absorption. The molarity was calculated by modifying equation (3-3), as follows:

$$M = \frac{W_t}{M_{wt} * \frac{V}{1000}} \qquad \text{... (3-3)}$$

Where:

M: molar concentration (mol/L),

W_t: Weight (g),

M_{wt}: Molecular weight (g/mol),

V: Volume of distilled water in (mL).

To compute the quantities of samples prepared to measure the absorbance, a suspension solution consisting of distilled water and powders of prepared materials has been prepared, where the volume of distilled water was (10 ml) with (0.01M) of molar concentration, as shown in the table (3-6).

Table. (3-6): *Amounts of powder added to distilled water*

Sample	*Molecular Weight (g/mol)*	*Mass (g)*
P1	*81.39*	*0.008139*
P2	*79.33575*	*0.007933*
P3	*84.9201*	*0.00849*
M1	*82.8658*	*0.008286*
M2	*86.3959*	*0.008639*
M3	*89.9261*	*0.00899*
M4	*93.4561*	*0.009345*
C1	*80.8116*	*0.00808*
C2	*78.7573*	*0.007875*
C3	*76.7031*	*0.00767*

Fig. (3-16): *UV- visible spectrometer*

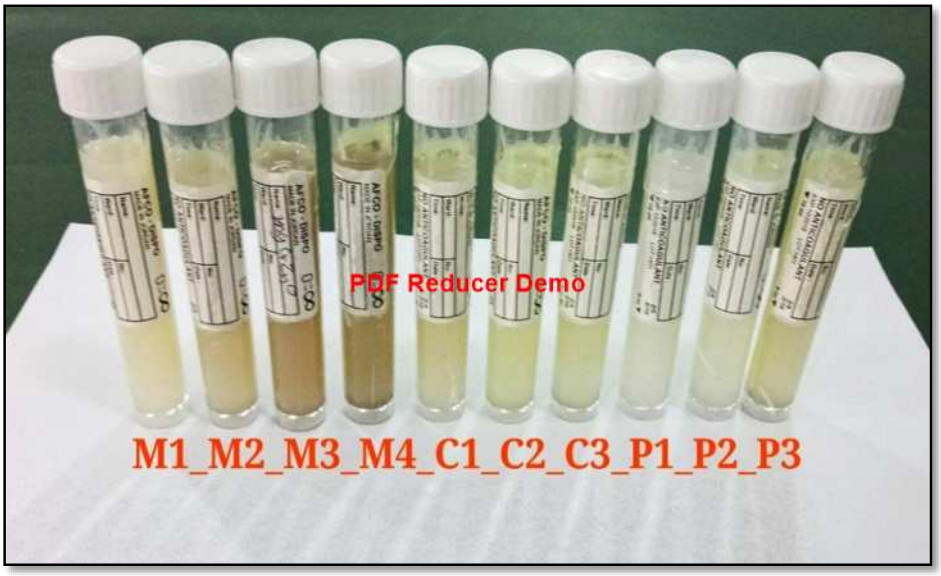

Fig. (3-17): *Samples prepared for UV-visible test*

3.12. Electrical Properties Measurement

After compacted the prepared nanopowders in form of pellets, as shown in figure (3-18). These pellets were connected with connectors of (LCR meter) device used to measure electrical properties. LCR meters are used to measure the inductance, capacitance, and resistance of components. The type of the device is Gwinstek, LRC-8105G (20 Hz-5 MHz) (GPIB, RS-232, Taiwan) as shown in figure (3-19). The device is connected to an electronic screen of a computer, which shows the results directly on the screen. This device can measure the capacitance Cp, and the tangent of loss angle (tan δ) as a function of frequency within the range (50 Hz-3MHz). In addition, the a.c. conductivity was measured at different temperatures, to identify the effect of the temperature variation on the a.c. conductivity.

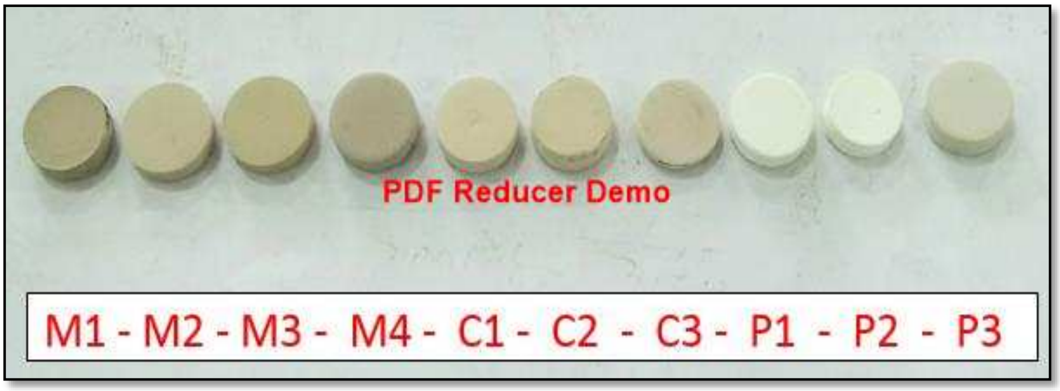

Fig. (3-18): *Samples prepared for electrical tests*

Fig. (3-19): *LCR meter device*

Chapter Four

Results and Discussion

4.1. Introduction

This chapter includes an overview of the results of measurements that were carried out, and the study of the structural, optical and electrical characteristics of pure and doped zinc oxide nanoparticles, as well as discussion of those results obtained from measurements of (XRD), (EDX), (SEM), (UV-visible), and (LCR-meter) devices, and comparing these results with the results of published studies and previous researches.

4.2. Structural Studies

The structural characteristics of pure and doped ZnO, have been studied for diagnosis their nature and types using X-ray diffraction of type (Shimadzu XRD- 6000), where it was found to have a hexagonal structure.

The crystal structure and of prepared pure ZnO and different composition of (Mg, Cr) doped ZnO nanoparticles calcined at (600 °C) were characterized using X-ray diffraction. Figure (4-1), shows a typical XRD patterns of pure ZnO and $Mg_xCr_yZn_{1-x-y}O$ nano-particles. The XRD patterns revealed that the diffraction peaks of undoped and (Mg, Cr) doped ZnO nanoparticles, can be indexed to hexagonal (wurtzite) structure. From the diffraction patterns of all prepared samples, strongest four clear peaks of zinc oxide were observed, within the angular range of the X-ray diffraction (20^o - 80^o), ascribed to the crystalline surfaces (101), (100), (002) and (110), and the preferred orientation was at the surface (101), which is in good agreement with the standard (JCPDS) file for ZnO, (JCPDS36-1451, a = 0.3279 nm, c = 0.5204 nm), with space group of P63mc. It is suggested that the wurtzite structure is the same, with all different doping concentrations. A slightly shifted was observed in the peaks in the diffraction pattern of doped samples, as compared to un-doped ZnO. The nanoparticles exhibited changes in relative intensities and crystallite size with changing the doping concentrations. The intensity of ZnO peaks, especially at the clear peak (101), increases with increasing magnesium amount and decreases with increasing chromium amount, Fig. (4-1), this indicates that phase segregation has occurred, and such structural degradation in the ZnO lattice may be attributed to the introduction of a foreign impurity [154].

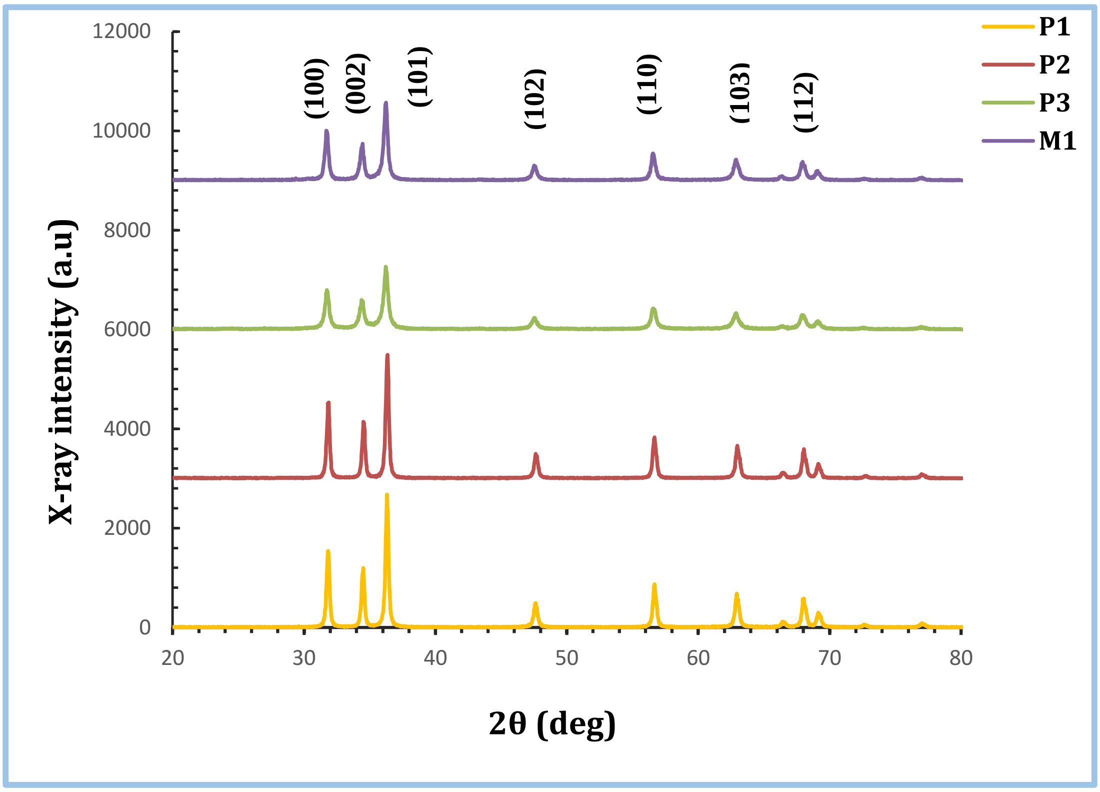

Fig. (4-1a): *The XRD patterens of the prepared samples (P1, P2, P3 and M1), where the patterens of samples P1 and M1 were used for comparing with other samples.*

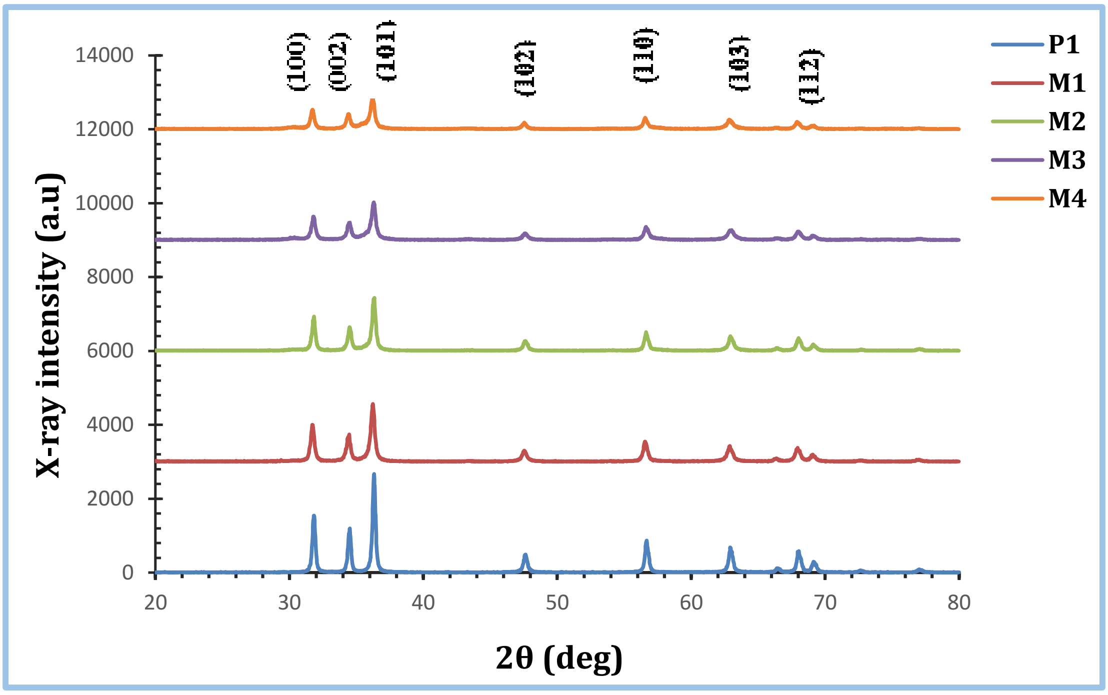

Fig. (4-1b): *The XRD patterens of the prepared samples (P1, M1, M2, M3 and M4).*

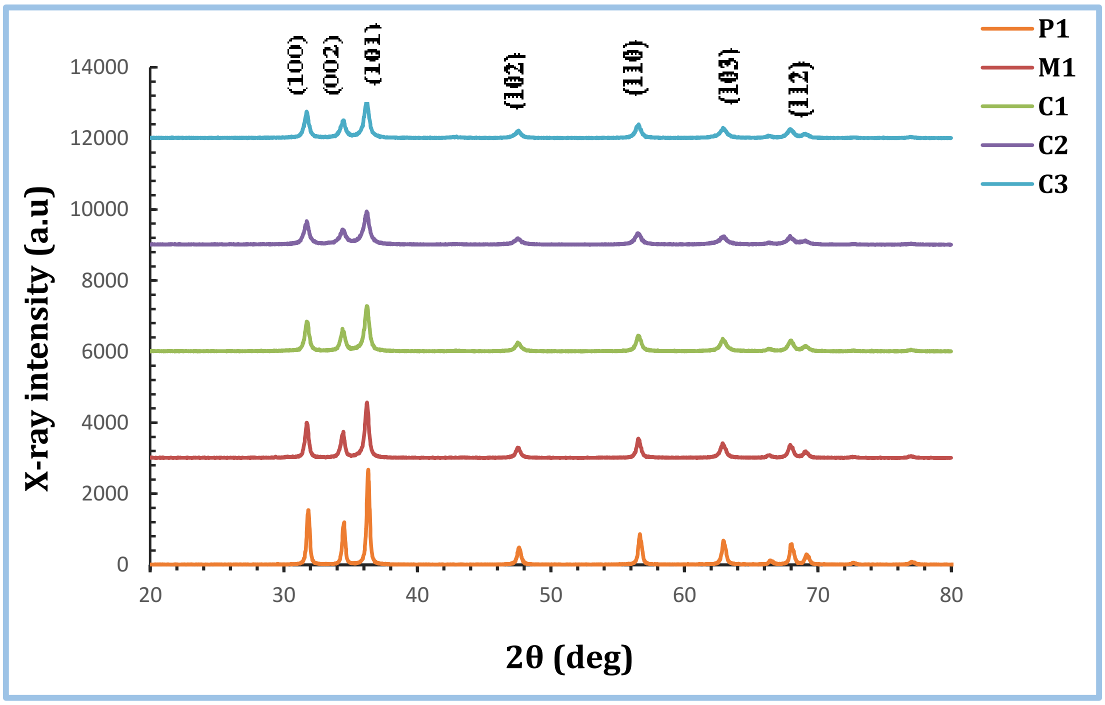

Fig. (4-1c): *The XRD patterens of the prepared samples (P1, M1, C1, C2 and C3).*

4.2.1. Crystal Structure: Indexing and Refinement

The above-mentioned diffraction patterns were automatically indexed to obtain the Miller indices and the lattice constants for each sample by using the following program (FULLPROF; 2015 ver. 3.00). As well as, the refinement of the crystal structure was done using (win PLOTR) program, annexed to the (FULLPROF) program. Nevertheless, the results of lattice constants, unit cell volume and crystalline system are listed in table (4-1).

The qualitative analysis of the phase of prepared samples was done using Reitveld method. The density of all the samples using x-ray data was calculated according to the relation (2-4), the results of the calculated x-ray density for each sample are presented in table (4-1).

From the table (4-1), we note a small variation in the lattice constants, occurs as the concentrations doping increases. Where, the lattice constants decrease as Cr concentration increased, such a decreasing of lattice parameters is clear, as the ionic radii of (Cr) ion is smaller than Zn [155]. Nevertheless, with increasing Mg concentration the lattice constants stay almost same because both Mg and Zn have very similar ionic radii (0.57 Å) and (0.60 Å), this can be interpreted that the Mg ions are successfully substituted in Zn ions [38]. With regard to density calculated from the XRD data, it is matched well with the reported data for the undoped ZnO; for doped samples, an obvious increasing was observed as the doping concentration increased with both (Mg, Cr) dopants. The unit cell volume was also noted to decrease with increasing the dopants contents; this indicates that (Cr, Mg) ions go to Zn site in ZnO lattice structure [156].

Table (4-1): *The crystalline system, lattice constants, density and the unit cell volume of the prepared samples*

Sample code	***Space group***	***crystalline system***	***lattice constants (Å)***		***Unit Cell Vol. (Å)^3***	***ρ x-ray (g/cm^3)***
			a = b	***c***		
P1	P63mc	Hexagonal	3.247	5.201	47.488	5.693
P2	P63mc	Hexagonal	3.248	5.197	47.481	5.692
P3	P63mc	Hexagonal	3.246	5.201	47.459	5.694
M1	P63mc	Hexagonal	3.244	5.193	47.327	5.706
M2	P63mc	Hexagonal	3.247	5.197	47.451	5.695
M3	P63mc	Hexagonal	3.246	5.194	47.395	5.699
M4	P63mc	Hexagonal	3.247	5.198	47.460	5.697
C1	P63mc	Hexagonal	3.247	5.196	47.442	5.698
C2	P63mc	Hexagonal	3.247	5.192	47.406	5.695
C3	P63mc	Hexagonal	3.248	5.191	47.426	5.7

4.2.2. Calculation of Crystallite Size Using Scherrer's Formula

The crystallite size was calculated by compensating the values obtained from the X-ray diffraction results in the Scherrer's equation (2-5) based on values of (FWHM), and the (d) spacing was calculated using the equation (2-3). Table (4-2) demonstrates the results of crystallite size calculations and inter-planner spacing of prepared samples.

***The table (4-2)**: Bragg's diffraction sites, (FWHM), d spacing and the calculated crystallite size according to Scherrer's equation*

Sample code	***(hkl)***	***2θ (deg)***	***FWHM (deg)***	d_{hkl} ***(Å)***	D_{Sh} ***(nm)***
P1	101	36.3291	0.2466	2.47091	33.543
	100	31.8459	0.2601	2.80778	31.425
	002	34.5013	0.2494	2.59752	32.998
	110	56.6685	0.2461	1.62300	36.281
P2	101	36.3470	0.2594	2.46974	31.889
	100	31.8592	0.2547	2.80664	32.091
	002	34.5509	0.2503	2.59390	32.884
	110	56.6594	0.2572	1.62324	34.713
P3	101	36.2577	0.3919	2.47562	21.105
	100	31.7867	0.3651	2.81288	22.383
	002	34.4315	0.3947	2.60262	20.846
	110	56.6087	0.3958	1.62457	22.552
M1	101	36.2290	0.3410	2.47751	24.251
	100	31.7420	0.3253	2.81674	25.118
	002	34.4287	0.3446	2.60283	23.877
	110	56.5602	0.3011	1.62585	29.638
M2	101	36.3171	0.2972	2.47170	27.831
	100	31.8286	0.2846	2.80927	28.717
	002	34.5123	0.2873	2.59671	28.646
	110	56.6322	0.3078	1.62396	29.003
M3	101	36.2882	0.3831	2.47360	21.589
	100	31.8145	0.3437	2.81048	23.778
	002	34.4817	0.3533	2.59895	23.295

	110	56.6371	0.3718	1.62383	24.011
M4	101	36.2106	0.3604	2.47873	22.943
	100	31.7350	0.3233	2.81734	25.273
	002	34.4163	0.3358	2.60374	24.5025
	110	56.5629	0.3007	1.62578	29.678
C1	101	36.2314	0.3964	2.47735	20.861
	100	31.7512	0.3703	2.81594	22.066
	002	34.4350	0.4008	2.60237	20.529
	110	56.5577	0.3895	1.62592	22.911
C2	101	36.2032	0.4971	2.47922	16.634
	100	31.7157	0.4663	2.81901	17.522
	002	34.4367	0.4967	2.60224	16.566
	110	56.5123	0.4978	1.62712	17.923
C3	101	36.2088	0.4382	2.47885	18.870
	100	31.7225	0.4099	2.81842	19.933
	002	34.4470	0.4455	2.60149	18.471
	110	56.5200	0.4351	1.62691	20.506

The values of crystallite size were found to be decreased as Mg concentration increased, but the decrease is greater by increasing the concentration of Cr, table (4-2). This could be attributed to the ionic radii of Zn, Mg and Cr ions. This is mainly because of the nucleation and subsequent growth rate with increasing Cr and Mg due to the difference of ionic radii of Zn, Mg and Cr ions [33]. Moreover, this behaviour can be explained by the incorporation of the dopant atom inhibits the growth of ZnO nanostructures [157]. Respective values of crystallite size (D) are represented in table (4-2). The relatively high value of crystallite size confirms the well crystalline nature of the material.

4.2.3. Calculation of Crystallite Size Using Williamson-Hall Equation

To calculate the average crystallite size and the value of microstrain, the Williamson-Hall equation (2-6) was used, by comparing the (W-H) equation with the equation of the straight line of the plot which is drawn with the values of (β_{hkl} cos Ө) along the y-axis and values of (sinӨ) along the x-axis. The value of the crystallite size (D) can be extracted by the intersection of the y-axis, which represents the magnitude ($\frac{k\lambda}{D}$). The plots are shown in figure (4-2) and details are presented in table (4-3).

Table (4-3): *The calculated crystallite size and internal strain using the Williamson-Hall equation*

Sample code	***$D_{W\text{-}H}$ (nm)***	***$\varepsilon * 10^{-4}$***
P1	30.469	- 2.75
P2	29.807	- 3
P3	21.764	1
M1	23.239	- 3
M2	27.425	- 1.5
M3	26.367	6
M4	22.852	- 3.5
C1	20.465	- 2.25
C2	17.139	0.75
C3	20.774	4.75

From the table, there is a difference between the crystallite size calculated by the Scherrer's equation and the crystallite size calculated by the Williamson -Hall equation, as the Williamson-Hall calculated crystallite size is smaller than the crystallite size in Scherrer, except for the sample (P3). As it is known, that the change in the distance between the atomic surfaces means that, the space of the crystalline inter-planner is not equal at each point of crystal, and this leads to the expansion or compression. The compression means that the lattice is stressful, but the strain is a measure of the amount of material deformation because of the stress, as it increases with increasing of stress and reduce its deficiency and causes a deviation in the lattice constant from its original value. The effect of an internal strain of the grains is due to the width of peaks to crystallite size and internal strain at the same time. Anyway, the internal strain was supposed to be regular along all crystallographic directions, therefore considering an isotropic nature of a crystal, where the substance characteristics are independent along of the direction, which they are measured [158]. On the other hand, note that the small crystallite size increases the internal strain. The negative signal indicates the compression of the lattice, which led to the small surface area.

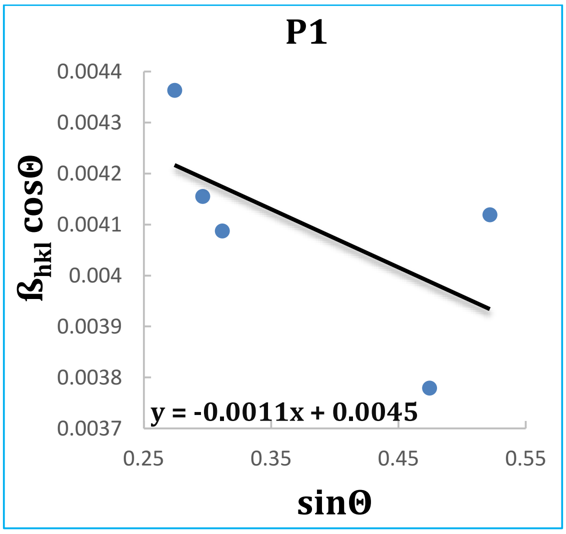

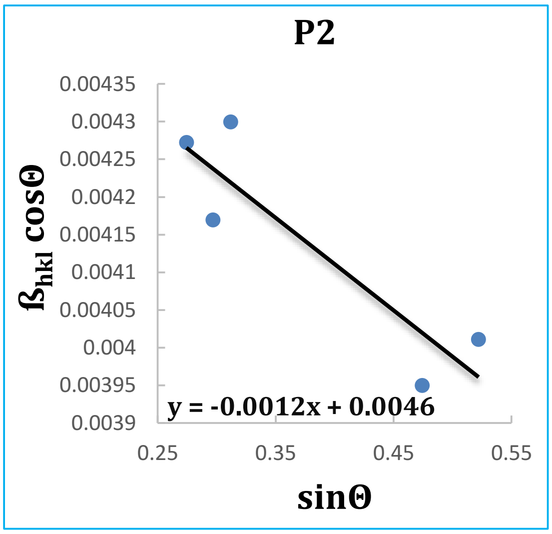

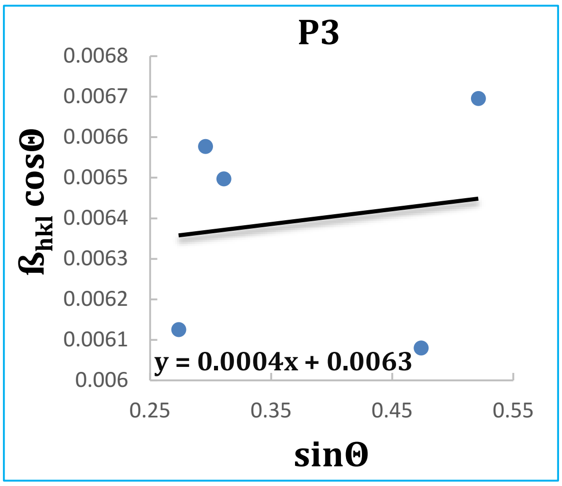
P3
ßhkl cosΘ
0.0068
0.0067
0.0066
0.0065
0.0064
0.0063
0.0062
0.0061
0.006
y = 0.0004x + 0.0063
0.25
0.35
0.45
0.55
sinΘ

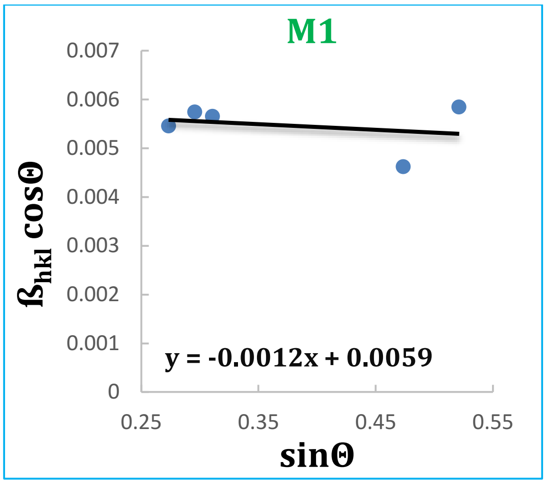
M1
ßhkl cosΘ
0.007
0.006
0.005
0.004
0.003
0.002
0.001
0
y = -0.0012x + 0.0059
0.25
0.35
0.45
0.55
sinΘ

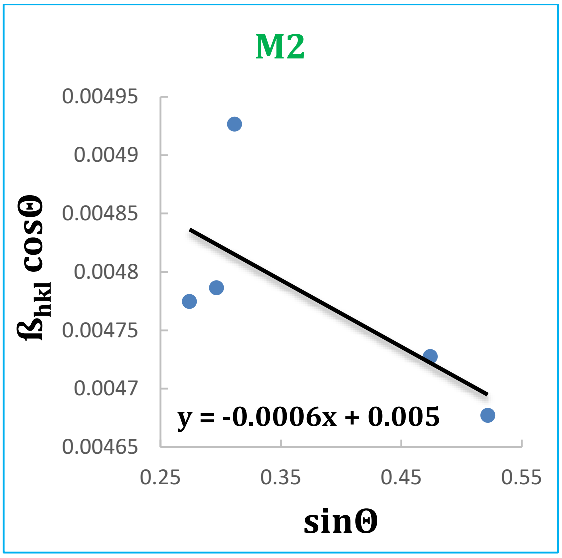
M2
ßhkl cosΘ
0.00495
0.0049
0.00485
0.0048
0.00475
0.0047
0.00465
y = -0.0006x + 0.005
0.25
0.35
0.45
0.55
sinΘ

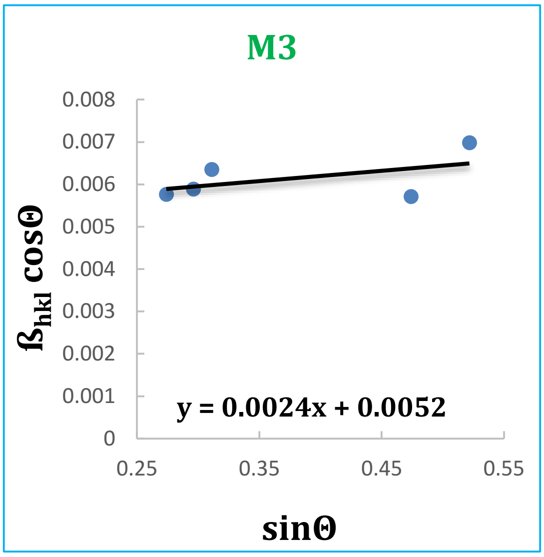
M3
ßhkl cosΘ
0.008
0.007
0.006
0.005
0.004
0.003
0.002
0.001
0
y = 0.0024x + 0.0052
0.25
0.35
0.45
0.55
sinΘ

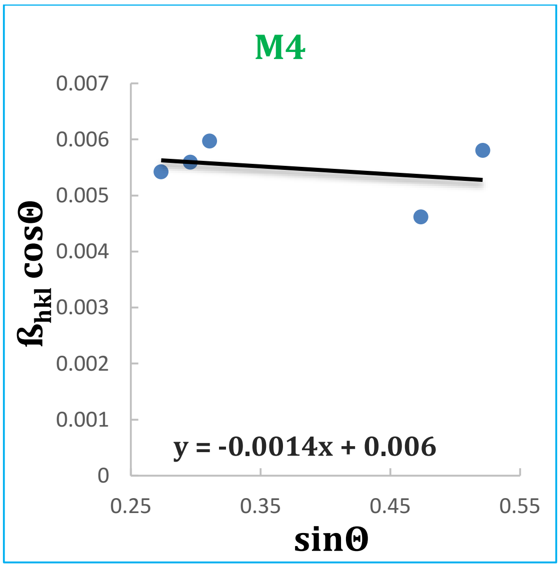
M4
ßhkl cosΘ
0.007
0.006
0.005
0.004
0.003
0.002
0.001
0
y = -0.0014x + 0.006
0.25
0.35
0.45
0.55
sinΘ

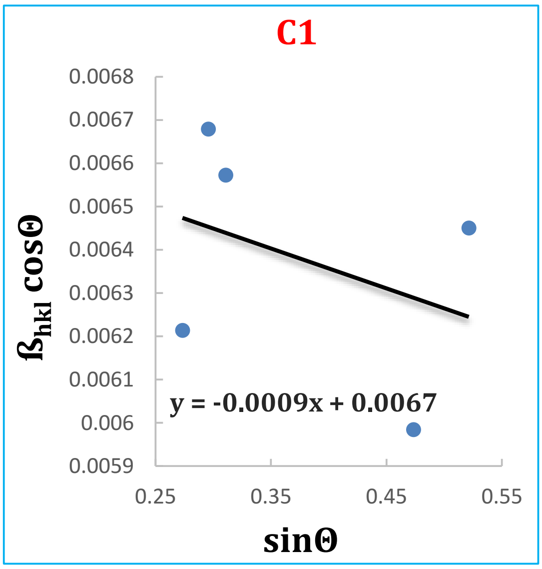
C1
ßhkl cosΘ
0.0068
0.0067
0.0066
0.0065
0.0064
0.0063
0.0062
0.0061
0.006
0.0059
y = -0.0009x + 0.0067
0.25
0.35
0.45
0.55
sinΘ

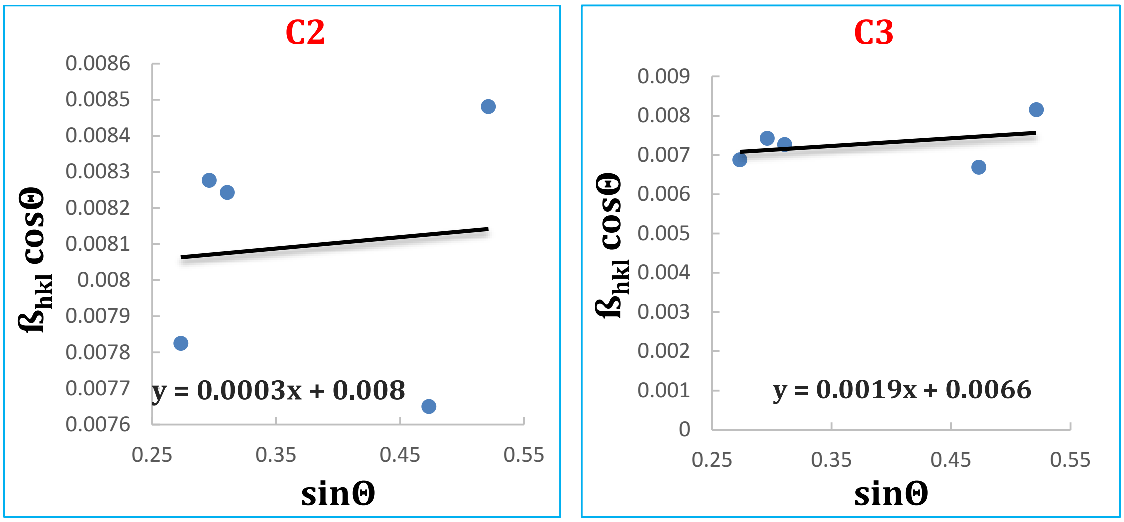

Figure. (4-2): *The calculation of the average crystallite size and internal strain from the Williamson-Hall equation for the prepared samples*

4.2.4. Calculation of the Specific Surface Area (SS.A)

The surface area of the particles was calculated for all pure and doped prepared samples, according to the relation (2-7), and the obtained results listed in table (4-4).

It was noted that the surface area (SS.A) of prepared nanoparticles increases with decreasing crystallite size calculated from both equations Williamson-Hall and Scherrer. Un-doped ZnO and 5% Mg-doped ZnO prepared samples exhibited lower (SSA) than other doped samples, the values of (SS.A) are presented in table (4-4). The increasing values of a specific area as the doping concentrations increased may be due to the preventing of crystal growth by the dopants ions and reside between the grains during the heat treatment process [159].

Table (4-4): *The calculated values of specific surface area of prepared samples*

Sample code	*D_{Sh} (nm)*	*$SS.A_{Sh}$ ($m^2.g^{-1}$)*	*D_{W-H} (nm)*	*$SS.A_{W-H}$ ($m^2.g^{-1}$)*
P1	33.507	31.454	30.469	34.589
P2	33.152	31.796	29.807	35.364
P3	21.472	49.073	21.764	48.416
M1	25.267	41.615	23.239	45.247
M2	28.702	36.705	27.42	38.419
M3	22.461	46.871	26.367	39.927
M4	25.202	41.788	22.852	46.086
C1	21.525	48.919	20.464	51.454
C2	16.962	62.111	17.139	61.471
C3	18.917	55.644	20.774	50.669

4.2.5. Calculation of the Morphology Index (M.I)

The morphology index of the crystalline surfaces of all samples was calculated according to the relation (2-9), and the results shown in the table (4-5) indicate the approximate values of the morphology index, and note that the surfaces that have the lowest value of the full width at half maximum have a large value Morphology index.

The table (4-5): *The values of morphology index of prepared samples*

Sample code	*FWHM Deg.*	*M.I (101)*	*FWHM Deg.*	*M.I (100)*	*FWHM Deg.*	*M.I (002)*	*FWHM Deg.*	*M.I (110)*
P1	0.246	0.558	0.26	0.545	0.249	0.555	0.246	0.559
P2	0.259	0.536	0.254	0.541	0.251	0.545	0.257	0.538
P3	0.395	0.534	0.365	0.555	0.395	0.533	0.395	0.532
M1	0.341	0.603	0.325	0.615	0.345	0.601	0.301	0.633
M2	0.297	0.589	0.285	0.599	0.287	0.597	0.307	0.581
M3	0.383	0.659	0.344	0.683	0.353	0.677	0.372	0.666
M4	0.360	0.678	0.323	0.702	0.336	0.694	0.301	0.717
C1	0.396	0.544	0.370	0.561	0.401	0.541	0.390	0.549
C2	0.497	0.590	0.466	0.605	0.497	0.591	0.498	0.590
C3	0.438	0.556	0.409	0.572	0.446	0.552	0.435	0.557

Experimental pure and doped ZnO nanopowders (M.I) is ranging between (0.5) to (0.72), and the details are presented in table (4-5). The convergence of (M.I) values for all samples have a clear indication of the good distribution of the crystallite sizes of each sample, where this factor is related to the degree of variation of the particles in the size of each sample. It also takes into consideration the width of each peak with the widest peak to identify how much difference between the crystallite sizes that caused different reflections from each surface of the crystalline surfaces [119].

4.2.6. Calculation of the Texture Coefficient (T_C)

The values of the Texture coefficient for each level and for all samples were calculated based on the equation (2-8), and obtained results shown in the table (4-6). The greater value of the texture coefficient is one, value greater of this value means the abundance of crystallization trend (hkl).

Table (4-6): *The values of the texture coefficient of prepared samples*

Sample code	*P1*	*P2*	*P3*	*M1*	*M2*	*M3*	*M4*	*C1*	*C2*	*C3*
Tc (101)	0.97	0.945	0.95	0.925	0.966	0.948	0.942	0.931	0.923	0.917
Tc (100)	0.97	0.995	1.033	1.022	1.034	1.015	0.975	1.062	1.085	1.078
Tc (002)	0.97	0.967	0.95	0.925	0.945	0.97	0.964	0.931	0.923	0.917
Tc (110)	1.091	1.093	1.068	1.127	1.056	1.067	1.119	1.076	1.068	1.089

From table (4-6), we note the highest value is (1.127) along the surface (110) ascribed to the sample (M1), as well as, a small preferential orientation along the surfaces of (100) and (110) for all samples was noted. In general, it can be said that the preferential orientation of the crystalline surfaces is not steady for a particular surface and for all samples, but varies according to the chemicals involved in the preparation process and the conditions of preparation. If T_c (hkl) ≈ 1, for all considered (hkl) planes, then the particles are irregularly oriented crystallites, which is matching well to the (JCPDS) indications. In the case of T_c(hkl) is more than 1, this suggests that the redundancy of grain is formed in a given [hkl] direction. Nevertheless, when ($1 > T_c$ (hkl) > 0), it denotes that there is a lack of grains in the specific direction. By increasing the texture coefficient, the preferential growth of the crystallites in the perpendicular direction to the (hkl) plane will be greater [110].

4.3. Study of the Morphological and Elemental Properties Using Scanning Electron Microscopy (SEM) and the Supplemented Device (EDX)

The (SEM) device was used to examine and analyze sample surfaces, where the resulting signal is a two-dimensional image showing information about surface morphology. While, (EDX) device identifies the elements present inside or on the surface of the model and measures the analytical structure of the elements. To obtain semi-quantitative results and identify the inorganic elements, the images produced by the (SEM) device were processed by Image-j program, to determine the diameter of the grains obtained from the test, and that was for the sample (M1). The surface morphology and elemental analysis of the prepared nanoparticles ($Mg_{0.05}Cr_{0.05}Zn_{0.90}O$), was analysed by the scanning electron microscope (SEM), fitted with (EDX).

The SEM micrograph have shown the particles have a spherical or semispherical formation aggregated in the form of clusters, with an average particle size of (30.399) nm. In SEM, the particle size was calculated by taking the noticeable grain boundaries. While in XRD, measurements are taken from the crystalline area that diffracts the X-ray waves. Thus, the particle size measurement of ($Mg_{0.05}Cr_{0.05}Zn_{0.90}O$) using XRD was found to be smaller than that with SEM measurement [160].

EDX relatively is considered a rapid and nondestructive approach for surface analysis. Composition and purity of the sample were studied using EDX. It is often used to survey surface problems and elemental analysis. The higher a peak in a spectrum, the more concentrated the element is in the sample. The observed peaks reveal the presence of Zn, Mg, Cr and O, that is confirming the formation of the analysed sample. From fig. (4-3d) the EDX spectra for the (Mg, Cr) doped ZnO sample confirmed the presence of zinc, oxygen, magnesium and chromium. The peak at (1.25) keV shows the presence of magnesium. The peak values at (1) keV and (8.6) keV, confirm the presence of zinc, the peak at (0.53) keV exhibits the presence of oxygen, the peak at (0.6 and 5.4) keV shows the presence of chromium and the peak at (1.3) keV reveals the presence of in the EDX spectra.

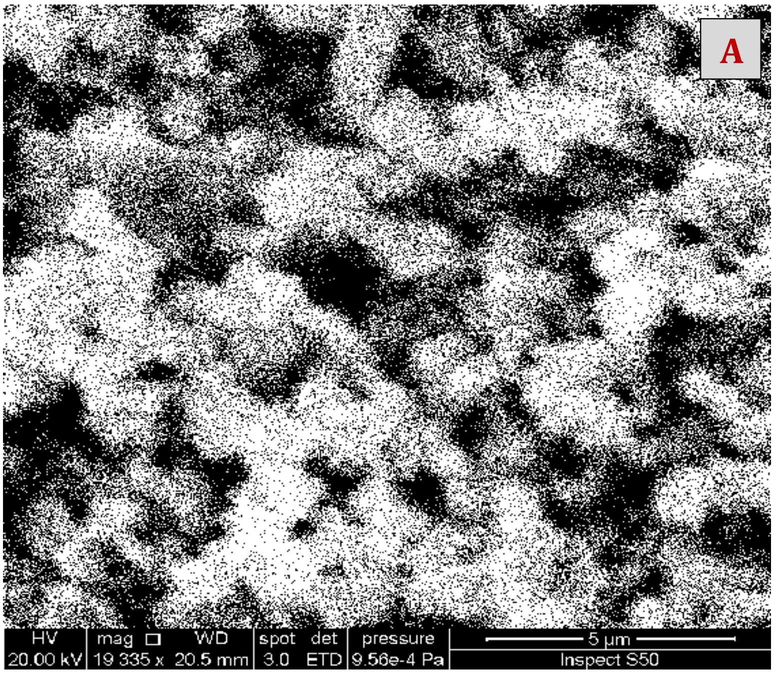

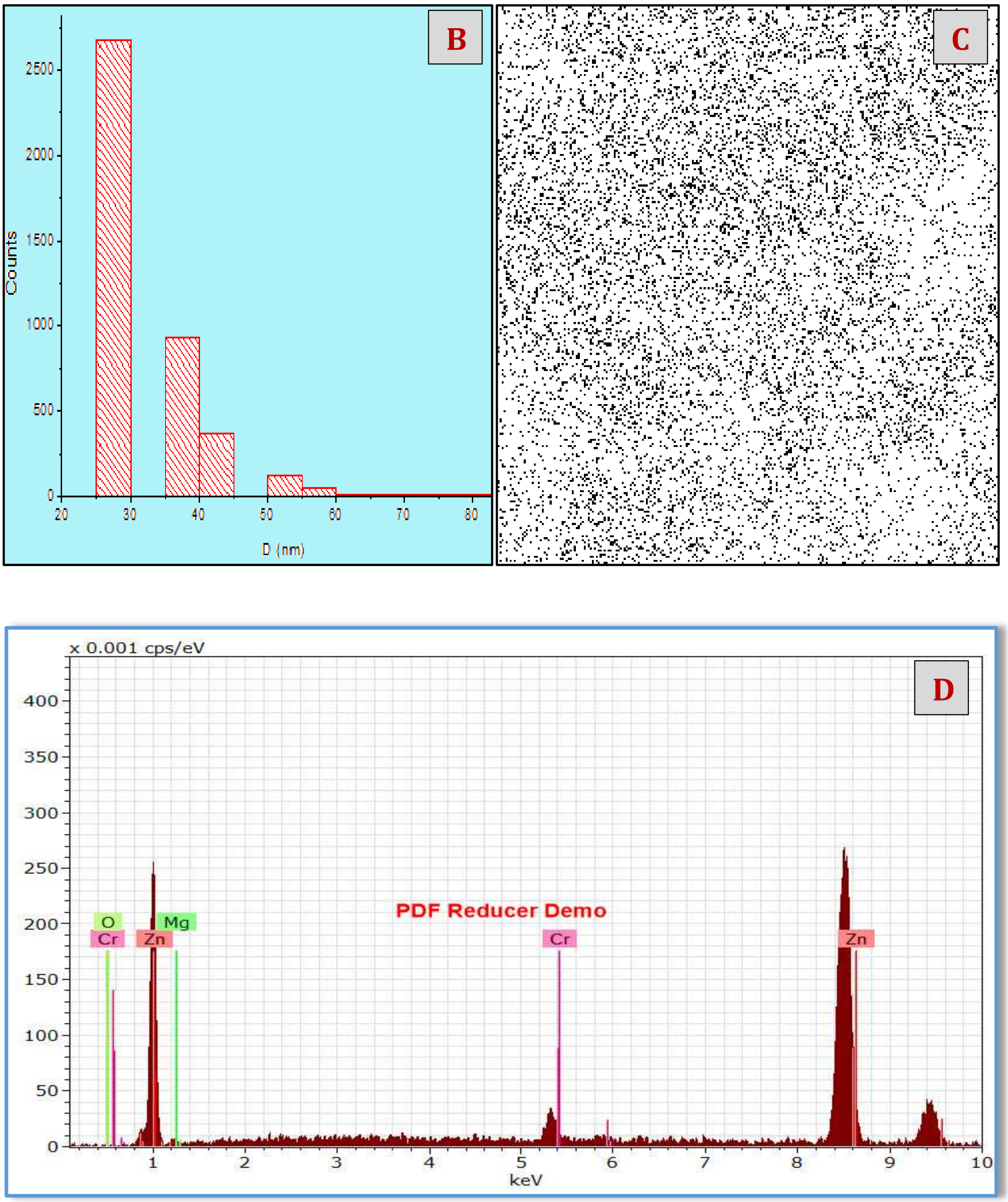

Fig. (4-3): ***A****. SEM image;* ***B****. Particle size calculated from SEM image;* ***C****. processed SEM image using (Image-j) program, and* ***D****. EDX spectra for the sample (5% Mg & 5% Cr) doped ZnO.*

4.4. Optical Calculations

The optical properties of pure and doped zinc oxide nanoparticles were studied using the absorption spectra within the wavelength range of (300-900) nm. These properties also included the calculation of optical constants such as absorbance, transmittance, reflectance and the optical band gap.

4.4.1. Absorbance (A) and Transmittance (T)

The absorbance and transmittance curves were plotted as a function of the wavelength (nm) of all prepared samples, as shown in figure (4-4), and the transmittance and absorbance values were calculated using the equations (2-15) and (2-16) respectively.

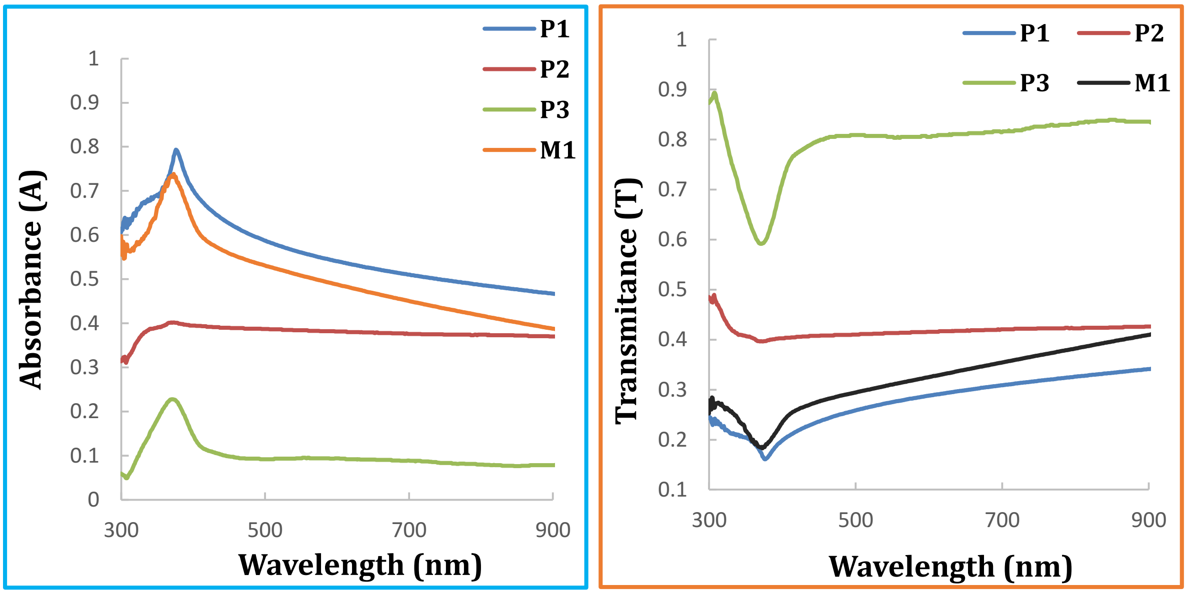

Fig. (4-4a): *The absorbance and transmittance spectra as a function of wavelength of the samples (P1, P2, P3 and M1)*

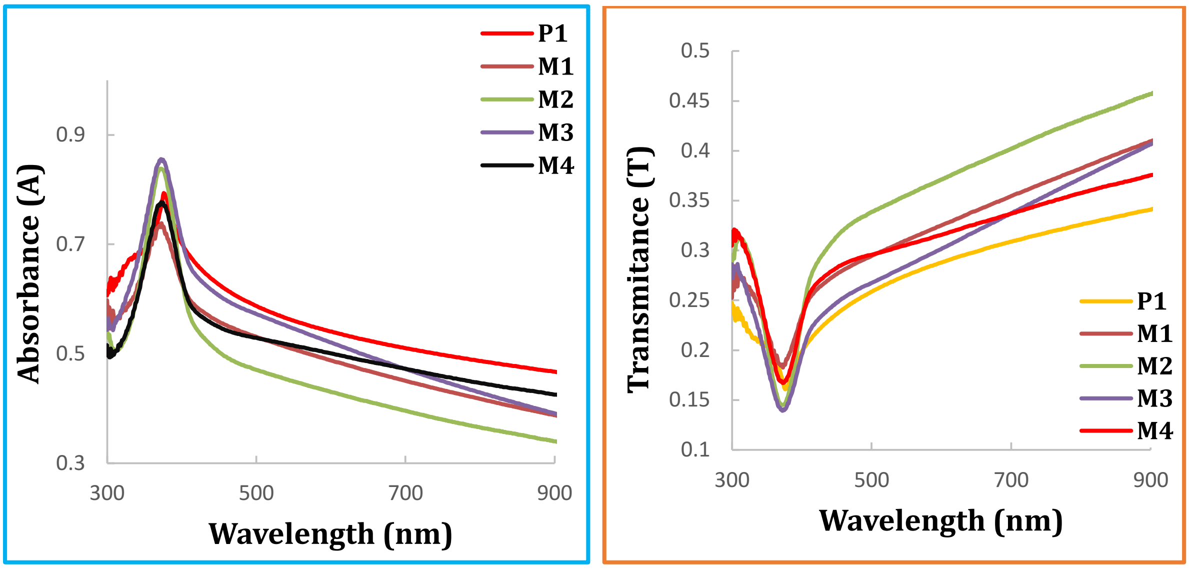

Fig. (4-4b): *The spectra of absorbance and transmittance as a function of wavelength of the samples (P1, M1, M2, M3 and M4)*

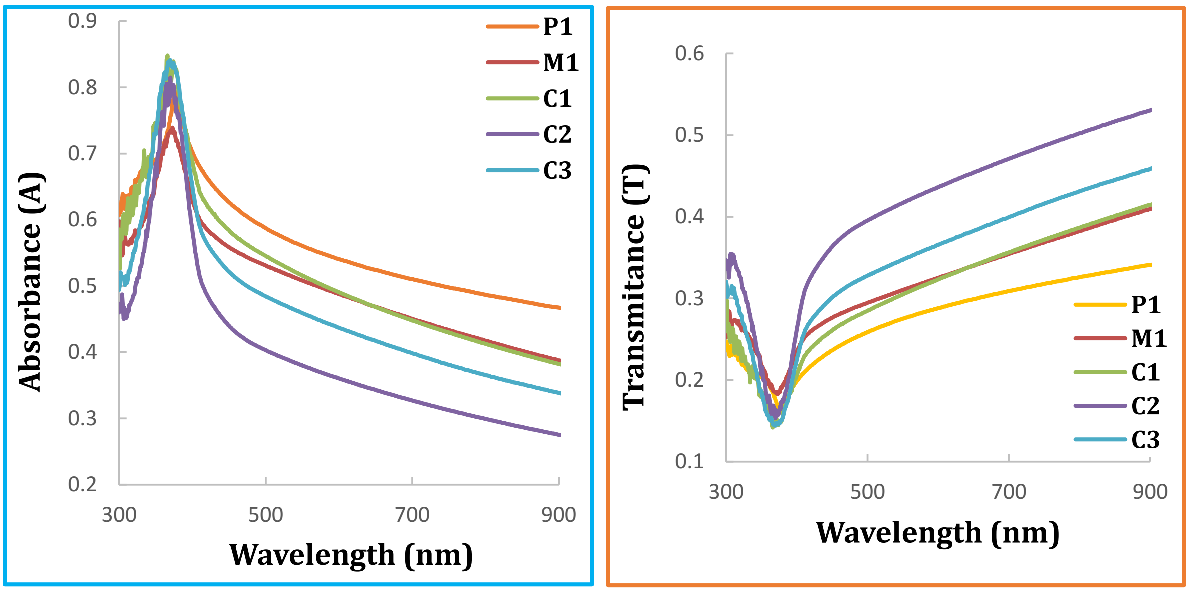

Fig. (4-4c): *The spectra of absorbance and transmittance as a function of the wavelength of the samples (P1, M1, C1, C2, and C3)*

The absorbance of materials is influenced by several factors such as the type of material and the wavelength of the incident radiation. The absorbance was measured as a function of wavelength in the range (300-

900 nm). Figure (4-4) clearly shows that the absorbance decreases with increasing wavelength for all prepared samples, as it suffers a sudden and rapid decline, and this is consistent with published research [29, 42]. Physically, this can be explained by the fact that the incident photon could not excite and transfer the electron from the valance band to the conduction band, because the incident photon energy is less than the energy gap value of the semiconductor, and thus the absorbance is reduced by increasing the wavelength [119]. It is also noticed that absorbance is reduced when the rate of doping increases and this confirms the introduction of atoms of the dopant material within the crystalline structure of the prepared samples, resulting in the formation of local levels within the energy gap, which in turn leads to the absorption of photons with low energies [8]. From the absorbance spectra as a function of the wavelength, where the absorption edge for all the prepared samples was between the wavelengths range of (350-375) nm.

From figure (4-4), we observe that the transmittance spectrum behaves differently from absorbance behaviour, where, it was noticed that the transmittance increases gradually with increasing wavelength for all samples [128]. Where the highest transmittance was obtained from the sample (P3) (0.05 % Cr) doped ZnO, where it was about (85%) at the wavelength (750-900) nm, this corresponds to a lower absorbance obtained and a decreasing reflectance of the sample itself, according to the energy conservation law. We also observed that the values of transmittance begin to increase in the wavelength range extending from (300-500) nm, where the increase from the area of visible light until reaching the greatest value at (900 nm). These values of transmittance show the growing interest of researchers for using of ZnO as optical windows in solar cells.

4.4.2. Reflectance (R)

The reflectance was calculated from the absorbance and transmittance spectra, under the energy conservation law using equation (2-17). Fig. (4-5) shows the reflectance as a function of the wavelength of the prepared samples. Generally, we noted there is an increase in reflectance with increasing the wavelength. The apparent general behaviour of the reflectance curves is to decrease the value of the reflectance and then increases with increasing wavelength. The decreasing lying between wavelength range (330-370) nm and the increasing begins between the wavelengths (380-900) nm. The spectrum of UV-VIS reflectance has a minimal effect in scattering than absorbance. The sudden decreasing at a particular wavelength of the reflectance, corresponding to the optical band gap denotes that the particles are almost regularly distributed in the prepared specimen [161].

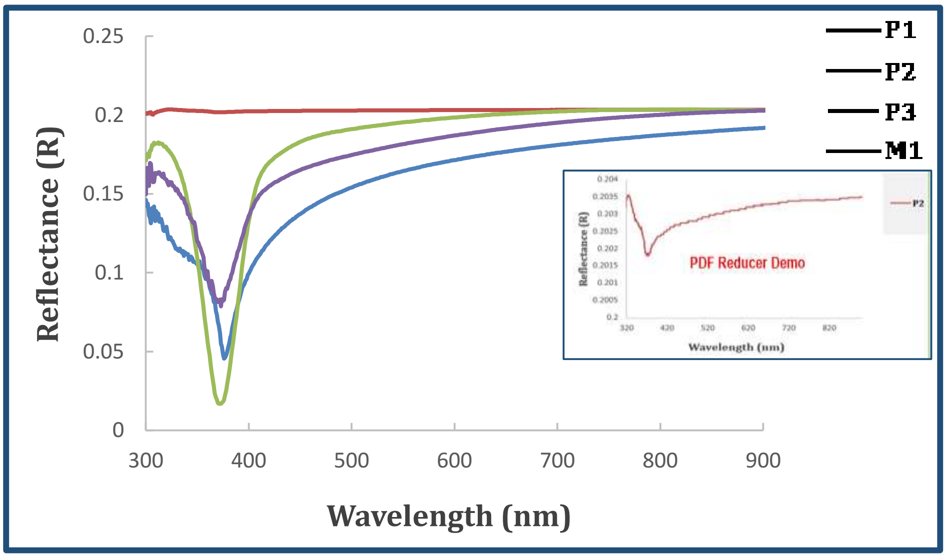

Fig. (4-5a): *Reflectance of the samples (P1, P2, P3 and M1)*

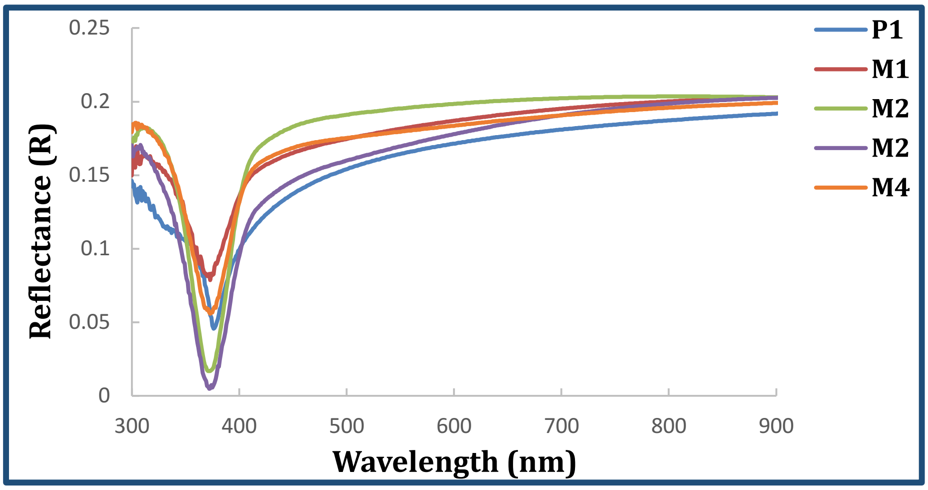

Fig. (4-5b): *Reflectance of the samples ((P1, M1, M2, M3 and M4)*

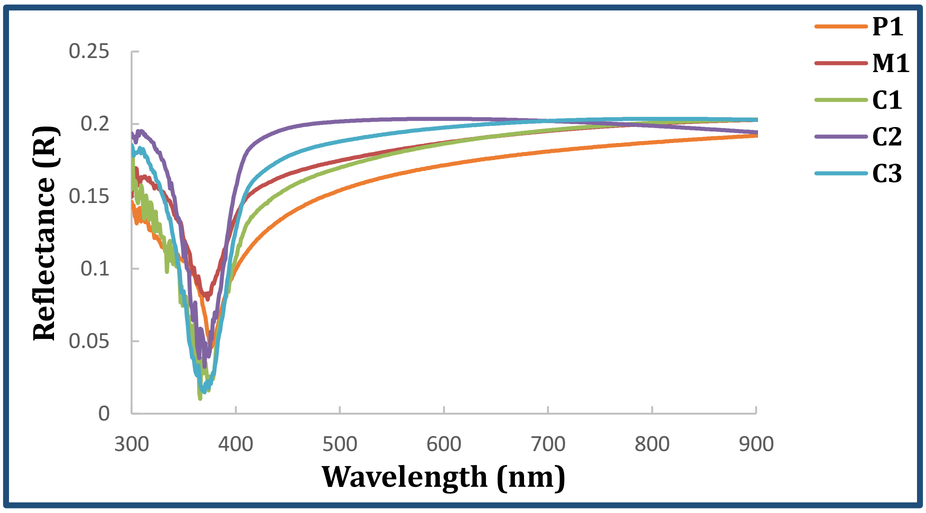

Fig. (4-5c): *Reflectance of the samples (P1, M1, C1, C2, and C3)*

4.4.3. Optical Band Gap (Eg)

It is one of the most important optical constants that are based on the physics of semiconductors, to manufacture many electronic devices such as solar cells, reagents, optical diodes and others. The selection of the semiconductor materials for manufacturing, based on the forbidden energy gap, which must be approximate to the energy of the photons within the visible UV and IR of the electromagnetic spectrum, in order to identify the amount of transmitted, absorbed or reflected photons affecting on the material under analysis [133].

The value of allowed indirect band gap can be obtained from Tauc's plot, by extrapolation the straight part of resulting curve at the point (αhν)² = 0, which is between values of (hν) (eV) along the x-axis with (αhν)² (eV.cm⁻¹) ² along the y-axis, where the intersection represents the optical energy gap of the material being studied.

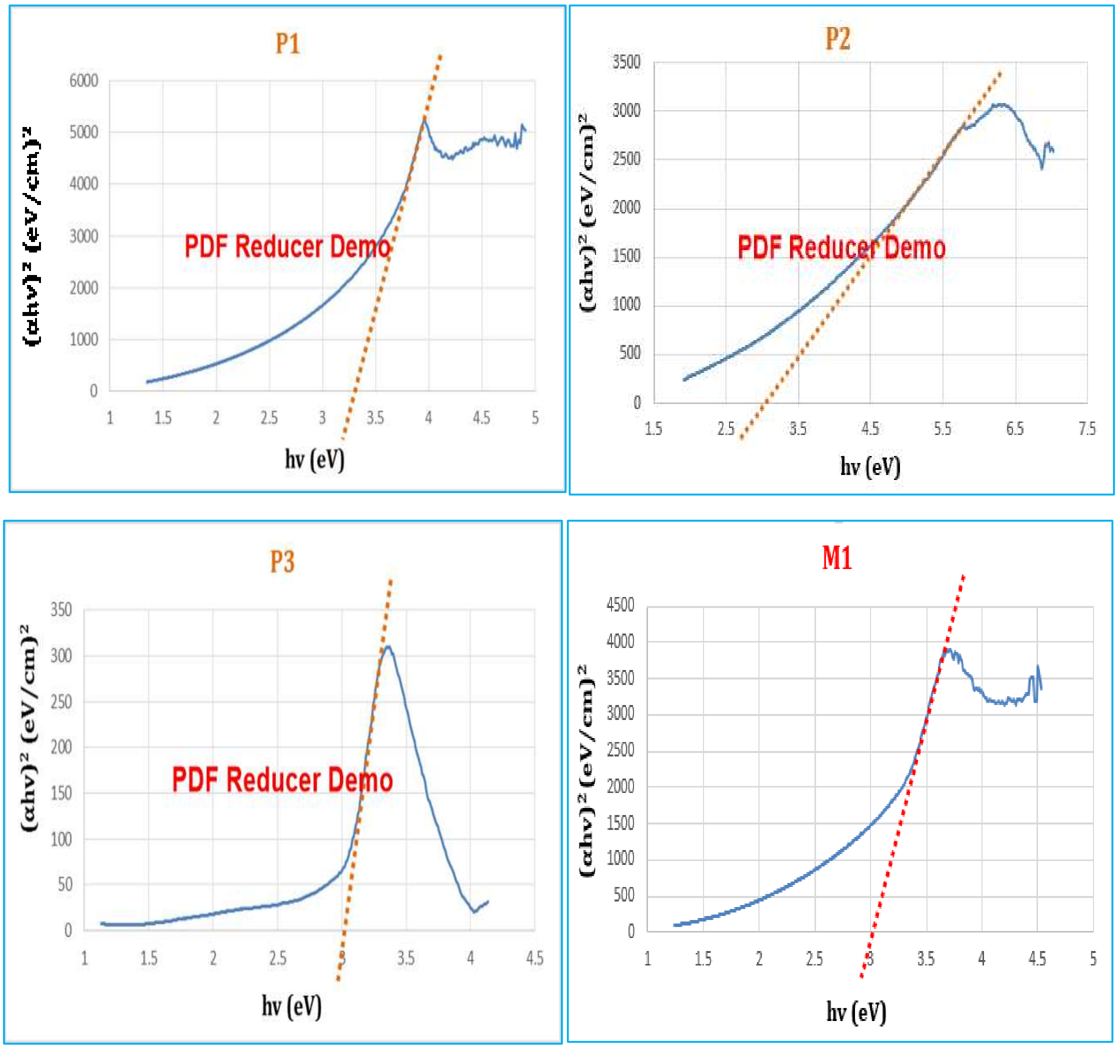

Fig. (4-6a): *Optical band gaps according to Tauc's relation of samples (P1, P2, P3 and M1)*

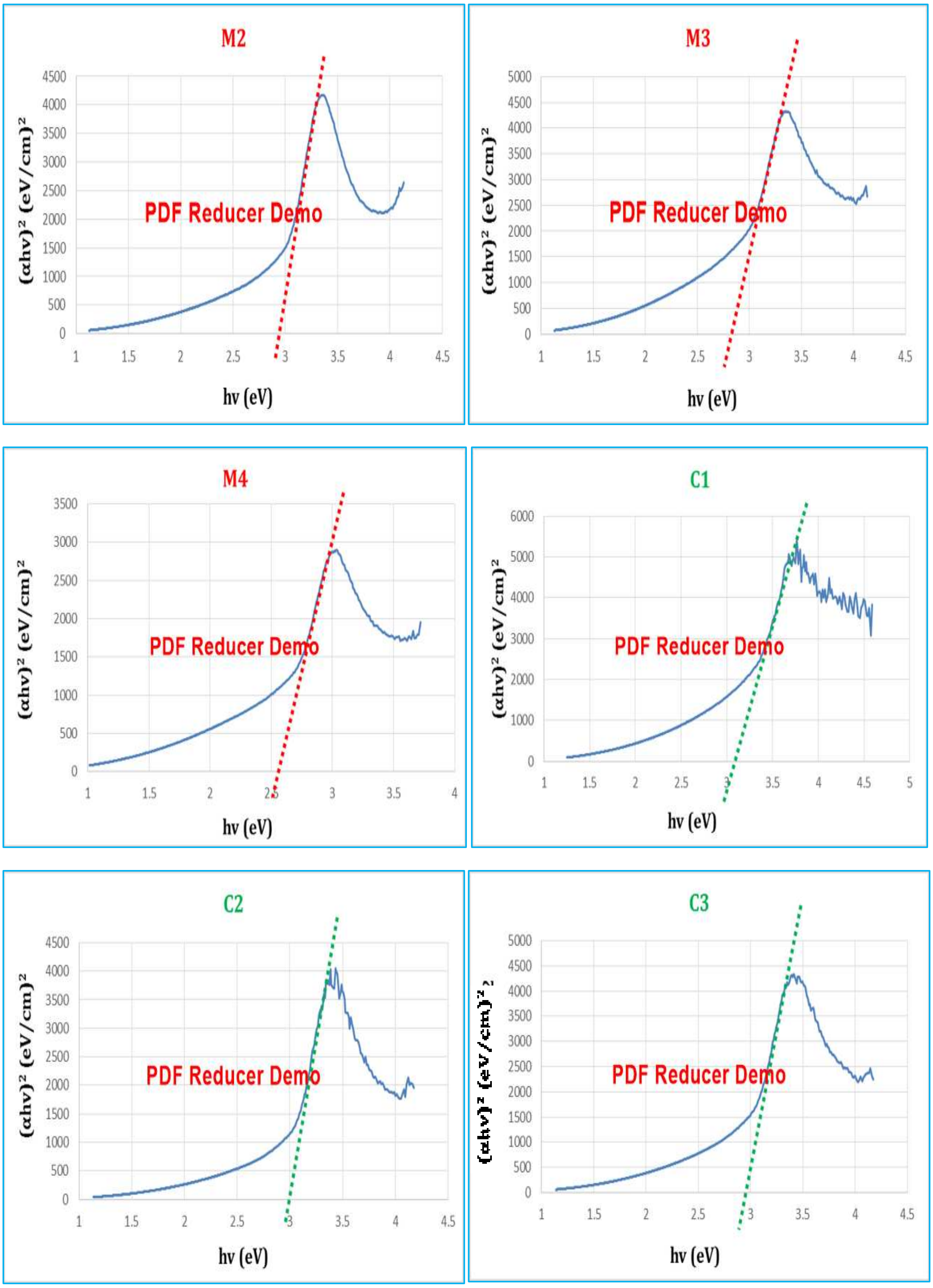

Fig. (4-6b): *Optical band gaps according to Tauc's relation of the samples (M2, M3, M4, C1, C2, and C3)*

It can be deduced from the above figures that the value of the energy gap decreases by increasing the rate of doping with both elements Mg and Cr, and this is consistent with the findings of others [32, 33]. This means that the doping has led to displace of the absorption edge towards the low energies, as shown in the figure (4-6). This decrease can be explained by the fact that the impurities led to the formation of donor levels within the energy gap and near the conduction band and thus absorbing of low energy photons [2]. The energy gap values for the allowed indirect transition of prepared samples are present in table (4-7).

This apparent decrease in energy gap values from 3.36 eV (bulk ZnO) to 2.61 eV could be attributed to the effect of the dopants, behaved as a substitutional impurity located in the lattice position of ZnO. This decreasing of the energy gap of doped ZnO nanoparticles formed more imperfects sites on the ZnO surface. These surface defects are qualified for absorbing more visible-light [162].

***Table (4-7)**: The calculated values of energy gap of prepared samples*

Sample	***Energy gap (eV)***
P1	***3.36***
P2	***3.28***
P3	***3.01***
M1	***3.02***
M2	***2.93***
M3	***2.83***
M4	***2.61***
C1	***3.13***
C2	***2.96***
C3	***2.93***

4.5. A.C. Electrical Measurements

The alternating electrical properties were studied as a function of the electric field frequency within the range (50 Hz-3MHz), using the (LCR meter) device, which gives the values of each (tan δ, Cp and D) on the electronic screen as a function of frequency.

4.5.1. Dielectric Constant (ε')

The dielectric constant was calculated within the frequencies range (50 Hz - 3MHz) using the equation (2-24). It is clear from fig. (4-7), a similar behaviour, was observed in all samples, where, with increasing the frequency of the applied electric field, the dielectric constant is clearly reduced. This can be explained by that the increase of frequency of the electric field caused a decrease in the contribution of the space charge polarization, and this phenomenon is common in most of the dielectrics.

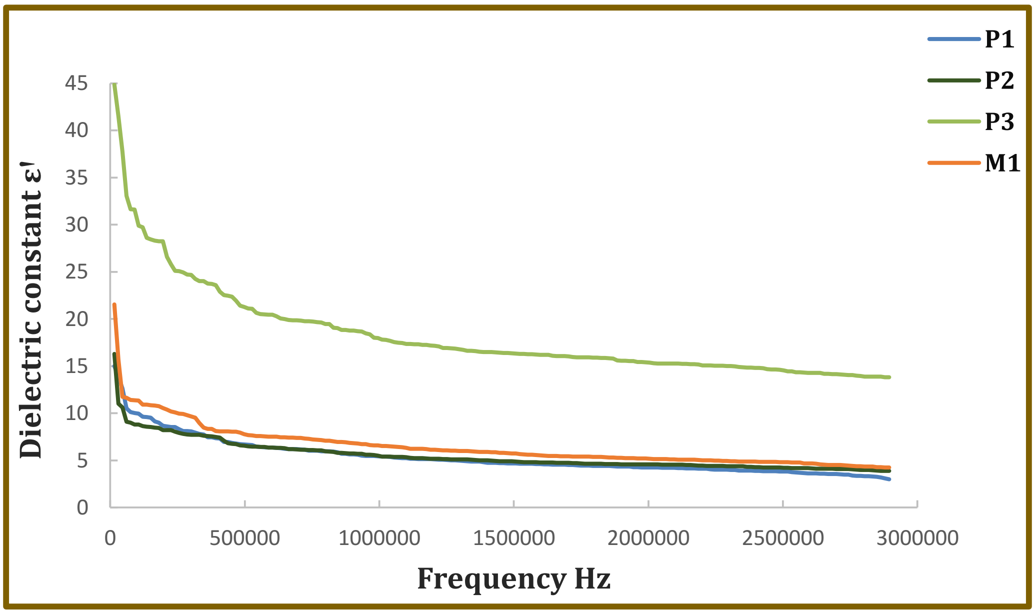

Fig. (4-7a): *Variation of dielectric constant as a function of frequency for the samples (P1, P2, P3 and M1)*

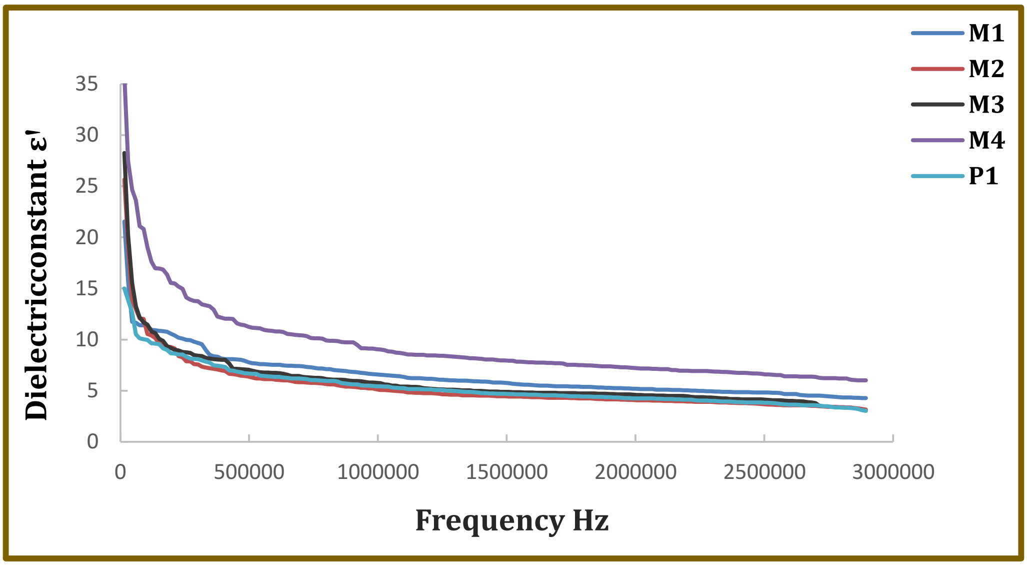

Fig. (4-7b): *Variation of dielectric constant as a function of frequency for the samples (P1, M1, M2, M3 and M4)*

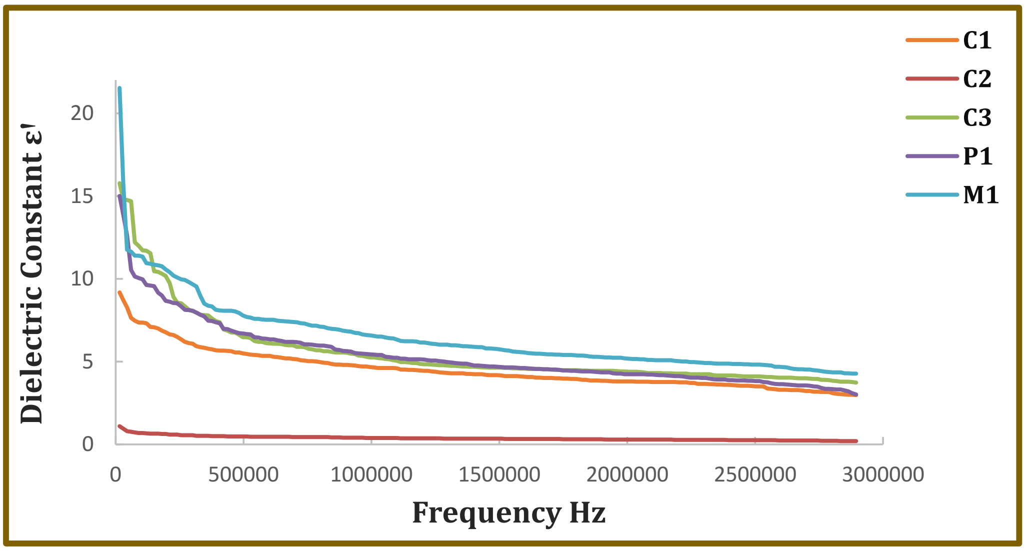

Fig. (4-7c): *Variation of dielectric constant as a function of frequency for the samples (P1, M1, C1, C2 and C3)*

Generally, ZnO is described as a polar molecule this fact is well known. It has a permanent dipole moment and quickly responds to the applied electric field. In addition, it was also noticed that the values of the dielectric constant at higher frequencies approximately remained constant. At low frequencies, pure ZnO have high values of dielectric constant, this is due to the domination of species of vacancies such as oxygen and defects of grain boundary etc. Whereas, the decreasing of dielectric constant with applied frequency is normal, in respect of the fact that any species participating to polarizability is bound to exhibit lagging behind the applied electric field at greater frequencies. From the observed higher value of dielectric constant of doped ZnO, we can conclude that the electron exchange between Zn^{2+}, Mg^{2+} and Cr^{3+} ions is predominant at lower frequencies. At higher frequencies, the dielectric constant tends to reach almost a constant value due to the fact, that beyond certain frequency the electron exchange between Zn^{2+}, Mg^{2+} and Cr^{3+}cannot follow the applied alternating field [47, 137].

4.5.2. Dielectric Loss (ε'')

The dielectric loss factor was calculated within the frequencies (50Hz - 3MHz), which is directly proportional to the dissipation of the energy in ceramic materials using equation (2-27). Figure (4-8) shows a similar behaviour for all samples. Where the highest value of dielectric loss factor is at low frequencies and decreases as the frequency of the applied electric field increased. This decrease is because of the space charge polarization. This exotic behaviour, as well as, the very low loss factor in comparison to the parent ZnO turns out that the synthesized nano samples appropriate for high-frequency device applications [41].

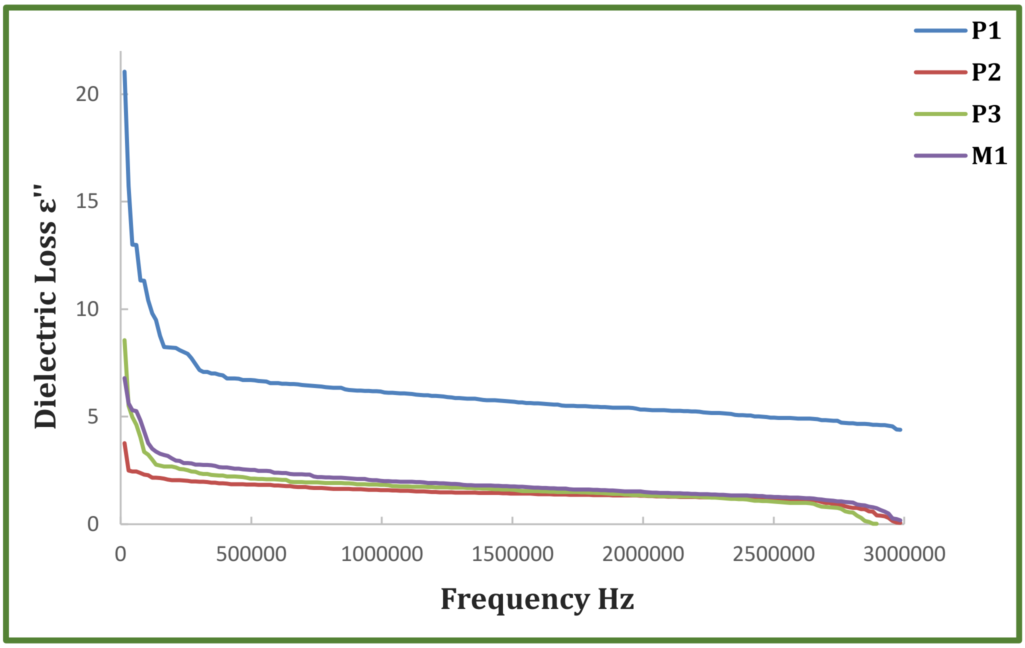

Fig. (4-8a): *Variation of dielectric loss as a function of frequency for the samples (P1, P2, P3 and M1)*

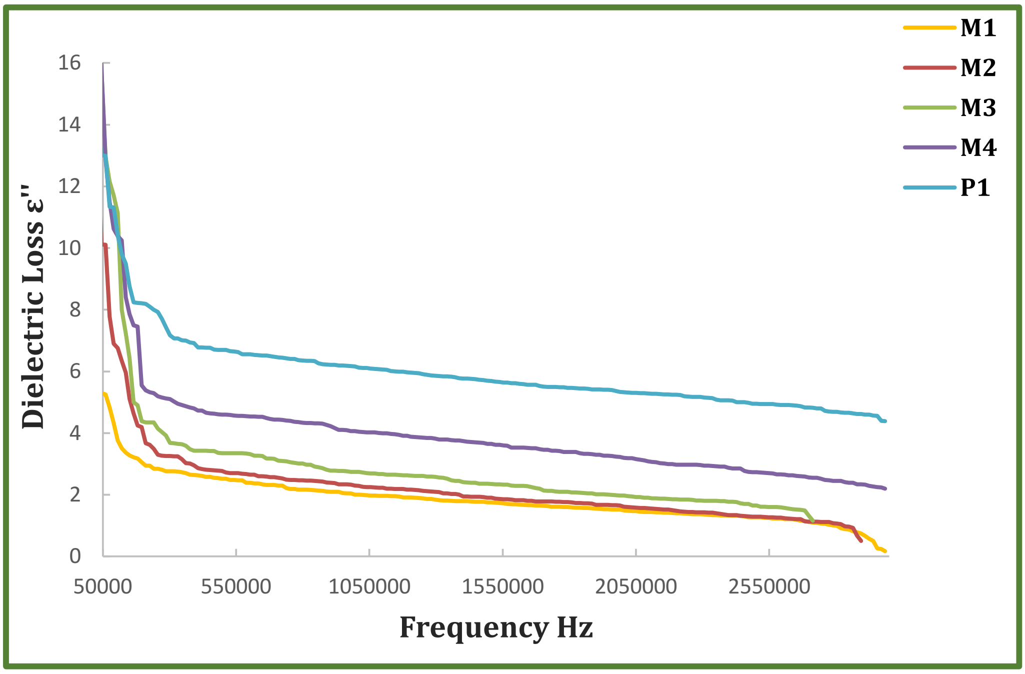

Fig. (4-8b): *Variation of dielectric loss as a function of frequency for the samples (P1, M1, M2, M3 and M4)*

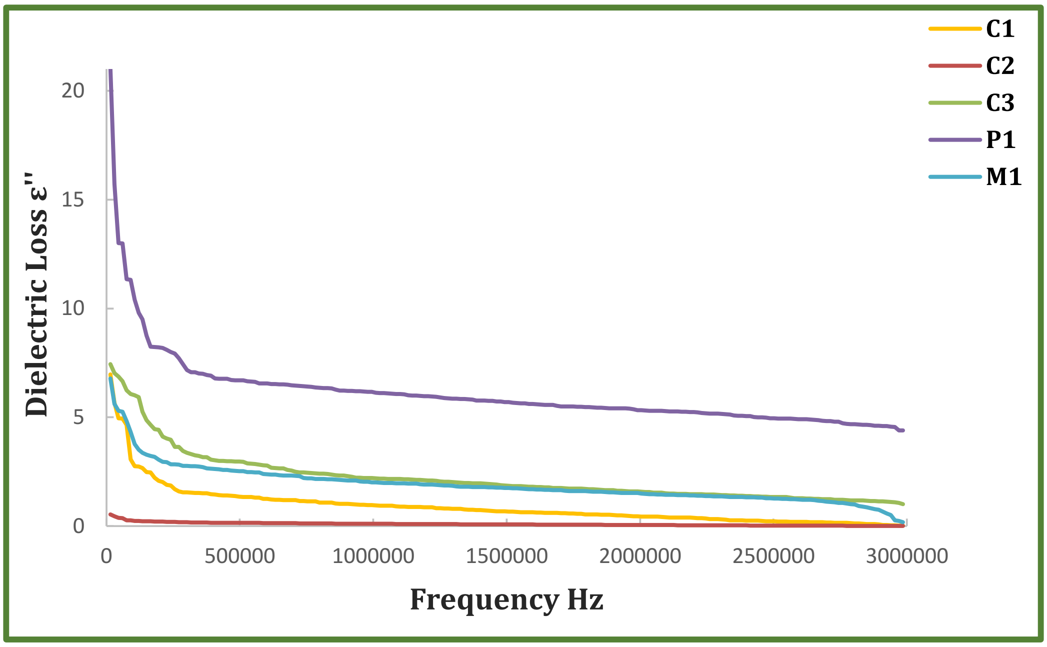

Fig. (4-8c) *Variation of dielectric loss as a function of frequency for the samples (P1, M1, C1, C2 and C3)*

From figures above, we noticed that the samples (P2, M1 and C2) have small dielectric loss compared to samples P1, M3 and M4. This indicates that they can store more energy due to a small loss. Hence, they possess a dielectric behaviour. Meanwhile, the samples P1, M3 and M4 with high losses rate. Thus, they cannot store energy; therefore, they possesses a conductor behaviour. It is obvious that the overall values of tanδ were observed to increase as the concentration of Cr^{3+} ions increased for all samples, and decrease as Mg^{2+} concentration decreased.

It is well known that high values of loss factor below (10 kHz) frequencies are caused by the existence of the space charge in the nanostructure, such as micro-pores, dangling bonds and vacancies due to the grain boundaries of their large surface grain. Beyond this frequency, the orientation polarization is the dominant mechanism. Furthermore, at low frequencies, the hopping electrons are trapped by these structural in-homogeneities that lead to a dominant space charge polarization at this range of frequency. The possible source of orientation polarization is the presence of oxygen vacancies and zinc interstitials in the nano-sized ZnO. When an external field is applied, the Zn ions and the oxygen vacancies in the neighbourhood can change the positions by a single jump and try to align along the direction of the field, which can be described by the notation of Kröger- Vink [46, 137].

4.5.3. Frequency and Temperature Dependent a.c. Conductivity ($\sigma_{a.c}$)

The a.c. conductivity of the prepared samples was measured at room temperature, 50, 100, 150 ^{0}C, within the frequency range of (50 Hz-3MHz) using Eq. (2-28). Figure (4-9), shows the change in conductivity as a function of a.c. electric field frequency. For all samples, results showed that the a.c conductivity increases as the frequency of applied a.c. field increased.

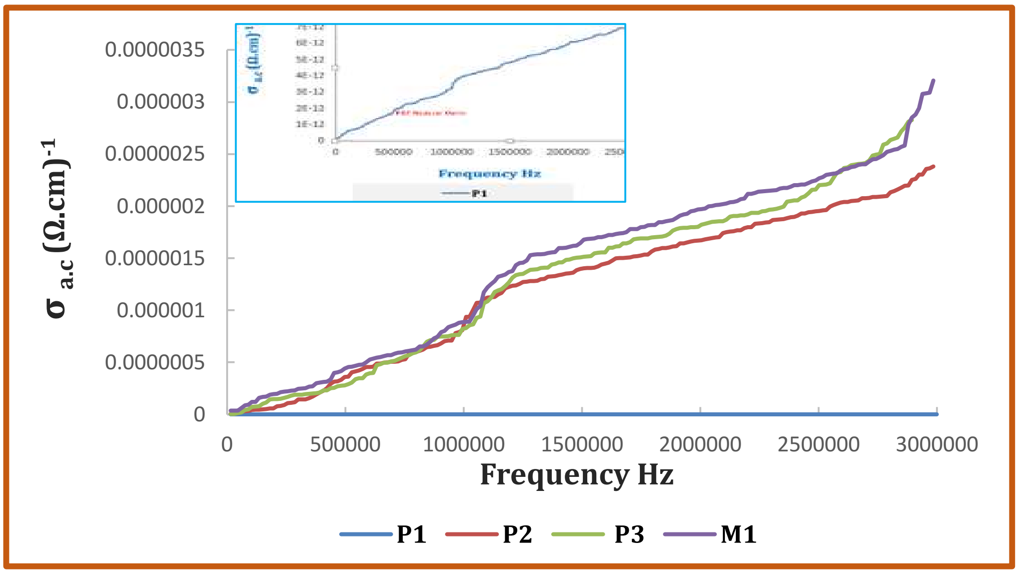

Fig. (4-9a): *Variation of a.c. conductivity as a function of frequency at room temperature for the samples (P1, P2, P3 and M1)*

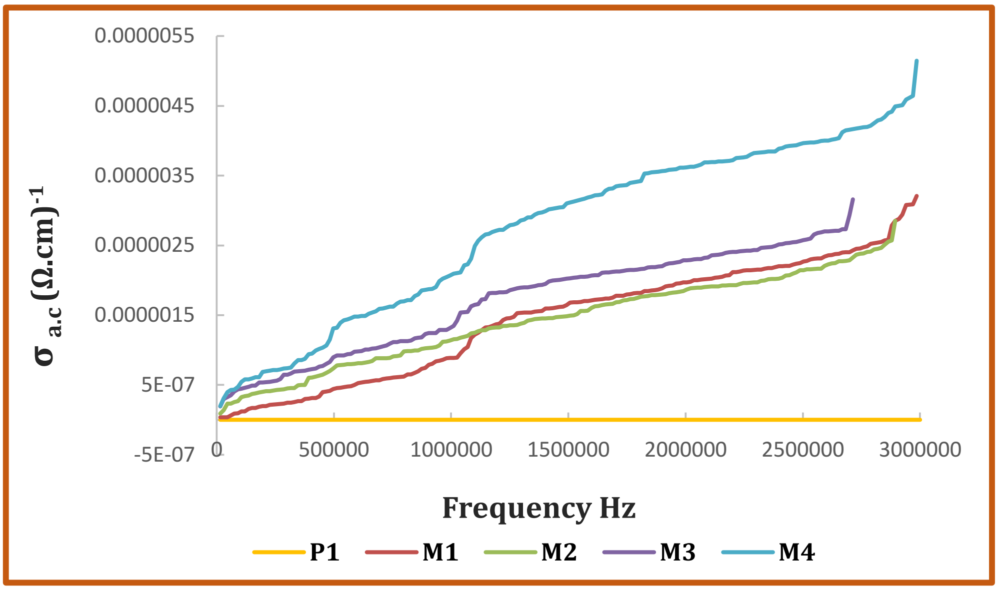

Fig. (4-9b): *Variation of a.c. conductivity as a function of frequency at room temperature for the samples (P1, M1, M2, M3 and M4)*

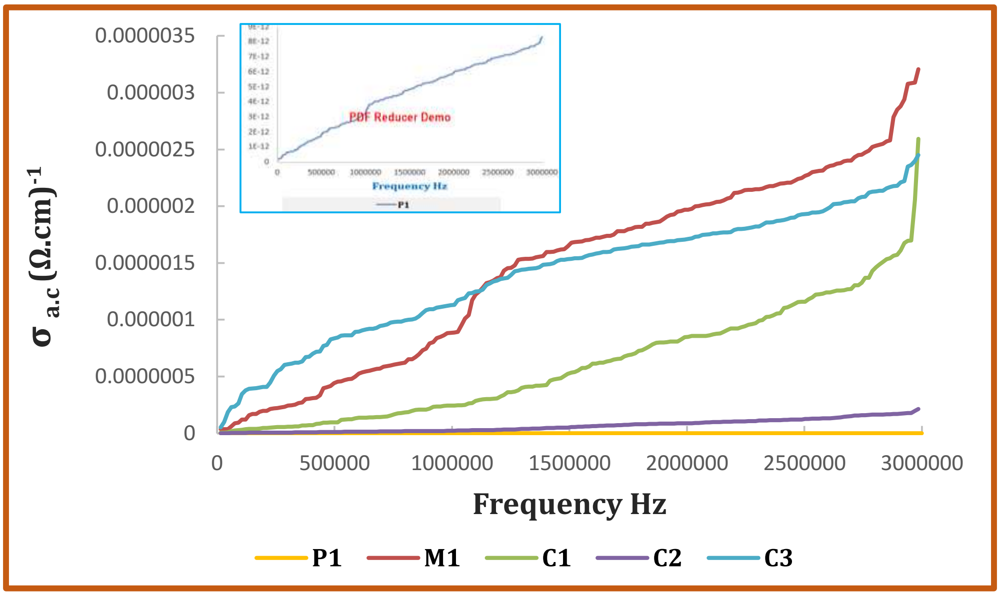

Fig. (4-9c): *Variation of a.c. conductivity as a function of frequency at room temperature for the samples (P1, M1, C1, C2 and C3)*

The variation of a.c. conductivity ($\sigma_{a.c}$) with the frequency at room temperature is illustrated by Fig. (4-9), which shows the variation in conductivity as a function of the electric field frequency. For all samples, results showed that the a.c. conductivity increases with the increase of the electric field frequency. A Linear increase in conductivity with increasing the frequency can be interpreted as the increasing frequency can improve the electrons hopping between the charges carriers, which dominated over the charge carriers plugging effect, and thus increasing the electric conductivity of the nanoparticles [145]. In the hopping model, it is probable to characterize various particular regions of frequency. Where, the conductivity is almost constant at low frequencies, as the transport takes place on the infinite paths. For a certain region of frequencies, where the a.c. conductivity strongly increases as the frequency increased, the transport is predominated by contributions from hopping infinite clusters. That is to say, that the region where the high-frequency cutoff starts to play a role is encountered. The model of electron hopping can be interpreted the mechanism of the electrical conduction [163].

Generally, at room temperature, the semiconductor materials are described as having intermediate electrical conductivity and increases with the input of energy. And so on, the overall electrical behaviour of semiconductors is described via the band model, involving electrons moving from different energy levels forming bands [164]. Therefore, undoped ZnO has shown less electrical conductivity equal to $(8.3*10^{-12})$ $(\Omega.cm)^{-1}$, than rest doped samples. Thus, we found that the doping with (Mg, Cr) has enhanced the electrical conductivity of zinc oxide at room temperature, where the highest conductivity value at room temperature was for the sample (M4) equal to $(5.2*10^{-6})$ $(\Omega.cm)^{-1}$.

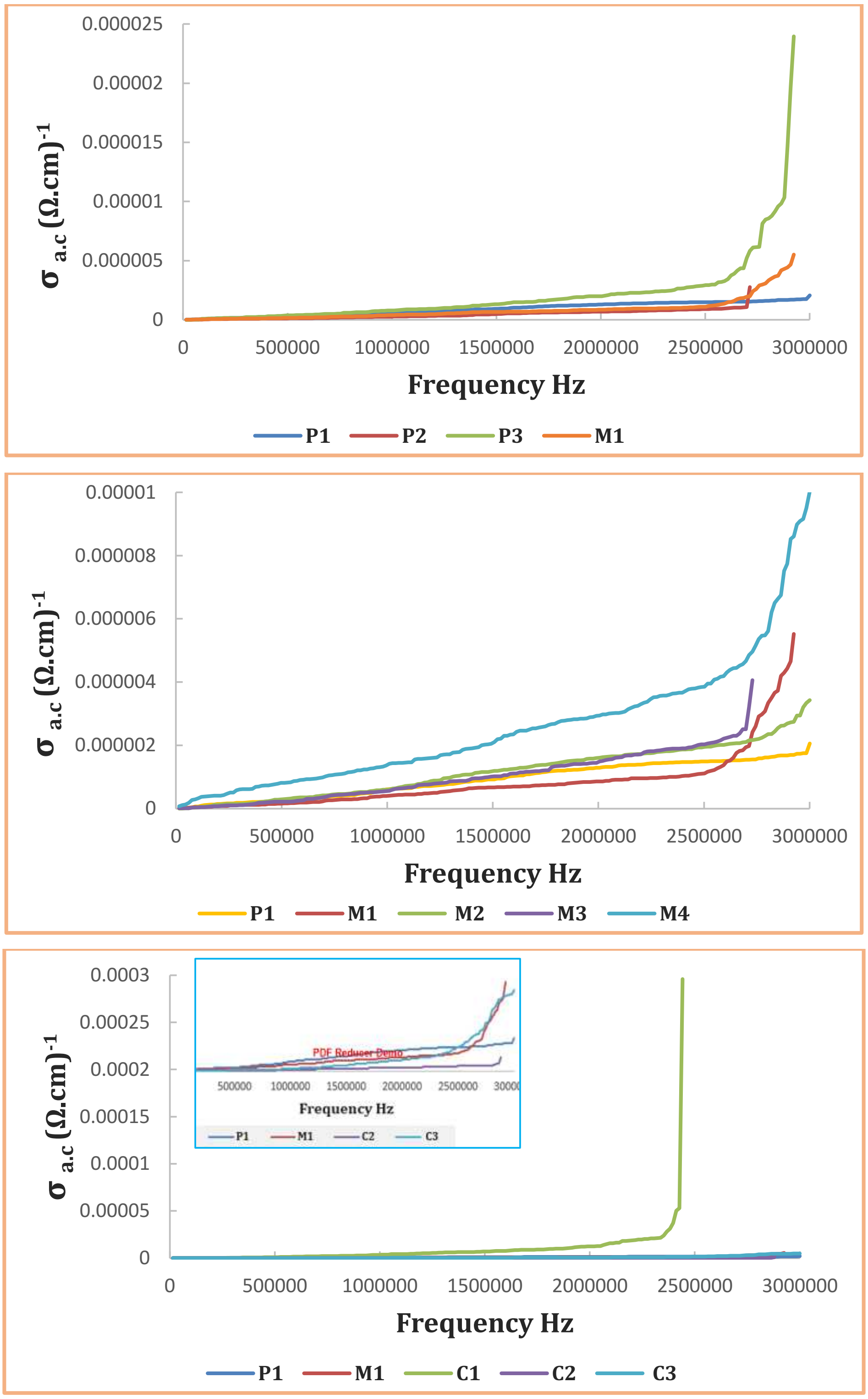

Fig. (4-10): *Variation of a.c. conductivity as a function of frequency for all samples at 50 °C*

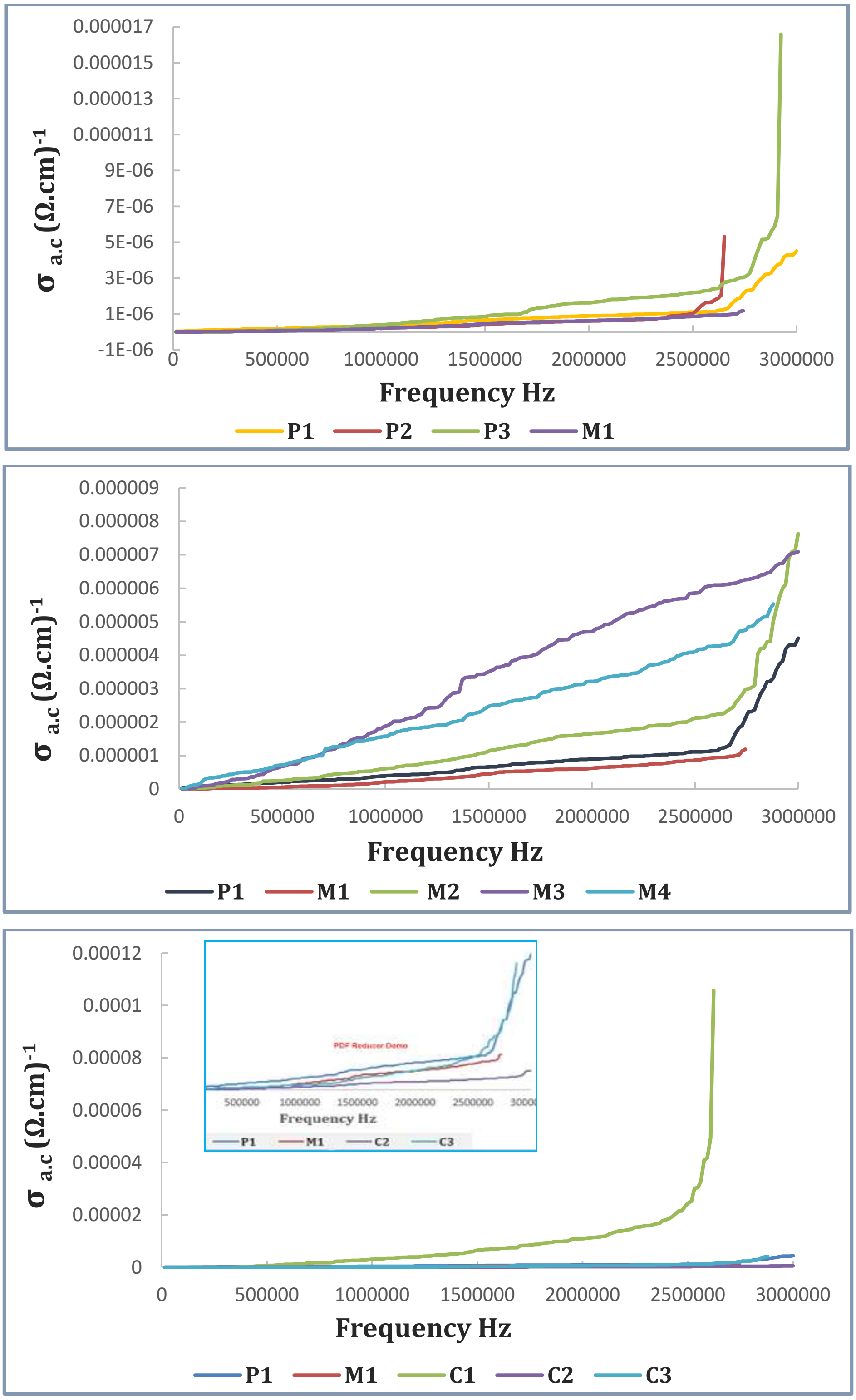

Fig. (4-11): *Variation of a.c. conductivity as a function of frequency for all samples at 100 °C*

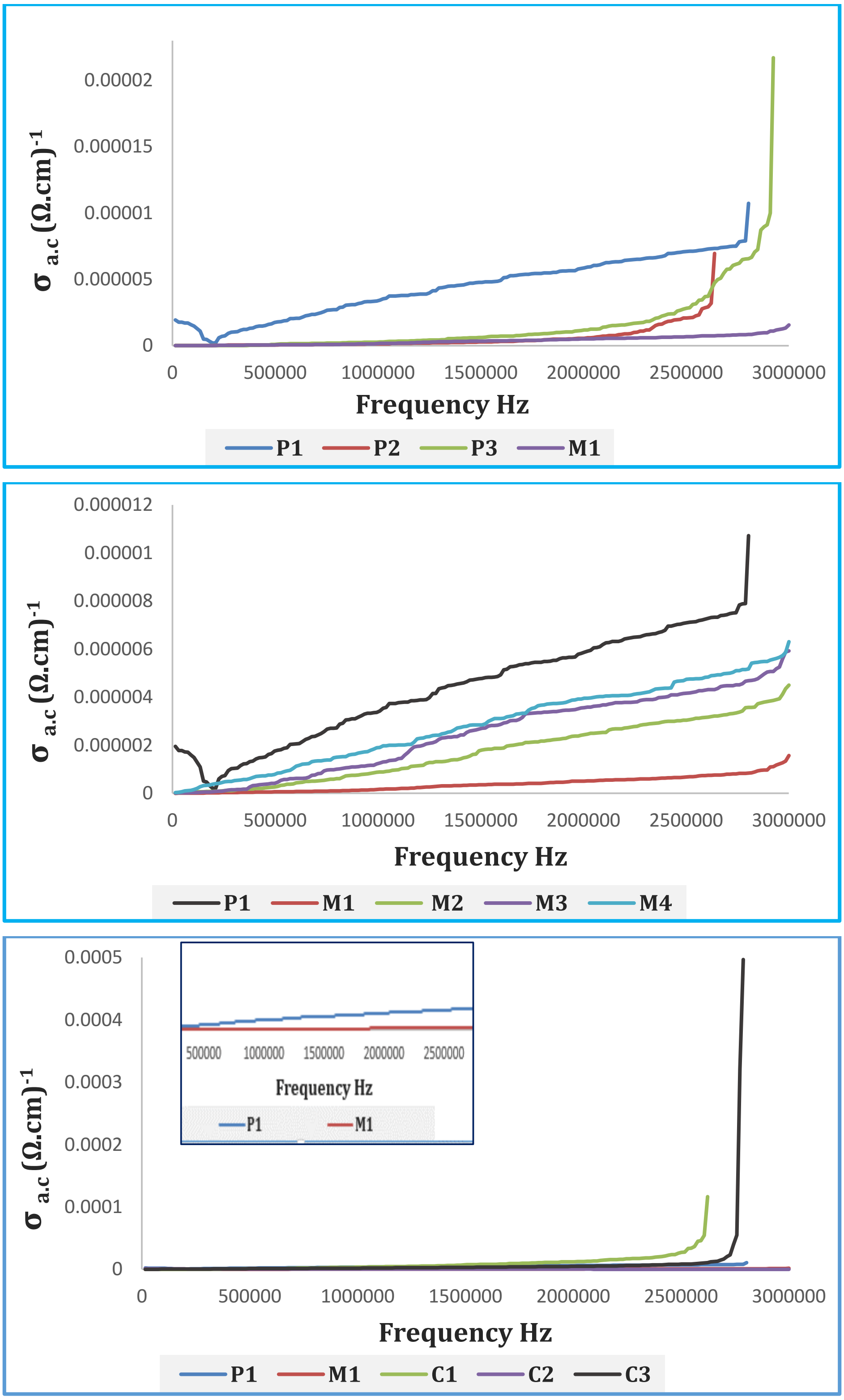

Fig. (4-12): *Variation of a.c. conductivity as a function of frequency for all samples at 150 °C*

***Table (4-8)**: The increase in a.c. conductivity values with increasing temperature at 2 MHz of prepared samples*

Sample	***a.c. conductivity (Ω.cm)$^{-1}$ at 2 MHz***			
	25 ^{0}C	***50 ^{0}C***	***100 ^{0}C***	***150 ^{0}C***
P1	$6*10^{-12}$	$1.3*10^{-6}$	$9*10^{-6}$	$5.9*10^{-6}$
P2	$1.7*10^{-7}$	$6.9*10^{-7}$	$6.2*10^{-7}$	$5.6*10^{-7}$
P3	$1.8*10^{-6}$	$2*10^{-6}$	$1.6*10^{-6}$	$1.9*10^{-6}$
M1	$2*10^{-7}$	$8.6*10^{-7}$	$6.3*10^{-7}$	$5.1*10^{-7}$
M2	$1* 10^{-6}$	$1.6*10^{-6}$	$1.7*10^{-6}$	$2.4*10^{-6}$
M3	$2.3*10^{-6}$	$1.5*10^{-6}$	$4.7*10^{-6}$	$3.6*10^{-6}$
M4	$3.6*10^{-6}$	$2.9*10^{-6}$	$3.2*10^{-6}$	$4*10^{-6}$
C1	$8.* 10^{-7}$	$1.2*10^{-5}$	$1.1*10^{-5}$	$1.2*10^{-5}$
C2	$8.8*10^{-8}$	$2.3*10^{-7}$	$2.7*10^{-7}$	$9.4*10^{-7}$
C3	$1.7*10^{-7}$	$7.1*10^{-7}$	$6.3*10^{-7}$	$4.2*10^{-6}$

As concerning to temperature effect on a.c conductivity, generally, it was found that the a.c. conductivity was increased by increasing the temperature, this confirms the semiconducting behaviour of the synthesized material. The increase in a.c. electrical conductivity as increasing temperature and frequency may be attributed to the increase in the drift mobility of the electrons and holes by the hopping conduction. Moreover, the increase in a.c. conductivity can be explained as that the increase in temperature can thermally activate the charge carriers that in turn increases the charge exchange interactions; this means that the increase in temperature has led to resistance with negative thermal coefficient [145, 165].

From figure (4-10) and the obtained results, at 50 ^{0}C, we can observe that the sample (C2) has exhibited a less electrical conductivity equal to (8.2*10^{-7}) (Ω.cm)$^{-1}$, while the highest conductivity value was for the sample (C1) equal to (3*10^{-4}) (Ω.cm)$^{-1}$. At 100 ^{0}C, from figure (4-11) and the obtained findings, we have noticed that the sample (C2) has exhibited a less electrical conductivity equal to (6.4*10^{-7}) (Ω.cm)$^{-1}$, while the highest conductivity value was for the sample (C1) equal to (1*10^{-4}) (Ω.cm)$^{-1}$. Moreover, at 150 ^{0}C, from figure (4-12) and the calculation results, it was observed that the sample (C2) has exhibited a less electrical conductivity equal to (9*10^{-10}) (Ω.cm)$^{-1}$, whereas, the highest conductivity value was for the sample (C3) equal to (5*10^{-4}) (Ω.cm)$^{-1}$. From the above, we find that the sample (C3), in which the concentration of Mg is a higher (20 %), has the highest a.c conductivity at 150 ^{0}C. This is because of the dopant has influenced the properties ZnO nanomaterial such as the electrical conductivity, band gap and optical property [166].

The general behavior of the increase in the a.c. conductivity by increasing the temperature can be noticed by the values shown in table (4-8), at manually selective frequency range (2 MHz).

Another reason can explain the increased conductivity of semiconductors by increasing temperature that is possession of a negative thermal coefficient, which is considered as one of the most important features of semiconductor materials. This leads to increase the electrical conductivity of the semiconductor with increasing temperature due to the collapse of the bonds and the transfer of electrons from the valence band to the conduction band, these features have made semiconductor very useful in many electronic applications [147].

Chapter Five

Conclusions and Future Works

5.1. Conclusions

From this work, the followings are concluded:-

1. The sol-gel combustion technique successfully proves to be capable for synthesizing of un-doped and (Mg, Cr) doped ZnO nanopowder, utilizing a zinc nitrate as a precursor and citric acid as fuel.
2. The XRD patterns revealed that the diffraction peaks of pure and ($Mg_xCr_yZn_{1-x-y}O$) doped ZnO nanoparticles, can be indexed to a hexagonal wurtzite structure, and it is suggested that the (wurtzite) structure is unchanged, with the different doping concentrations.
3. Mg and Cr ions were successfully substituted Zn lattice positions; this has led to a little variation in relative intensities and lattice parameters, as compared to the reported data of un-doped ZnO.
4. The incorporation of the Mg and Cr dopants and due to the difference in ionic radii of Zn, Mg and Cr ions, have led to decreasing the crystallite size of un-doped and ($Mg_xCr_yZn_{1-x-y}O$) doped ZnO Nanopowder.
5. The relatively high values of crystallite size of ZnO nanomaterial confirms the well crystalline nature of the synthesized material.
6. The behaviour of Mg and Cr dopants as substitutional impurities located in the lattice position of ZnO, have led to decrease band gap values from 3.36 eV (bulk ZnO) to 2.61 eV of the sample M4 with doping concentrations of (0.05 Mg 0.20 Cr).
7. Un-doped ZnO has shown less electrical conductivity equal to ($8.3*10^{-12}$) $(\Omega.cm)^{-1}$, than rest doped samples. Thus, we found that the doping with (Mg, Cr) has enabled controlling and optimizing the electrical conductivity of zinc oxide at room temperature.

5.2. Propositions for Future Works

In addition to the current research works, the followings are suggested:-

1. Using another solvent instead of water such as methanol and Ethanol in the combustion method for preparing un-doped and (Mg, Cr) doped ZnO. As well as, using another fuel instead of citric acid as a combustion agent such as urea.
2. Investigate mechanical and magnetic properties of un-doped and ($Mg_xCr_yZn_{1-x-y}O$) ZnO prepared by combustion method.
3. Investigate the temperature effect on structural and optical properties of undoped ZnO and $Mg_xCr_yZn_{1-x-y}O$ prepared by combustion method.
4. Study the doping effect on structural and morphological properties using (TEM) device.
5. The sample (0.05%Cr doped ZnO), have exhibited high transmittance value, which is possible to be employed for manufacturing these materials for certain applications such as transparent conductive and optical windows in solar cells.
6. Study the doping effect on optical properties using (FT-IR) device.
7. Study the doping effect on electrical and dielectric properties using (precession impedance analyzer) device.
8. Utilizing of other materials for doping ZnO and study their effect on its properties.
9. High increased electrical conductivity that displayed by (Mg, Cr) doped ZnO samples at room temperature can be suggested as promising materials for optoelectronic and electronic applications gadgets.

10. Cr doped ZnO prepared nanomaterial can be employed as Ferro-fluid magnetic and biomedical applications.

11. Cr doped ZnO prepared samples are promising for employing these materials in different applications, such as chemical sensors, electrically controlled magnetic sensors and actuators, and advanced optical switches, because Cr is a good candidate to enhance some others characteristics of ZnO for.

12. By doping with MgO, which has a wider band-gap, the band-gap of ZnO can be modulated for the realization of light-emitting devices operating in a wider wavelength region.

Bibliography

[1] B. Bhusan, "Springer handbook of nanotechnology." *Heidelberg7 Springer-Verlag* (2004).

[2] زياد طارق خضير المجمعي، "تصميم وتصنيع التراكيب النانوية المنماة بتقنية APCVD ودراسة بعض الخواص الفيزيائية وظروف الترسيب للمركب (ZnO:Fe)"، أطروحة دكتوراه، كلية التربية للعلوم الصرفة- ابن الهيثم، جامعة بغداد، (2011).

[3] S. Günter, ed. *Nanotechnology: Principles and fundamentals*. Vol. 1. Wiley-Vch, (2008).

[4] H. Bruus, “Introduction to nanotechnology", MIC – Department of Micro and Nanotechnology Technical University of Denmark, Lyngby, spring (2004).

[5] A. H. Abed, “Study of Some Physical Properties of Chemically Prepared Nano Magnesium Oxide (MgO) Doped With Iron and Cerium Ions", M.Sc. Thesis, College of Science, University of Diyala, (2016).

[6] عمار عيسى عباس نجم الربيعي،"دراسة الخصائص التركيبية والكهربائية والمغناطيسية للفرايت النانوي ذي التركيب المغزلي ($Ni_xCu_{0.2}Zn_{0.8-x}Fe_2O_4$) المحضر بطريقة السول– جل ذات الاحتراق التلقائي"، رسالة ماجستير، كلية التربية للعلوم الصرفة- ابن الهيثم، جامعة بغداد، (2015).

[7] M. W. Muayad, “Synthesis and Characteristics Study of ZnO/Porous Si Hetrojunctiion", M.Sc. Thesis, Department of Applied Sciences, University of Technology, (2013).

[8] مصطفى عبد الكريم جهاد الأوجي، "تحضير ودراسة متراكبات بوليمرية مدعمة من نوع PMMA/Graphene و PMMA/ZnO النانوية"، رسالة ماجستير، كلية التربية للعلوم الصرفة- ابن الهيثم، جامعة بغداد، (2015).

[9] إيناس ياسين عبد،"دراسة تأثير درجة حرارة القاعدة وزمن التلدين على الخواص التركيبية والبصرية لأغشية (ZnO) " رسالة ماجستير، كلية التربية للعلوم الصرفة- ابن الهيثم ، جامعة بغداد، (2010).

[10] عمر دحام جرذي ،" دراسة تأثير السمك ودرجة حرارة التلدين على الخواص التركيبية والبصرية لأغشية (ZnO) الرقيقة "، رسالة ماجستير، كلية التربية للعلوم الصرفة- ابن الهيثم، جامعة بغداد، (2012).

[11] إسراء محمد كاظم الخفاجي ،"دراسة تأثير البلازما غير الحرارية في الخواص التركيبية والبصرية لأغشية أوكسيد الخارصين النانوية (ZnO) الرقيقة المحضرة بطريقة التحلل الكيميائي الحراري "، رسالة ماجستير، كلية العلوم للبنات – جامعة بغداد ، (2014).

[12] M. E. H. Ahmed, “A study of Effect of Yttria Stabilized Zirconia Addition on the Mechanical and Electrical Properties of Zinc Oxide Ceramic ", M.Sc. Thesis, College of Education- Ibn AL-Haitham, University of Bagdad, (2011).

[13] مشري خولة،" دراسة الخصائص الفيزيائية للأغشية الرقيقة لأكسيد الزنك (ZnO) المطعمة باللانثانوم (La) و المرسبة بتقنية رذاذ الانحلال الحراري "، رسالة ماجستير، جامعة قاصدي مرباح ورقلة /كلية الرياضيات وعلوم المادة-قسم الفيزياء، (2015).

[14] علي محمد رحيمة الساعدي ،" تصنيع ودراسة خصائص كاشف ضوئي من اغشية ZnO:Al الرقيقة "، أطروحة دكتوراه، كلية التربية للعلوم الصرفة- ابن الهيثم، جامعة بغداد، (2012).

[15] سهام حسن سلمان،" تصميم وتصنيع متحسس من شبه موصل ZnO للكشف عن الغازات"، رسالة ماجستير، كلية التربية للعلوم الصرفة- ابن الهيثم، جامعة بغداد، (2010).

[16] آسيا چاسب يوسف،" دراسة تأثير المواد البوليمرية على الخواص البصرية لأغشية ZnO "، رسالة ماجستير، كلية التربية للعلوم الصرفة- ابن الهيثم، جامعة بغداد، (2013).

[17] نور محمد علي الكرخي،" دراسة الخصائص التركيبية والبصرية لأغشية (ZnO:Sn) المحضرة بطريقة التحلل الكيميائي الحراري"، رسالة ماجستير، كلية العلوم – جامعة ديالى، (2012).

[18] مريم زهير عبد الواحد طعمة،" تأثير اوكسيد المغنيسيوم و ثاني اوكسيد السليكون النانوي على بعض الخواص الميكانيكية والحرارية لمتراكبات الايبوكسي "، رسالة ماجستير، كلية العلوم للبنات - جامعة بغداد، (2015).

[19] D. Junkai, M. Mortazavi, N. V. Medhekar, and J. Zhe Liu. "Band engineering of Ni1− xMgxO alloys for photocathodes of high efficiency dye-sensitized solar cells." *Journal of Applied Physics* 112, no. 12, (2012).

[20] S. Balamurugan, L. Ashna, and P. Parthiban. "Synthesis of nanocrystalline MgO particles by combustion followed by annealing method using hexamine as a fuel." *Journal of Nanotechnology, vol.* 2014 (2014).

[21] S. A. SALIH, “Study of Some Physical Properties of Epoxy Reinforce With Nano Particles “, Ph.D. Dissertation, College of Education for pure science-ibn al-Hiatham, University of Baghdad, (2016).

[22] M. M. Abdullah, F. M. Rajab, and S. M. Al-Abbas. "Structural and optical characterization of Cr_2O_3 nanostructures: Evaluation of its dielectric properties." *AIP Advances* 4, no. 2, (2014).

[23] حبيبة كاظم العتابي، " تاثير اشعة كاما على الخواص التركيبية والبصرية لاغشية Cr_2O_3 الرقيقة " رسالة ماجستير، كلية التربية للعلوم الصرفة-ابن الهيثم، جامعة بغداد، (2009).

[24] ايناس سلمان المزبان، "دراسة الخواص البصرية والكهربائية لأغشية أوكسيد الكروم (Cr_2O_3) واوكسيد الكوبلت (Co_3O_4) الرقيقة ومزيجهما" رسالة ماجستير، كلية التربية للعلوم الصرفة-ابن الهيثم، جامعة بغداد، (1997).

[25] M. H. M. Ahmed," Metal Oxide Surfaces; Beyond UHV", Ph.D. dissertation, Faculty of Engineering and Physical Sciences, The University of Manchester, (2014).

[26] S. B. Rana, P. Singh, A. K. Sharma, A. W. Carbonari, and R. Dogra. "Synthesis and characterization of pure and doped ZnO nanoparticles." *Journal of optoelectronics and Advanced Materials*, vol.12, no. 2, pp. 257- 261, (2010).

[27] A. K. Zak, WH A. Majid, M. E. Abrishami, and R. Yousefi. "X-ray analysis of ZnO nanoparticles by Williamson–Hall and size–strain plot methods." *Solid State Sciences* 13, no. 1, pp. 251-256, (2011).

[28] J. Zhang, D. Gao, G. Yang, J. Zhang, Z. Shi, Z. Zhang, Z. Zhu and D. Xue, , “Synthesis and magnetic properties of Zr doped ZnO Nanoparticles”, *Nanoscale research letters*, vol. *6, no.*(1), p.587, (2011).

[29] T. V. Kolekar, H. M. Yadav, S. S. Bandgar, and P. Y. Deshmukh. "Synthesis by sol–gel method and characterization of ZnO nanoparticles." *Indian streams research journal* 1, no. 1 (2011).

[30] R. Garcia, R. Nuñez-Gonzalez, D. Berman-Mendoza, M. Barboza-Flores, and R. Rangel. "Synthesis and characterization of In-doped ZnO nano-powders produced by combustion synthesis." *Revista Mexicana de Física* 57, no. 2, pp.10-12, (2011).

[31] S. P. Ghosh, "Synthesis and Characterization of Zinc Oxide Nanoparticles by Sol-Gel Process." PhD diss., National Institute of Technology, Rourkela, (2012).

[32] R. Viswanatha, Y. Arthoba Nayaka, C. C. Vidyasagar, and T. G. Venkatesh. "Structural and optical properties of Mg doped ZnO nanoparticles." *J Chem Pharm Res* 4, no. 4, pp. 1983-89, (2012).

[33] V. D. Mote, V. R. Huse, and B. N. Dole. "Synthesis and characterization of Cr doped ZnO nanocrystals." *World Journal of Condensed Matter Physics* 2, no. 04, pp.208-211, (2012).

[34] M. A .Hassan." Preparation and characterization ZnO nanoparticles and study of morphology at high temperature", *Iraqi Journal of Physics,* Vol.10, No.18, PP. 17-23, (2012).

[35] T. M. Hammad, J. K. Salem, and R. G. Harrison. "Structure, optical properties and synthesis of Co-doped ZnO superstructures." *Applied Nanoscience* 3, no. 2, pp.133-139, (2013).

[36] K. Sanjeev, A. Kumara, F. Singhb, and A. Kapoora. "Preparation of Mg-doped ZnO nanoparticles by Sol-gel method and their Optical & structural properties." *Stress (GPa)* 3, no. 2.381, pp.701-712, (2013).

[37] T. M. Hammad, S. Griesing, M. Wotocek, S. Kuhn, R. Hempelmann, U. Hartmann, and J. K. Salem. "Optical and magnetic properties of Fe-doped ZnO nanoparticles prepared by the sol-gel method." *International Journal of Nanoparticles* 6, no. 4, pp.324-337. (2013).

[38] S. F. Shayesteh, and A. A. Dizgah. "Effect of doping and annealing on the physical properties of ZnO: Mg nanoparticles." *Pramana* 81, no. 2, pp.319-330, (2013).

[39] A. Ghosh, N. Kumari, and A. Bhattacharjee. "Investigations on structural and optical properties of Cu doped ZnO." *J. Nanosci. Nanotechnol* 2, no.4, pp.485-489, (2014).

[40] C. Jayachandraiah, and G. Krishnaiah. "Erbium induced raman studies and dielectric properties of Er-doped ZnO nanoparticles." *Adv. Mater. Lett. Adv. Mater. Lett* 6 (2015): 743-748.

[41] N. K. Divya, P. U. Aparna, and P. P. Pradyumnan. "Dielectric Properties of Er^{3+} Doped ZnO Nanocrystals." *Advances in Materials Physics and Chemistry* 5, no. 08, pp.287-294, (2015).

[42] S. R. Brintha, and M. Ajitha. "Synthesis and characterization of ZnO nanoparticles via aqueous solution, sol-gel and hydrothermal methods." *IOSR J. Appl. Chem* 8, no. 11, pp.66-72. (2015).

[43] A. Sh. AL-Gurabi, Sh. S. Al-Ani, and E. A. Al-Ajaj," Preparation and characterization of ZnO nano-particles", *Journal of University of Kerbala*, The international ^{3}rd. Scientific Conference of the College of Science, pp.24-34, (2015).

[44] S. Jurablu, M. Farahmandjou, and T. P. Firoozabadi. "Sol-Gel Synthesis of Zinc Oxide (ZnO) Nanoparticles: Study of Structural and Optical Properties." *Journal of Sciences, Islamic Republic of Iran* 26, no. 3, pp.281-285, (2015).

[45] M. S. Hamza, S. S. Shaker and kh. S. Shaker," Preparation and Study of morphological properties of ZnO nano Powder", *Journal of Engineering*, Vol. 22, Issue.4, pp. 116-126, (2016).

[46] Ch. Yacine, A. Chaouchi, Y. Lorgoilloux, M. Rguiti, A. Kadri, and Ch. Courtois. "Electrical, dielectric and photocatalytic properties of Fe-doped ZnO nanomaterials synthesized by sol gel method." *Processing and Application of Ceramics* 10, no. 3, pp.125-135, (2016).

[47] T. Iqbal, S. Ghazal, S. Atiq, N. R. Khalid, A. Majid, S. Afsheen, and N. A. Niaz. "Influence of Manganese on Structural, Dielectric and Magnetic Properties of Zno Nanoparticles." *Digest Journal of Nanomaterials and Biostructures* 11, no. 3, pp. 899-908, (2016).

[48] David J. Lockwood, "Nanostructure Science and Technology." (2005).

[49] Nassiopoulou, Androula G., and Xanthi Zianni. "*Microelectronics, Microsystems and Nanotechnology": Papers Presented at MMN 2000, Athens, Greece, 20-22 November 2000*. World Scientific, (2001).

[50] Nouailhat, Alain. “*An Introduction to Nanosciences and Nanotechnology*. Vol. 10. John Wiley & Sons”, (2010).

[51] S.L. Kakani and A. Kakani,"Material science “New Age International, New Delhi, (2004).

[52] S. A. Busk, “Nanostructured titanium dioxide: fate in the aquatic environment and effects on the marine mussel Mytilus edulis." Master's thesis, University of Stavanger, Norway, (2011).

[53] V. Pokropivny, R. Lohmus, I. Hussainova, A. Pokropivny, and S. Vlassov, “Introduction to nanomaterials and nanotechnology”. Ukraine: Tartu University Press, (2007).

[54] M. S. Hameed, “Doping effect on some Physical Properties of ZnO Nanoparticles”, Master’s thesis, College of Science for Women , University of Baghdad, (2014),

[55] N. L. Pacioni, C. D. Borsarelli, V. Rey, and A. V. Veglia. "Synthetic routes for the preparation of silver nanoparticles." In *Silver Nanoparticle Applications*, Springer International Publishing, pp. 13-46, (2015).

[56] S. A. Johari, I. Sourinejad, N. Bärsch, S. Saed-Moocheshi, A. Kaseb, and N. Nazdar, "Does physical production of nanoparticles reduce their ecotoxicity? A case of lower toxicity of AgNPs produced by laser ablation to zebrafish *(Danio rerio)*." *International Journal of Aquatic Biology* 2, no. 4, pp.188-192, (2014).

[57] C. Daraio and S. Jin. "Synthesis and patterning methods for nanostructures useful for biological applications." In *Nanotechnology for Biology and Medicine*, Springer New York, pp. 27-44, (2012).

[58] A. El-Badawy, D. Feldhake, and R. Venkatapathy. "Scientific, Technical, Research, Engineering and Modeling Support Final Report." *State of the Science Literature Review: Everything Nanosilver and More, Washington, DC: US Environmental Protection Agency. Office of Research and Development,* p.34, (2010).

[59] C. A. Milea, C. Bogatu, and A. Duta, "The influence of parameters in silica sol-gel process," *Bulletin of TheTransilvania University of Brasov* 4, No. 1, pp.59-66, (2011).

[60] A. Sengupta, and C. K. Sarkar, eds. “Introduction to Nano: Basics to Nanoscience and Nanotechnology”. Springer, 2015.

[61] C. A. Charitidis, P. Georgiou, M. A. Koklioti, A.-Flora Trompeta, and V. Markakis. "Manufacturing nanomaterials: from research to industry." *Manufacturing Review* 1, (2014): 11.

[62] لؤي جعفر خضر عباس السعدي، "تحضير مسحوق الفضة النانوية بطريقة الصول-جل ودراسة خصائصها التركيبية" رسالة ماجستير، كلية التربية للعلوم الصرفة- ابن الهيثم، جامعة بغداد، (2014).

[63] C. J. Gommes, and A. P. Roberts. "Structure development of resorcinol-formaldehyde gels: microphase separation or colloid aggregation." *Physical Review E* 77, no. 4: 041409, (2008).

[64] Patra, Sunil. “Synthesis and Characterization of $CaCu_3Ti_4O_{12}$ and Lanthanum Doped $CaCu_3Ti_4O_{12}$ by Auto-Combustion Technique." PhD diss., Department of Ceramic Engineering, National Institute of Technology, Rourkela, (2009).

[65] A.R. Aparna, Dr. V. Brahmajirao, Dr. T.V. Kartikeyan and Dr. M. Fernandes” Synthesis and Structural, Morphological & FTIR Studies on Ferrite Powders Bafe $_{(12-X)}$ Ti $_{x}$O $_{19}$, Using Sol-Gel Method” Sensors, *IOSR Journal of Applied Physics, Volume 8, Issue. 1, Ver. III,* PP. 18-26, (2016).

[66] J. Azadmanjiri, S.A. Seyyed Ebrahimi, and H. K. Salehani. "Magnetic properties of nanosize $NiFe_2O_4$ particles synthesized by sol–gel auto combustion method." *Ceramics International* 33, no. 8, pp.1623-1625, (2007).

[67] I. Ahmad, T. Abbas, A. B. Ziya, Gh. Abbas, and A. Maqsood. "Size dependent structural and magnetic properties of Al substituted Co–Mg ferrites synthesized by the sol–gel auto-combustion method." *Materials Research Bulletin* 52, pp.11-14, (2014).

[68] J. Ungula, "Growth and Characterization ZnO Nanoparticles by Sol-gel Process." M.Sc. Thesis., University of the Free State (Qwaqwa Campus), South Africa, (2015).

[69] Ch. D. Snyders, E. E. Ferg, J. Schuelein, and H. Loewe. "A review of using spray pyrolysis through sol-gel materials in the synthesis of cathode materials for lithium-ion batteries." *South African Journal of Chemistry* 69, pp.88-97, (2016).

[70] Asseel Sh. M. Al-Najdi," Sintering Behavior of Prepared Nano-Sized ZnO Powder", M.Sc. Thesis, Department of Materials Engineering, University of Technology, (2011).

[71] Ana C. Marques," Sol-gel process: an overview", Department of Materials Science and Engineering, Lehigh University, USA, (2007).

[72] K. E. Geckeler and H. Nishide, "*Advanced nanomaterials*". John Wiley & Sons, 2009.

[73] L. Radev, B. Samuneva, I. Mihailova, L. Pavlova, and E. Kashchieva. "Sol-gel synthesis and structure of cordierite/tialite glass-ceramics." *Processing and Application of Ceramics* 3, no. 3, pp. 125-130, (2009).

[74] L. John and P. Sobota. "Alkoxide molecular precursors for nanomaterials: a one step strategy for oxide ceramics." In *Ceramic Materials*. InTech, (2010).

[75] M. Wang, T. Wang, Sh. Song, Q. Ma, and R. Liu. "Effect of sintering temperature on structural, dielectric, and magnetic properties of multiferroic $YFeO_3$ ceramics fabricated by spark plasma sintering." *Materials* 10, no. 3: 267, (2017).

[76] شيماء جبار عبد الرزاق و عبد العزيز عبيد موسى، "دراسة الخواص البصرية لأشباه موصلات جديدة محضرة من مواد بلورية سائلة وبعض من معقداتها"، مجلة جامعة بابل/ العلوم الصرفة والتطبيقية، العدد 5، مجلد 21، (2013).

[77] C. Chen, B. Yu, P. Liu, J. Liu, and L. Wang. "Investigation of nano-sized ZnO particles fabricated by various synthesis routes." *Journal of Ceramic Processing Research* 12, no. 4: 420-425, (2011).

[78] Mohammed W. Muayad, “Synthesis and Characteristics Study of ZnO/Porous Si Hetrojunction”, M.Sc. thesis, Department of Applied Sciences, University of Technology, (2013).

[79] عباس حيدر حسين، "دراسة الخواص التركيبية والبصرية لأغشية CdSe:Al الرقيقة كدالة لنسب التشويب ودرجة حرارة التلدين" رسالة ماجستير، كلية التربية للعلوم الصرفة- ابن الهيثم، جامعة بغداد، (2015).

[80] X. Wen, “Ultrafast spectroscopy of semiconductor nanostructures”, Ph.D. diss., Swinburne University of Technology, Centre for Atom Optics and Ultrafast Spectroscopy, (2007).

[81] T. Menke, "Molecular Doping of Organic Semiconductors: A Conductivity and Seebeck Study." PhD diss., Dresden, Technische Universität Dresden, Diss., (2013).

[82] A. Dragoneas, "Organic Semiconductor Devices: Fabrication, Characterisation and Sensing Applications", PhD diss., University of Sheffield, (2013).

[83] Brian S. Mitchell, *“An introduction to materials engineering and science for chemical and materials engineers”*. John Wiley & Sons, (2004).

[84] William D. Callister, Jr., and David G. Rethwisch, “Materials Science and Engineering”, (seven Ed.), Vol. 5, NY: John Wiley & Sons, (2007).

[85] A. Seyhan, "Photoluminescence Specroscopy of CdS and GaSe." Ph.D. diss., METU, (2003).

[86] S. Tongay, *“Graphite-graphene semiconductor junctions and magneto-dielectric coupling in Schottky diodes”*. University of Florida, (2010).

[87] طاهر حمد محمود، "دراسة الخواص التركيبية والبصرية لأغشية CdO المشوبة بـ Sn والمحضرة بتقنية التبخير الحراري في الفراغ"، رسالة ماجستير، كلية التربية للعلوم الصرفة-ابن الهيثم، جامعة بغداد، (2011).

[88] B. M. Maoz, “Synthesis and Properties of Highly Defective MgO Nanosheets”, M.Sc. Thesis, Tel Aviv University, (2010).

[89] A. L. Abdelhady, M. I. Saidaminov, B. Murali, V. Adinolfi, O. Voznyy, Kh. Katsiev, E. Alarousu et al., "Heterovalent dopant incorporation for bandgap and type

engineering of perovskite crystals." *The journal of physical chemistry letters* 7, no. 2: 295-301, (2016).

[90] Schmidt, Rüdiger. "Perylene Bisimide and Acene Derivatives as Organic Semiconductors in OTFTs." (2008).

[91] هناء إبراهيم محمد، “الخواص الالكتروبصرية لأغشية CdTe الرقيقة المشوبة بـ Zn "، رسالة ماجستير، كلية التربية للعلوم الصرفة-ابن الهيثم، جامعة بغداد، (2008).

[92] سلام حميد فياض، "تحضير ودراسة الخواص التركيبية والبصرية لأغشية CdTe:Cu" رسالة ماجستير، كلية التربية للعلوم الصرفة-ابن الهيثم، جامعة بغداد، (2015).

[93] Aram K. Majeed, “Structural and Dielectric Properties of ($Bi_{1-X}Sr_XFeO_3$) Ferrites Prepared Using (Sol-Gel) Auto Combustion Method” M.Sc. Thesis, College of Science- University of Diyala, (2014).

[94] Amira A. Abdel-Wahab, “Study of The Physical Properties of Some Semiconductor Materials." PhD diss., HELWAN University, (2012).

[95] زياد طارق وموفق كاظم عبد الرضا وزينب طارق العاني، "دراسة الخصائص البصرية لغشاء CuBr" مجلة ابن الهيثم للعلوم الصرفة والتطبيقية، المجلد 21، العدد 3، (2008).

[96] ردينة صديق عبد الستار الدليمي، "دراسة الخصائص التركيبية و البصرية لأغشية $Ni_{(1-x)}Zn_xO$ المحضرة بطريقة التحلل الكيميائي الحراري"، رسالة ماجستير، كلية العلوم، جامعة ديالى، (2013).

[97] G. Amin, "ZnO and CuO nanostructures: low temperature growth, characterization, their optoelectronic and sensing applications." PhD diss., Linköping University Electronic Press, (2012).

[98] Langford, J. Ian, and Daniel Louer. "Powder diffraction." *Reports on Progress in Physics* 59, no. 2, : 131 (1996).

[99] F. Sher, "Crystal Structure Determination I." (2007).

[100] E. Napolitano, "Applications of the diffraction technique in solid state chemistry from" AB-INITIO" structure solution to final structure refinement: powder and single crystal.” Ph.D diss., University of Sassari: 1-168, (2011).

[101] Hugo M. Rietveld, "The early days: a retrospective view." *The Rietveld Method, Oxford University Press, Oxford*: 39-42, (1993).

[102] M. Mazhdi, and P. Hossein Khani. "Structural characterization of ZnO and ZnO: Mn nanoparticles prepared by reverse micelle method." *International Journal of Nano Dimension* 2, no. 4: 233-240, (2012).

[103] S. S. Kulkarni, and M. D. Shirsat. "Optical and structural properties of zinc oxide nanoparticles." *International Journal of Advanced Research in Physical Science (IJARPS)* Vo. 2, Issue 1, PP. 14-18, (2015).

[104] B. Nandan, and M. C. Bhatnagar. "Effect of sintering treatment on structural and magnetic properties of Ni0. 5Co0. 5Fe2O4 ferrites." In *AIP Conference Proceedings*, vol. 1728, no. 1, p. 020506. AIP Publishing, (2016).

[105] V. Kumar, S. Kumari, P. Kumar, M. Kar, and L. Kumar. "Structural analysis by rietveld method and its correlation with optical propertis of nanocrystalline zinc oxide." *Adv. Mater. Lett.* 6, pp. 139-147, (2015).

[106] H. Sarma, and K. C. Sarma. "X-ray peak broadening analysis of ZnO nanoparticles derived by precipitation method." *Int. J. Sci. Res. Publ* 4, no. 3, pp. 1-7, (2014).

[107] B. Nath and T. F. Barbhuiya," Studies on the density and surface area of nanoparticles from Camellia sinensis, A natural source", *Journal of Chemical and Pharmaceutical Research*, vol. 6(11):608-610, (2014).

[108], S. Sönmezoğlu and E. Akman, "Improvement of physical properties of ZnO thin films by tellurium doping." *Applied Surface Science* 318: 319-323, (2014).

[109] D. Djouadi, M. Meddouri, A. Chelouche, L. Hammiche, and A. Aksas. "Structural and morphological characterizations of ZnO nanopowder synthesized by hydrothermal route using inorganic reactants." *Journal of Semiconductors* 35, no. 12: 123001, (2014).

[110] A. Singh, and H. L. Vishwakarma. "Study of structural, morphological, optical and electroluminescent properties of undoped ZnO nanorods grown by a simple chemical precipitation." *Materials Science-Poland* 33, no. 4: 751-759, (2015).

[111] R. Jacob, H.G. Nair and J. Isac, “Structural and morphological studies of nano-crystalline ceramic $BaSr_{0.9}Fe_{0.1}TiO_4$”. *International Letters of Chemistry, Physics and Astronomy*, *41*, pp.100-117, (2014).

[112] Y.T. Prabhu, K.V. Rao, V.S.S. Kumar and B.S. Kumari, “Synthesis of ZnO Nanoparticles by a novel surfactant assisted amine combustion method”. *Advances in Nanoparticles*, *2*(01), p.45, (2013).

[113] Criterion, I., and V. I. I. Annexure. "I. Executive Summary 2 II. Profile of the Institution 7 III. Action Taken Report 17 IV. Criteria-Wise Inputs.” (2014).

[114] S. Schmitt-Rink, D. S. Cchemla, D. A. B. Miller, "Linear and Nonlinear Optical Properties of Semiconductor Quantum Wells”, *ADVANCED IN PHYSICS*, Vol. 38, no. 2, pp. 89-188, (1989).

[115] Daniel R. Harada, “The synthesis, optical, and transport properties of $SnZrS_3$." M.Sc. diss., Oregon State University, (2010).

[116] عبد المجيد عيادة إبراهيم و نيران فاضل عبدالجبار و قاسم حمادي محمود، “دراسة تأثير التشعيع بأشعة كاما على الخواص البصرية للأغشية الرقيقة"، مجلة جامعة كركوك - الدراسات العلمية المجلد – (5)، العدد (1)، (2010) .

[117] R. H. Jabbar, “Physical Properties of Aluminum and Boron co-doped Zinc Oxide Thin Films”, Ph.D. diss., College of Science, Al–Mustansiriyah University, (2015).

[118] نادر فاضل حبوبي و صباح انور سلمان و كاظم مصطفى كاظم، “الخصائص البصرية لأغشية اوكسيد الخارصين المشوب بالفناديوم المحضرة بالتحلل الكيميائي الحراري"، مجلة ديالى للعلوم الصرفة، المجلد 8، العدد 3، (2012).

[119] كرار أمين قدوري محمد، "تحضير SnO_2 النانوي ودراسة تأثير التشويب على الخواص التركيبية والبصرية" رسالة ماجستير، كلية التربية للعلوم الصرفة-ابن الهيثم، جامعة بغداد، (2015).

[120] A. A. Ramadhan, “Structural, Optical and Photovoltaic Effect of Thermal Evaporated Tin Selenide Thin Films”, M.Sc. Thesis, College of Science, University of Baghdad, (2013).

[121] فاطمة شهيد عيسى و خالد ابراهيم عجيل، “تحضير ود راسة الخواص الضوئية للبوليمر الموصل بولي (أورثو-أنسدين) النقي والمشوب بحامض الهيدروكلوريك (HCl)“، مجلة أبحاث البصرة (العلميات)، العدد 38، الجزء B.3، (2012).

[122] منى جايد العيداني، “استقرارية الصفات الضوئية لأغشية CdS:Al المحضرة بطريقة الرش الكيميائي الحراري “، مجلة أبحاث البصرة (العلميات)، العدد 32، الجزء 3، :(1-6)، (2012).

[123] Dr. S. A. A. Taha, Dr. A. A. Abdul-Hamead, Ass. Lec. Marwa S. Mehsin, Eng.Roaa S. Mahmood, “Study Some Structural and Optical Properties of Copper Nano Film”, *International Journal of Application or Innovation in Engineering & Management (IJAIEM),* Vol. 4, Issue 1, (2015).

[124] مصطفى خالد كامل، "الخواص البصرية والكهربائية لأغشية (CdO) النقية والمطعمة بـ(Se) " رسالة ماجستير، كلية التربية للعلوم الصرفة-ابن الهيثم، جامعة بغداد، (2012).

[125] R. T. Hussain, “Study the Optical and Electrical Properties of PMMA/Metal Oxide Composites”, M.Sc. Thesis, College of Education for Pure Science Ibn-AL-Haitham, University of Baghdad, (2016).

[126] علياء حسين علي ،محمد سامي عبد علي، محمد حميد عبد الله،" دراسة تأثير أشعة كاما على فجوة الطاقة البصرية لأغشية البولي مثيل ميثاكريلات (PMMA) “مجلة ديالى للعلوم الصرفة، المجلد 6، العدد 4، (2010).

[127] M. S. Dresselhaus , *“Optical Properties of Solids”* Part II , (1998).

[128] عماد محمد احمد عبدالله المرسومي، "تأثير جسيمات الفضة النانوية على اخواص البصرية لزجاج التليريوم المشوب بأيونات العنصر الأرضي النادر السماريوم" رسالة ماجستير، كلية التربية للعلوم الصرفة-ابن الهيثم، جامعة بغداد، (2016).

[129] حلا إبراهيم جاسم،" إمكانية استخدام أفلام التشخيص الفوتوغرافي كمقياس جرعة للأشعة فوق البنفسجية ودراسة خواصها البصرية “،مجلة علوم الرافدين، المجلد 24، العدد 1، ص. 108- 120، (2013).

[130] ميخائيل عيسى منصور،" دراسة الخواص التركيبية والبصرية لأغشية (ZnO:Cu) المحضرة بطريقة APCVD “،المجلة الأردنية للفيزياء، المجلد 5، العدد 2، ص ص. 89- 103، (2012).

[131] شوق محمد علي الغامدي، "دراسة بعض الخواص الفيزيائية للمركب العضوي رباعي سيانو كينو ثنائي الميثان" رسالة ماجستير، كلية التربية العلمية للبنات ،جامعة الملك عبد العزيز، (2009).

[132] عدوية جمعة حيدر و ناهده بخيت حسن و علي صلاح حسن،" دراسة تأثير التطعيم بالمنغنيز Mn على الخصائص البصرية لأغشية كبريتيد الخارصين ZnS المحضرة بتقنية الترسيب بالليزر النبضي "،مجلة جامعة بابل/ للعلوم الصرفة والتطبيقية، المؤتمر العلمي السنوي لكلية العلوم، جامعة بابل، المجلد 22، العدد 1، ص ص. 152- 161، (2012).

[133] عبد المجيد عيادة إبراهيم و زهير ناجي مجيد و سوزان عبد الله حسن،" تأثير التلدين والتشويب على بعض الخواص البصرية لأغشية كبريتيد الخارصين الرقيقة "،مجلة جامعة كركوك- الدراسات العلمية، المجلد 8، العدد 1، (2013).

[134] A.M. Hassana, Ayman H. Ahmeda, Hosni A. Gumaaa, Bassem H. Mohamed and Ahmed M. Eraky, “Manganese (II) complexes of N,O-chelating dihydrazone: Synthesis, characterization, optical properties and corrosion inhibition on aluminum in HCl solution”, *Journal of Chemical and Pharmaceutical Research*, Vol. 7(7): 91-104, (2015).

[135] H. Kumar and R. Rani, “Structural and Optical Characterization of ZnO Nanoparticles Synthesized by Microemulsion Route”, *International Letters of Chemistry, Physics and Astronomy,* Vol.14, pp.26-36, (2013).

[136] Hashim M. Jabbar, Eman M. Jaboori and Ali Q. Abdullah, “Dispersion Parameters, Optical Constant and Photoluminescence of Poly Vinyl Alcohol Grafted Eosin –Y Dye (PVA-g-Ei)”, *Journal of Basrah Researches ((Sciences))*, Vol. 36, No.3, (2010).

[137] M. L. Dinesha, G. D. Prasanna, C. S. Naveen, and H. S. Jayanna. "Structural and dielectric properties of Fe doped ZnO nanoparticles." *Indian Journal of Physics* 87, no. 2: 147-153, (2012).

[138] Luigi S. Amato, “Recombination dynamics in zinc oxide." PhD diss., Università degli Studi di Napoli Federico II, (2010).

[139] وسن كامل حسن،" دراسة الخصائص الكهربائية لمتراكب بولي ستايرين - بنتونايت والعوامل المؤثرة فيها "،مجلة الكوفة- الفيزياء، المجلد 3، العدد 2، (2011).

[140] رولا عبد الخضر عباس،" دراسة بعض الخصائص الكهربائية العزلية والعوامل المؤثرة فيها لمواد متراكبة من راتنج النوفولاك “،مجلة الهندسة والتكنولوجيا، المجلد 25، العدد 8، (2007).

[141] I. Latif, E. E. AL-Abodi, D. H. Badri and J. Al Khafagi, “Preparation, Characterization and Electrical Study of (Carboxymethylated Polyvinyl Alcohol/ZnO) Nanocomposites”, *American Journal of Polymer Science*, 2(6): 135-140, (2012).

[142] K. Omar, M. D. Johan Ooi and M. M. Hassin, “Investigation on Dielectric Constant of Zinc Oxide”, *Modern Applied Science,* Vol. 3, No. 2, (2009).

[143] Li, Li. “Dielectric properties of aged polymers and nanocomposites”. , Ph.D. diss., Iowa State University, (2011).

[144] S. Suresh, “Synthesis, structural and dielectric properties of zinc sulfide nanoparticles”, *International Journal of Physical Sciences,* Vol. 8(21), pp. 1121-1127, (2013).

[145] P. Donta, V. K. Katrapally and V. R. Pendyala, “Dielectric Response of $Ni_x\ Zn_{1-x}\ Al\ Fe\ O_4$ Nanoferrites”, *NanoWorld J,* 2(2): 27-34, (2016).

[146] Aly M. Badr, Haroun A. Elshaikh and Ibraheim M. Ashraf, “Impacts of Temperature and Frequency on the Dielectric Properties for Insight into the Nature of the Charge Transports in the Tl_2S Layered Single Crystals”, *Journal of Modern Physics 2, pp.12-25*, (2011).

[147] علاء خضير هاشم و صالح مهدي حداوي و عوده مزعل ياسر،" أنواع جديدة من أشباه موصلات بلورية سائلة “،المجلة القطرية للكيمياء، المجلد 24، ص ص. 475 - 487، (2006).

[148] A. K. Mahapatra, B. L. Jones, C. N. Nguyen, and G. Kannan, "Experimental determination of the electrical resistivity of beef." *Agricultural Engineering International: CIGR Journal* 12, no. 3-4: 124-128, (2010).

[149] William D. Callister, Jr., “Fundamentals of Materials Science and Engineering”, fifth Edition, John Wiley & Sons, (2001).

[150] D. A. Tuan, V. T. Tung, L. V. Phuong, “Analyzing 2D Structure Images of Piezoelectric Ceramics Using ImageJ”, *International Journal of Materials and Chemistry,* 4(4): 88-91, (2014).

[151] J. I. Goldstein, D. E. Newbury, P. Echlin, D. C. Joy, C. E. Lyman, E. Lifshin, L. Sawyer, and J. R. Michael. "Special Topics in Scanning Electron Microscopy." In *Scanning Electron Microscopy and X-Ray Microanalysis*, pp. 195-270. Springer US, (2003).

[152] Santiago, Miguel. "Introduction to X– ray Diffractionmeter." *Melalui http://geology. uprm. edu/facilities/Class% 20Forms/xrd. Pdf*, (2007).

[153] Instruments, Kevex. "Energy-Dispersive X-Ray Microanalysis—An Introduction." (1989).

[154] S. Husain, F. Rahman, N. Ali, and P. A. Alvi. "Nickel sub-lattice effects on the optical properties of ZnO nanocrystals." *Journal of Optoelectronics Engineering* 1, no. 1: 28-32, (2013).

[155] S. S. Sartiman, N. F. Djaja, R. Saleh, “Chromium-Doped ZnO Nanoparticles Synthesized by Co-Precipitation: Chromium Effects,” *Materials Sciences and Applications*, Vol. 4: 528-537, (2013).

[156] M. Sharma and P. Jeevanandam,” Magnesium doping in hierarchical ZnO nanostructures and studies on optical properties”, *Superlattices and Microstructures,* 52: 1083–1092, (2012).

[157] R. A. Rakkesh and S. Balakumar, “Structural, electrical transport and optical studies of Li ion doped ZnO nanostructures,” *Processing and Application of Ceramics, Vol.* 8 (1): 7-13, (2014).

[158] H. Sarma, K.C. Sarma, “X-ray Peak Broadening Analysis of ZnO Nanoparticles Derived by Precipitation method”, *International Journal of Scientific and Research Publications*, Volume 4, Issue 3, (2014)

[159] J. R. Reddy, K. Sivalingam, G. K. Mani, P. Shankar and J. B. B. Rayappan,”Synthesis and Characterization of Sol-Gel Dip Coated Pure and Mn-

Doped ZnO Thin Films”, *Research Journal of Pharmaceutical, Biological and Chemical Sciences RJPBCS*, 5(4), pp. 605-614, (2014).

[160] G. Varughese, P. W. Jithin and K.T. Usha, “Determination of Optical Band Gap Energy of Wurtzite ZnO: Ce Nanocrystallites”, *Physical Science International Journal,* 5(2): 146-154, (2015).

[161] M. S. Samuel, L. Bose and KC. George, “OPTICAL PROPERTIES OF ZnO NANOPARTICLES”, *SB Academic Review*, Vol. XVI: No. 1 & 2: 57-65, (2009).

[162] R. John and R. Rajakumari. "Synthesis and characterization of rare earth ion doped nano ZnO." *Nano-Micro Letters* 4, no. 2: 65-72, (2012).

[163] H. M. Mehedi, W. Khan, A. Azam, and A. H. Naqvi. "Influence of Cr incorporation on structural, dielectric and optical properties of ZnO nanoparticles." *Journal of Industrial and Engineering Chemistry* 21: 283-291, (2015).

[164] Thomas, Abegayl Lorenda Shara-Lynn. "Solution Combustion Synthesis of Oxide Semiconductors.” Ph.D. diss., the University of Texas at Arlington, (2015).

[165] سامي سلمان جياد ، د .نادر فاضل حبوبي، د .عبد الرحمن الحسن محمد عثمان،" الخصائص الكهربائية والبصرية لأغشية ثنائي أوكسيد القصدير المشوب بالأنتمون"، المؤتمر العلمي الثالث لكلية العلوم، جامعة بغداد، ص-ص. 2230-2238، (2009).

[166] Chan O. Chey, "Synthesis of ZnO and transition metals doped ZnO nanostructures, their characterization and sensing applications." Ph.D diss., Linköping University Electronic Press, (2014).

Appendix

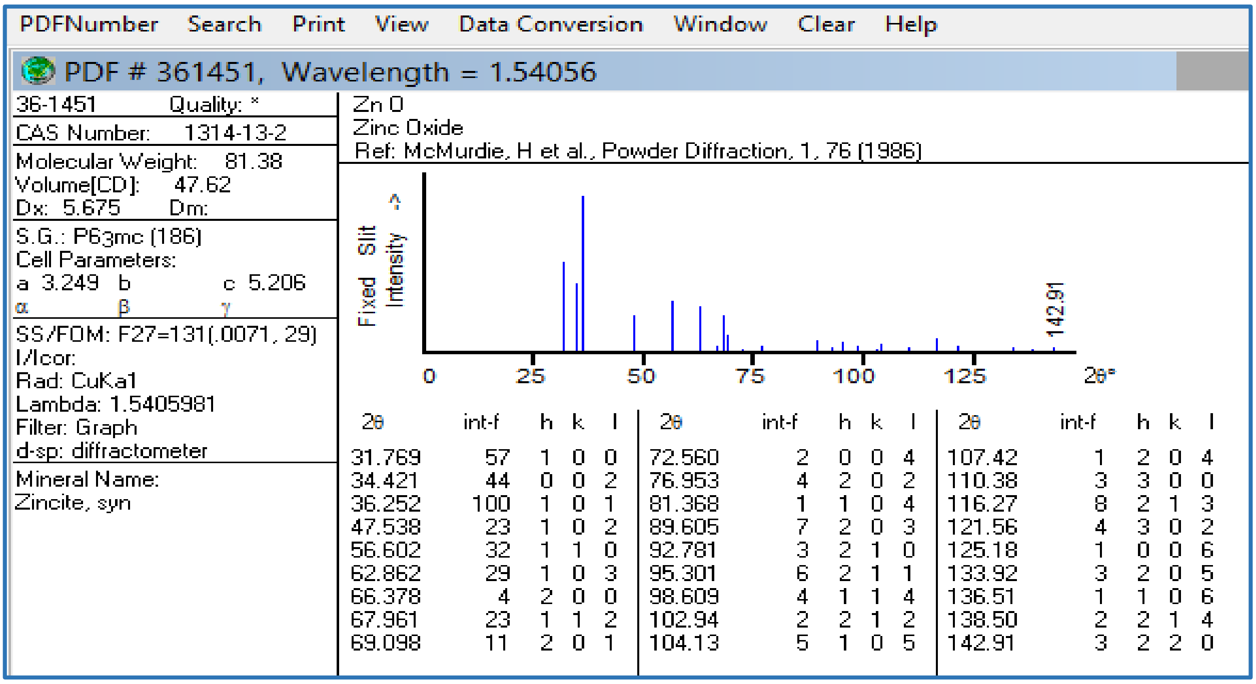

PDF # 361451, Wavelength = 1.54056

36-1451 Quality: *
CAS Number: 1314-13-2
Molecular Weight: 81.38
Volume[CD]: 47.62
Dx: 5.675 Dm:
S.G.: P6₃mc (186)
Cell Parameters:
a 3.249 b c 5.206
α β γ
SS/FOM: F27=131(.0071, 29)
I/Icor:
Rad: CuKa1
Lambda: 1.5405981
Filter: Graph
d-sp: diffractometer
Mineral Name:
Zincite, syn

Zn O
Zinc Oxide
Ref: McMurdie, H et al., Powder Diffraction, 1, 76 (1986)

2θ	int-f	h	k	l	2θ	int-f	h	k	l	2θ	int-f	h	k	l
31.769	57	1	0	0	72.560	2	0	0	4	107.42	1	2	0	4
34.421	44	0	0	2	76.953	4	2	0	2	110.38	3	3	0	0
36.252	100	1	0	1	81.368	1	1	0	4	116.27	8	2	1	3
47.538	23	1	0	2	89.605	7	2	0	3	121.56	4	3	0	2
56.602	32	1	1	0	92.781	3	2	1	0	125.18	1	0	0	6
62.862	29	1	0	3	95.301	6	2	1	1	133.92	3	2	0	5
66.378	4	2	0	0	98.609	4	1	1	4	136.51	1	1	0	6
67.961	23	1	1	2	102.94	2	2	1	2	138.50	2	2	1	4
69.098	11	2	0	1	104.13	5	1	0	5	142.91	3	2	2	0

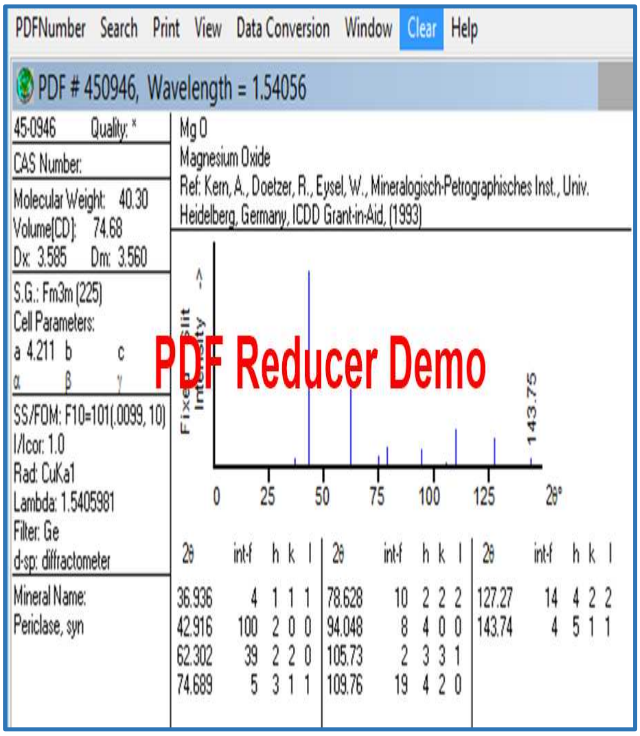

PDF # 450946, Wavelength = 1.54056

45-0946 Quality: *
CAS Number:
Molecular Weight: 40.30
Volume[CD]: 74.68
Dx: 3.585 Dm: 3.560
S.G.: Fm3m (225)
Cell Parameters:
a 4.211 b c
α β γ
SS/FOM: F10=101(.0099, 10)
I/Icor: 1.0
Rad: CuKa1
Lambda: 1.5405981
Filter: Ge
d-sp: diffractometer
Mineral Name:
Periclase, syn

Mg O
Magnesium Oxide
Ref: Kern, A., Doetzer, R., Eysel, W., Mineralogisch-Petrographisches Inst., Univ. Heidelberg, Germany, ICDD Grant-in-Aid, (1993)

2θ	int-f	h	k	l	2θ	int-f	h	k	l	2θ	int-f	h	k	l
36.936	4	1	1	1	78.628	10	2	2	2	127.27	14	4	2	2
42.916	100	2	0	0	94.048	8	4	0	0	143.74	4	5	1	1
62.302	39	2	2	0	105.73	2	3	3	1					
74.689	5	3	1	1	109.76	19	4	2	0					

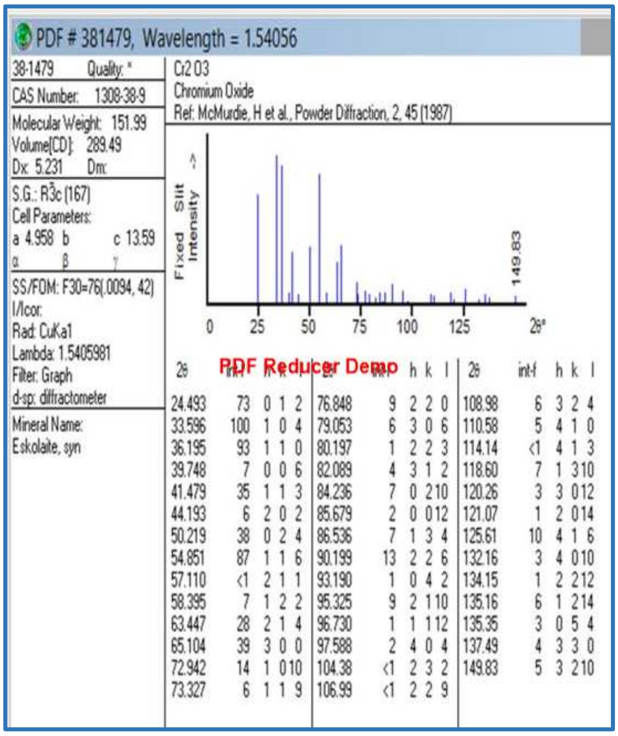

PDF # 381479, Wavelength = 1.54056

38-1479 Quality: *
CAS Number: 1308-38-9
Molecular Weight: 151.99
Volume[CD]: 289.49
Dx: 5.231 Dm:
S.G.: R3̄c (167)
Cell Parameters:
a 4.958 b c 13.59
α β γ
SS/FOM: F30=76(.0094, 42)
I/Icor:
Rad: CuKa1
Lambda: 1.5405981
Filter: Graph
d-sp: diffractometer
Mineral Name:
Eskolaite, syn

Cr2 O3
Chromium Oxide
Ref: McMurdie, H et al., Powder Diffraction, 2, 45 (1987)

2θ	int-f	h	k	l	2θ	int-f	h	k	l	2θ	int-f	h	k	l
24.493	73	0	1	2	76.848	9	2	2	0	108.98	6	3	2	4
33.596	100	1	0	4	79.053	6	3	0	6	110.58	5	4	1	0
36.195	93	1	1	0	80.197	1	2	2	3	114.14	<1	4	1	3
39.748	7	0	0	6	82.089	4	3	1	2	118.60	7	1	3	10
41.479	35	1	1	3	84.236	7	0	2	10	120.26	3	3	0	12
44.193	6	2	0	2	85.679	2	0	0	12	121.07	1	2	0	14
50.219	38	0	2	4	86.536	7	1	3	4	125.61	10	4	1	6
54.851	87	1	1	6	90.199	13	2	2	6	132.16	3	4	0	10
57.110	<1	2	1	1	93.190	1	0	4	2	134.15	1	2	2	12
58.395	7	1	2	2	95.325	9	2	1	10	135.16	6	1	2	14
63.447	28	2	1	4	96.730	1	1	1	12	135.35	3	0	5	4
65.104	39	3	0	0	97.588	2	4	0	4	137.49	4	3	3	0
72.942	14	1	0	10	104.38	<1	2	3	2	149.83	5	3	2	10
73.327	6	1	1	9	106.99	<1	2	2	9					

الخلاصة

تم في هذا البحث تحضير مساحيق نانوية من أوكسيد الزنك ZnO النقي والمطعم بعنصري الكروم والمغنيسيوم ذو الصيغة الكيميائية ($Mg_xCr_yZn_{1-x-y}O$) لتسع عينات وبتراكيز مختلفة بتقنية الصول-جل ذات الاحتراق التلقائي من نترات الزنك ($Zn\ (NO_3)_2.6H_2O$) ومحلول الامونيا (NH_3) كأساس وحامض الستريك ($C_6H_8O_4$) كعامل مساعد على الاحتراق والماء المقطر كمذيب . قسمت هذه التراكيز لمجموعتين، الأولى كان فيها تركيز المغنيسيوم ثابت وهو ($x=0.05$)، وتركيز الكروم متغير حيث ($y = 0, 0.05, 0.1, 0.15, 0.2$); بينما المجموعة الثانية كان فيها تركيز الكروم ثابت وهو ($y=0.05$)، وتركيز المغنيسيوم متغير حيث ($x = 0, 0.05, 0.1, 0.15, 0.2$). ان الظروف المثالية لتحضير العينات كانت عند درجة حامضية ($pH=7$) وحرارة تفاعل 85^oC.

تم دراسة الخصائص التركيبية والبصرية والكهربائية للعينات المحضرة باستخدام جهاز حيود الأشعة السينية (XRD) والمجهر الإلكتروني الماسح (SEM) ومقياس الاشعة السينية المشتتة للطاقة (EDX) ومطياف الاشعة فوق البنفسجية (UV-Vis) وجهاز القياسات الكهربائية (LCR meter)، حيث قورنت نتائج العينات المطعمة بنتائج عينة أوكسيد الزنك غير المطعم.

أظهرت نتائج حيود الشعاع السيني بأن جميع العينات المحضرة تمتلك تركيبا سداسياً، حيث تم ملاحظة أربع ذروات أساسية لأوكسيد الزنك عائدة للسطوح البلورية (101) و(100) و(002) و (110) ضمن المدى الزاوي (20^o -80^o). تم استخدام طريقة شرر وطريقة وليامسون-هول لحساب الحجم البلوري، حيث تبين ان المادة المحضرة تمتلك حجما نانوياً يتراوح بين (22-33 nm)، وبينت النتائج ان الحجم البلوري يقل بزيادة معدل التشويب. تم حساب العديد من الثوابت التركيبية مثل معلمات الشبيكة، وفسحة السطوح البلورية، والكثافة من بيانات XRD، وعامل التشكيل، والمساحة السطحية النوعية، ومعامل طبيعة السطح. قياسات المورفولوجيا والتركيب أجريت للعينة (M1) ذات التراكيز ($Mg_{0.05}Cr_{0.05}Zn_{0.9}O$)، حيث بينت صورة جهاز (SEM) بأن حبيبات المادة المحضرة تمتلك شكلاً كرويا او شبة كروي متجمعة بشكل عناقيد. أما فحص (EDX) فقد اثبت وجود عنصر الزنك والمغنيسيوم والكروم والأوكسجين، والذي يطابق مكونات العينة المفحوصة.

تم اجراء القياسات البصرية لمحلول ZnO ضمن مدى الطول الموجي nm (300-900)، حيث أظهرت النتائج بأن طيف الامتصاصية يقل بزيادة معدل التشويب. اما بالنسبة لفجوة الطاقة للانتقال غير المباشر المسموح فقد تم حسابها باستخدام معادلة (Tauc)، حيث وجد أنها تتناقص بزيادة نسبة التشويب لكل من Mg و Cr من (3.36 eV) الى (2.61 eV).

تم دراسة الخصائص الكهربائية والعزلية كدالة لتردد المجال الكهربائي ضمن مدى التردد (50Hz -3MHz). حيث أظهرت النتائج تناقصاً في قيمة ثابت العزل وعامل الفقد العزلي عند درجة حرارة الغرفة بزيادة التردد، وهذا نتيجة للنقصان الحاصل في توزيع استقطاب الشحنة الفراغية بزيادة التردد، وهذه الظاهرة شائعة في معظم المواد العازلة. أيضا تم دراسة تغير التوصيلية المتناوبة مع التردد عند درجة حرارة الغرفة ودرجة 50 و100 و150 سيليزية. حيث أظهرت النتائج زيادة خطية في التوصيلية الكهربائية بزيادة التردد ودرجة الحرارة، وهذا يثبت بأن المادة المحضرة هي شبه موصل. كذلك أظهرت النتائج بأن عينة ZnO النقية غير المطعمة كانت تمتلك اقل توصيلية كهربائية عند درجة حرارة الغرفة من باقي العينات المطعمة، ولهذا فقد اتضح بأن التطعيم بالمغنيسيوم والكروم قد ساهم في تحسين وتعديل التوصيلية الكهربائية ل ZnO عند درجة حرارة الغرفة.

جمهورية العراق
وزارة التعليم العالي والبحث العلمي
جامعة بغداد
كلية التربية للعلوم الصرفة -ابن الهيثم

تحضير المركب النانوي $(Mg_xCr_yZn_{1-x-y}O)$ بطريقة الصول - جل ذات الاحتراق التلقائي ودراسة خصائصه

رسالة مقدمة الى
مجلس كلية التربية للعلوم الصرفة ابن الهيثم وهي جزء من متطلبات نيل درجة
ماجستير في علوم الفيزياء

تقدم بها

رضوان شوبان محسن

(بكالوريوس علوم فيزياء / جامعة بغداد 2013)

بإشراف

أ. م. د. تغريد مسلم مريوش

1439 هـ **2017 م**